TECHNISCHE UNIVERSITÄT MÜNCHEN
Lehrstuhl für Zellbiophysik E27

Kinetics and Mechanics of Non-equilibrium Actin Networks

Kurt Michael Schmoller

Vollständiger Abdruck der von der Fakultät für Physik der Technischen Universität München zur Erlangung des akademischen Grades eines

Doktors der Naturwissenschaften (Dr. rer. nat.)

genehmigten Dissertation.

Vorsitzender: Univ.-Prof. Dr. M. Zacharias

Prüfer der Dissertation: 1. Univ.-Prof. Dr. A. Bausch

2. Univ.-Prof. Dr. E. Frey,
Ludwig-Maximilians-Universität München

Die Dissertation wurde am 23.05.2012 bei der Technischen Universität München eingereicht und durch die Fakultät für Physik am 31.07.2012 angenommen.

Summary

The actin cytoskeleton is a complex system, consisting of the dynamic biopolymer actin and numerous additional regulatory proteins. It provides mechanical stability, but is also responsible for force generation during dynamic processes such as cell division or cell migration. Force generation is achieved either by molecular motors which "walk" along the actin filaments, or through an ATP-driven process called treamilling, where the polar actin filaments continuously grow at one end while shrinking at the other. While basic functions of many actin binding proteins have been identified in *in vitro* experiments with well defined reconstituted systems, it is still elusive how cells regulate the extremely heterogeneous cytoskeleton in space and time. Studying the interplay of different actin binding proteins in reconstituted systems and investigating the effect certain external stimuli have on such defined actin systems can give important insights that contribute to a better understanding of cytoskeletal regulation mechanisms.

The first part of this thesis focuses on the intrinsic dynamics of actin filaments and how they are modified by the presence of cross-linking proteins. Despite the fundamental importance for our understanding of the actin cytoskeleton, even the steady state dynamics of an ensemble of pure actin filaments have so far not been observed directly. Here, following the length distribution of labelled filaments embedded in an unlabelled network over time allows to separate processes which cause filament growth from the once that cause the balancing shrinkage. By that, spontaneous fragmentation is identified as a dominating process of the steady state dynamics, whereas treadmilling surprisingly turns out to be too slow to be experimentally accessible by this approach. Because the steady state dynamics are so slow, the effect of cross-linking proteins on the actin dynamics is not studied in such a steady state situation, but instead, it is investigated how they alter the depolymerization behavior of actin filaments. It is shown that cross-linking proteins drastically slow down actin depolymerization in a concentration dependent manner. This is a generic effect observed for all actin binding proteins which bind at least two actin monomers simultaneously. Also the severing protein cofilin, which promotes disassembly of actin structures *in vivo*, is not sufficient to disintegrate highly cross-linked or bundled actin networks on a reasonable time scale *in vitro*. Only by a simultaneous action of cofilin and the molecular motor myosin-II even networks consisting of thick actin/filamin bundles can be disassembled.

Cross-linking proteins stabilize actin structures not only on the length scale of individual filaments, but can also provide macroscopic structural integrity by stably arranging actin filaments into a defined geometry. Recently, it has been shown that some cross-

linking proteins build extremely static and stable actin bundle networks, which are arrested in a non-equilibrium state. In the second part of the thesis, the unique properties of such kinetically trapped actin bundle networks, as they are formed e.g. by filamin or α-actinin, are investigated. A detailed characterization of actin/filamin networks reveals that the architecture of the branched bundle networks is given by the timescales of filament formation, elongation and bundling rather than by the cross-linker concentration. The insensitivity of the network structure towards the filamin concentration is reflected in the mechanical properties; in the bundle regime, a saturation of the non-linear viscoelastic properties with respect to the filamin concentration is observed. Only at very low shear rates, where a reorganization of the cross-linking proteins in the bundle can be expected to be possible, an increased filamin concentration results in a higher non-linear elasticity. The non-equilibrium nature of actin/filamin and actin/α-actinin bundle networks allows to irreversibly alter their structure by applying external forces. This results in a unique mechanical response to cyclic loads: if the networks are repeatedly sheared to a certain strain amplitude, they not only exhibit a softening at low deformations but surprisingly demonstrate a drastic increase of the non-linear elasticity which is reached near the maximal applied strain. The microscopic origin of this mechano-memory is identified by a combination of macrorheology and confocal microscopy, which allows to visualize the network during the shearing procedure. Cyclic loading is found to cause structural reorganizations that encode the maximal applied strain into the network architecture and account for the observed cyclic hardening behavior. Whereas cyclic hardening as observed here for kinetically trapped actin bundle networks has never been reported for any polymer system before, shape memory alloys surpisingly show a phenomenologically similar behavior.

Recent studies indicate that cells locally change the intracellular pH to tune the properties of actin binding proteins, and by that regulate cytoskeletal processes. Yet, it is still completely unclear, how a variation of pH affects structural and mechanical properties of cross-linked actin assemblies. Here, it is shown that the bundling propensity of filamin itself is hardly pH dependent. However, the rates of actin nucleation and filament elongation are both dependent on pH, resulting in a shift of the timescales which determine the aggregation controlled growth process of actin/filamin networks. This in turn results in an increase of the mesh size with increasing pH. The pH dependence of the network architecture goes along with a strong and complex pH dependence of the mechanical properties of the actin/filamin networks. It is shown that not only actin/filamin networks can be tuned via pH, but each type of cross-linking protein results in a characteristic pH dependence: the drastic pH dependence observed for actin networks in the presence of cortexillin-I can be traced back to the pH dependent bundling activity of cortexillin. On the other hand, the cross-linking protein fascin is shown to suppress even the intrinsic pH dependence of pure actin solutions. Finally, the pH dependence of the molecular motor myosin-II is shown to result in a pH dependent contractility of actomyosin systems. Using different cross-linking proteins with different pH dependencies

allows to adjust the pH range where contraction is observed. These findings suggest that cells can employ transient local variations of the intracellular pH to specifically modify distinct cross-linked actin structures.

The results described in this thesis suggest that *in vivo* cross-linking proteins not only provide mechanical stability but also fulfill important tasks as regulators of the cytoskeleton: As an example, the stabilizing effect of cross-linking proteins allows to directly couple the structure of an actin assembly with its internal dynamics. Moreover, it has been shown that cross-linked actin structures can passively adapt to mechanical forces, and triggering effects such as changes in pH will affect actin structures according to the present cross-linking proteins. *In vitro* studies with reconstituted systems are a powerful tool to identify potential cytoskeletal regulation mechanisms. In order to reveal how these mechanisms are actually employed by cells, future studies will have to increase the complexity of the reconstituted systems, e.g. by including additional regulatory proteins and physical constraints such as spatial confinement. At the same time, the regulatory mechanisms which are reconstituted in these systems will have to be directly compared with the processes that are occuring in the cytoskeleton of a living cell.

Contents

1 Introduction **1**

2 Materials and Methods **5**
2.1 Proteins . . . 5
2.1.1 Actin . . . 5
2.1.1.1 Covalently labeled actin . . . 6
2.1.1.2 Visualizing actin with labeled phalloidin . . . 6
2.1.2 Cross-linking and bundling proteins . . . 7
2.1.2.1 HMM . . . 7
2.1.2.2 Fascin . . . 8
2.1.2.3 Filamin . . . 8
2.1.2.4 α-actinin . . . 8
2.1.2.5 Cortexillin-I . . . 8
2.1.2.6 Anillin . . . 9
2.1.3 Other actin binding molecules . . . 9
2.1.3.1 Myosin-II . . . 9
2.1.3.2 Tropomyosin . . . 9
2.1.3.3 Cofilin . . . 9
2.1.3.4 Gelsolin . . . 10
2.1.3.5 Latrunculin B . . . 10
2.2 Microscopy . . . 10
2.2.1 Fluorescence microscopy . . . 10
2.2.2 Confocal microscopy . . . 11
2.3 Macrorheology . . . 11
2.3.1 Confocal rheology . . . 12
2.3.2 Surface effects in the non-linear rheology of biopolymer networks . 12

3 Steady state dynamics of actin filaments: Fragmentation is a crucial process **17**
3.1 Theoretical background . . . 18
3.1.1 Single-stranded polymer in thermal equilibrium . . . 18
3.1.1.1 Length distribution . . . 18
3.1.1.2 Fragmentation and annealing . . . 20

3.1.2 Single-stranded polar polymer in steady state . . . 20
3.2 Steady state dynamics of actin filaments directly visualized by fluorescence microscopy . . . 22
3.3 Phosphate release of a steady state F-actin ensemble . . . 27
3.4 Steady state dynamics are even slower at physiological salt concentrations 29
3.5 Discussion . . . 31

4 Slow down of actin depolymerization by cross-linking molecules 33
4.1 Fascin and HMM slow down LatB induced depolymerization of actin . . . 34
4.2 ABPs slow down LatB induced depolymerization . . . 37
4.3 ABPs slow down depolymerization induced by dilution . . . 39
4.4 ABPs slow down disintegration of actin networks induced by cofilin . . . 40
4.5 Simultaneous use of molecular motors and cofilin disrupts bundled actin networks . . . 40
4.6 Stabilization by cross-linking molecules is a generic effect . . . 42
4.7 Outlook on quantitative models . . . 45
4.8 Discussion . . . 47

5 Actin/Filamin Networks 49
5.1 Structure of actin/filamin networks . . . 51
5.2 Viscoelastic response of actin/filamin networks . . . 55

6 Cyclic hardening in actin bundle networks 61
6.1 Mullins effect . . . 62
6.2 Cyclic hardening in actin networks bundled by α-actinin . . . 64
6.3 Memory effect in actin networks bundled by α-actinin . . . 65
6.4 Structural reorganizations account for cyclic hardening . . . 65
6.5 Stepwise shearing of actin networks bundled by α-actinin . . . 68
6.6 Cyclic hardening is sensitive to network architecture . . . 70
6.7 Cyclic hardening in actin networks bundled by filamin . . . 73
6.8 Cyclic hardening – a unique property of actin bundle networks . . . 74
6.9 Analogy to shape memory alloys . . . 75
6.9.1 Shape memory alloys . . . 76
6.9.2 Cyclic hardening in actin bundle networks and shape memory alloys 78

7 pH modulates actin network mechanics in multiple ways 81
7.1 Actin/filamin networks exhibit a complex pH dependence . . . 82
7.2 The bundling activity of cortexillin is pH dependent . . . 84
7.3 Fascin suppresses the pH dependence of F-actin solutions . . . 86
7.4 HMM shows a pH dependent cross-linking activity . . . 87
7.5 Contractility of cross-linked active actin systems can be tuned via pH . . . 88

7.6 pH as a potential regulator of cross-linked actin structures in cells 91

8 Outlook **93**

Bibliography **97**

List of Figures **113**

1 Introduction

The cytoskeleton is a complex system, consisting of only a few types of proteins that are able to assemble into polymeric structures and a myriad of additional auxiliary proteins which organize these biopolymers in space and time. One of the most prominent of the cytoskeletal polymers is actin, which is essential for numerous cellular functions, ranging from cell locomotion to cell division. Despite decades of thorough investigation, it is far from understood how cells manage to precisely orchestrate their actin cytoskeleton. Even basic principles such as the intrinsic dynamics of actin filaments are still subject of controversial debate [Kueh et al., 2008, Li et al., 2009, Jégou et al., 2011]. A sound physical understanding of cytoskeletal processes is often impeded by their overwhelming complexity: one major obstacle is the fact that numerous – maybe even unknown – proteins are often simultaneously involved in fulfilling a certain task, makes it hard to unambiguously identify the function of a particular type of cytoskeletal protein. One way to overcome this dilemma is to study reconstituted *in vitro* systems, where type and concentration of the proteins as well as the buffer conditions are well defined [Bausch and Kroy, 2006]. This bottom-up approach has already been used extensively to study the role of actin cross-linking and bundling proteins [Lieleg et al., 2010, Stricker et al., 2010]. In cells, this broad class of proteins serves to locally arrange actin filaments into well defined geometries and to provide their mechanical stability. The cross-linking proteins often build up stable, bundle-like actin structures, which persist for a long period of time. Obviously, cross-linking proteins maintain the structural integrity of these assemblies by keeping the actin filaments together. On the other hand, cross-linking proteins provide mechanical stability also in rather dynamic actin systems such as the actin lamellipodium [Small et al., 2002], where the individual filaments exhibit a fast turn-over [Bugyi and Carlier, 2010]. It is still elusive how cells manage that only the particular actin filaments in the more static structures are specifically protected from the regulatory proteins that accelerate the internal actin dynamics. It has been speculated that cross-linking proteins could contribute to this task, which would drastically extend their function as regulators of the actin cytoskeleton [Tilney et al., 2003, Rzadzinska et al., 2005]. Along that line, although *in vitro* studies have identified regulatory proteins which can disassemble actin filaments, it is still unclear how their function is modified

by the presence of cross-linking proteins and whether they can be utilized by cells to disintegrate highly cross-linked or bundled actin structures if they are not needed any more. To address this questions, *in vitro* experiments are needed, which focus on the effect cross-linking proteins have on the intrinsic actin dynamics, and unravel the interplay of cross-linking proteins and proteins which have their major role as regulators of the actin dynamics.

In vitro experiments have shed light on the mechanical properties of cross-linked actin networks and how they correlate with the network architecture. However, while many studies focused on the equilibrium properties of such networks, little is known about their dynamic formation process. Only recently it turned out that even comparably simple reconstituted actin systems consisting of actin and a single type of cross-linking protein (e.g. filamin or α-actinin) can form non-equilibrium structures [Schmoller et al., 2008b, Lieleg et al., 2009b, Lieleg et al., 2011]: Their formation process results in networks that are kinetically trapped in a metastable, glass-like state. The potential non-equilibrium character of cytoskeletal networks has strong implications for our understanding of how cells regulate the architecture of actin structures. The state of a kinetically trapped network depends on the network history, which can be expected to complicate the challenge for cells to precisely control the actin assemblies. On the other hand, the intrinsic non-equilibrium character of cross-linked actin assemblies is also a powerful mechanism that can be employed by cells to build different structures with identical constituents. Yet, it is still an open question which parameters set the structural and mechanical properties of a non-equilibrium actin network – and by which means they can be tuned to modify the resulting network.

In this thesis an *in vitro* approach is applied to study cross-linked and bundled actin networks on different length scales (Fig. 1.1). Chapter 1 and 2 focus on the intrinsic dynamics of individual actin filaments and address the question how they are modified by the presence of different cross-linking proteins. It will be shown that cross-linking proteins not only stabilize actin assemblies on a mesoscopic length scale by maintaining their structural integrity but also on the level of individual filaments by slowing down their intrinsic dynamics and protecting them from depolymerization factors. In chapter 3 confocal microscopy and macrorheology are used to investigate how the aggregation controlled growth process of kinetically trapped actin/filamin networks is reflected in the resulting network architecture and the macroscopic mechanical properties. Finally, in chapter 4 and 5 it will be demonstrated that the non-equilibrium character of such actin bundle networks allows to tune the structural and mechanical network properties by applying external forces or a variation of pH.

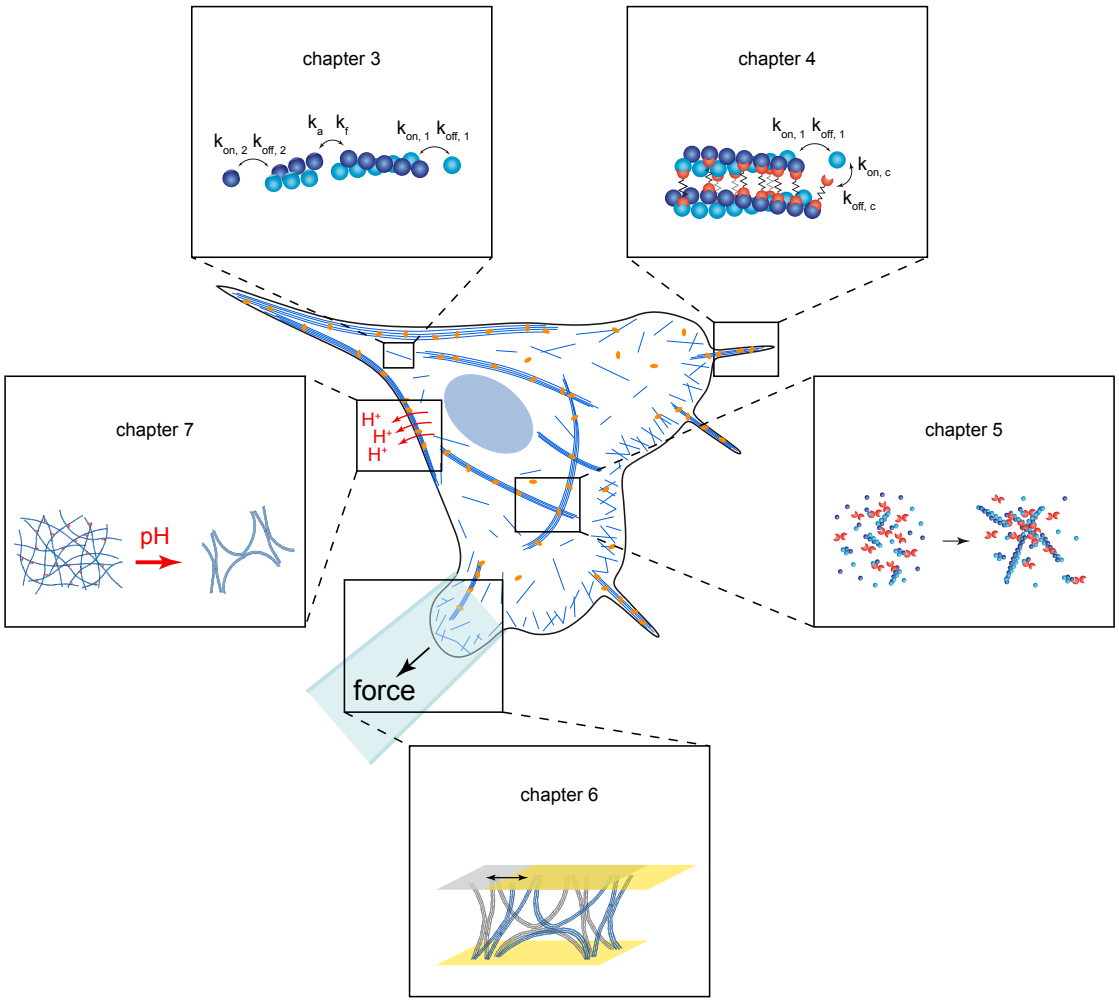

Figure 1.1: Cross-linking proteins fulfill multiple functions by regulating actin assemblies on different levels, ranging from individual filaments to macroscopic networks. In chapter 3 of this thesis, it is shown that spontaneous fragmentation plays a major role in the internal dynamics of an ensemble of steady state actin filaments. In chapter 4 it is investigated how cross-linking and bundling proteins affect the depolymerization of actin filaments. The structural and mechanical properties of kinetically trapped actin bundle networks are studied in chapter 5. Chapter 6 demonstrates that the structure and the mechanical response of such networks can be tuned by cyclic loading. In chapter 7 it is studied how a variation of pH affects actin networks cross-linked by different types of cross-linking proteins.

2 Materials and Methods

2.1 Proteins

2.1.1 Actin

In eukaryotic cells, the globular 42-kDa protein actin is abundant and fulfills numerous tasks. In its polymerized form it not only is an essential part of the contractile elements in muscle cells, but also is one of the three major biopolymers of the cytoskeleton. Here, G-actin is obtained from rabbit skeletal muscle by a modified protocol of [Spudich and Watt, 1971], where an additional gel filtration (Sephacryl S-300 HR) step is done [MacLean-Fletcher and Pollard, 1980]. The actin is stored in lyophilized form at -21 °C [Spudich and Watt, 1971]. The G-actin solution is prepared by dissolving lyophilized actin in deionized water and dialyzing against G-buffer (pH 8; 2 mM TRIS, 0.2 mM ATP, 0.2 mM $CaCl_2$, 0.2 mM DTT and 0.005 % NaN_3) at 4 °C. The G-actin solution is kept at 4 °C and used within two weeks. Polymerization is initiated in the presence of the respective actin binding proteins by addition of 10 % volume of different 10x polymerization buffers. A low salt 10x polymerization-buffer(pH 7.5; 20 mM TRIS, 20 mM $MgCl_2$, 2 mM DTT, 5 mM ATP) is used in chapter 3. $CaCl_2$ is added such that a final concentration of 0.2 mM is reached. For phosphate release measurements lower concentrations of ATP are used such that including the ATP in the G-buffer a total concentration of $\approx 175 - 290$ µM ATP is obtained. A standard 10x F-buffer (pH 7.5; 20 mM TRIS, 5 mM ATP, 20 mM $MgCl_2$, 2 mM $CaCl_2$, 1 M KCl, 2 mM DTT) is used in chapter 4, 5 and 6. In chapter 4, F-buffer without ATP is used for actin/rigor-HMM networks. For the actin/filamin networks polymerized in the presence of myosin II a different 10x polymerization buffer (pH 7.2; 100 mM Imidazol, 30 mM $MgCl_2$, 2 mM $CaCl_2$, 0.05 % NaN_3) is used. In chapter 7, 10x-AB-buffer with different pH values (40 mM $MgCl_2$, 10 mM EGTA, 10 mM ATP, 20 mM DTT, 250 mM KCl (no KCl was used for macroscopic contraction assays) and 250 mM MES for pH 4.8-6.5, Imidazole for pH 6.5-7.5 or TRIS for pH 7.5-9) are used. In the case of actin/cortexillin and actin/filamin networks, additional cortexillin buffer (see section 2.1.2.5) or filamin buffer (pH 7.5; 20 mM TRIS, 250 mM KCl, 0.5 mM EDTA and 0.5 mM DTT) is added to be comparable to the highest cross-linker concentration. For contraction experiments, an ATP regeneration system

consisting of 20 mM creatine phosphate and 0.1 mg/ml creatinephosphokinase (Sigma) and additional buffer of the respective cross-linking proteins are added: The cross-linking proteins anillin, filamin and α-actinin are diluted in filamin buffer to a concentration fivefold higher than the final concentration in the sample. Cortexillin is diluted in cortexillin buffer to the twofold of the final concentration. Fascin is diluted in fascin buffer (pH 8; 2 mM TRIS, 150 mM KCl) to the fivefold of the final concentration. In the case of pure actin/myosin-II systems either 20 % filamin or fascin buffer or 50 % cortexillin buffer is added to ensure comparable buffer conditions. No significant difference between these conditions is observed. In Fig. 7.7B only the data obtained with cortexillin buffers, respectively are shown. After sample preparation a part of the sample is used to measure the actual pH of the sample using a microelectrode (Schott instruments).

2.1.1.1 Covalently labeled actin

For fluorescence microscopy experiments which address the internal dynamics of actin filaments (as performed in chapter 3 and chapter 4), actin is labeled with the amine-reactive dye Alexa Fluor 555 carboxylic acid succinimidyl ester (Invitrogen A20009) or with Atto 488-NHS ester (Sigma Aldrich 41698). For this purpose, G-actin is dialyzed against Borat-buffer (pH 8; 50 mM boric acid, 0.2 mM $CaCl_2$, 0.2 mM ATP). After polymerization induced by addition of 10 % of polymerization buffer (pH 7.2; 100 mM Imidazol, 10 mM ATP, 30 mM $MgCl_2$, 2 mM $CaCl_2$, 0.05 % NaN_3) the dye (dissolved in DMSO) is added in 1-2 fold molar excess. After centrifugation the pellet is resuspended in G-buffer and dialyzed against G-buffer. The sample is clarified by centrifugation and the supernatant is stored in lyophilized form at -21 °C. A degree of labeling of $\approx 14 - 25$ % for Alexa Fluor 555 and ≈ 125 % for Atto 488 is achieved.

For pyrene assay experiments, actin is labeled with pyrene by a modification of the method of [Kouyama and Mihashi, 1981] as described in [Cooper et al., 1983].

2.1.1.2 Visualizing actin with labeled phalloidin

Phalloidin is a small actin binding molecule, which stabilizes actin filaments against depolymerization and by that also inhibits the internal dynamics of actin filaments. For fluorescence microscopy experiments which do not address the internal dynamics, actin can be visualized using labeled phalloidin. By this, a better contrast than by covalent labeling can be obtained. In this work, Alexa 488-phalloidin (Invitrogen) (chapter 3, 7), phalloidin-TRITC (Sigma-Aldrich) (chapter 5) and Atto 488 phalloidin (Invitrogen) (chapter 6) is used.

2.1.2 Cross-linking and bundling proteins

Actin binding proteins which simultaneously bind two actin filaments can arrange actin filaments into different geometries. Using numerous types of such cross-linking proteins enables cells to build highly diverse structures which are specifically tailored for certain tasks. Although a lot effort has been put into understanding how different cross-linking proteins tune the architecture of actin assemblies [Lieleg et al., 2009b], the critical parameters which determine the effect of a specific cross-linking protein remain rather elusive. Reprensentative confocal images of actin bundle networks as formed by bundling proteins studied in this thesis are shown in Fig. 2.1. In order to allow a meaningful comparison of the effect of different cross-linking proteins, in this thesis concentrations of cross-linking proteins which act as dimers are given as the dimer concentrations. Since the effect of a certain concentration of cross-linking protein strongly depends on the actin concentration, it is often useful to use the molar ratio between the actin binding protein (ABP) and actin, $R_{\mathrm{ABP}} = c_{\mathrm{ABP}}/c_{\mathrm{a}}$, to characterize the system.

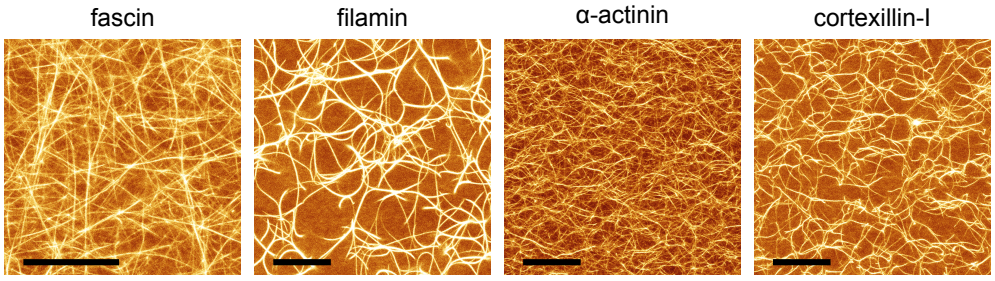

Figure 2.1: Representative images (maximum projections of confocal z-stacks) of actin networks bundled by different cross-linking proteins. The scale bars denote 20 µm.

2.1.2.1 HMM

Heavy meromyosin (HMM) is the larger fragment ($\approx$ 350 kDa) obtained from myosin II by chymotrypsin digestion as described by [Uhde et al., 2004]. HMM is still working as a molecular motor, but in contrast to the full myosin II does not assemble into filaments. In the absence of ATP it cross-links and decorates actin filaments. In contrast to all other actin cross-linking proteins used in this thesis, HMM does not induce bundling even if present at very high concentrations. This makes actin/HMM networks an ideal model system to study properties of point-to-point cross-linked actin filaments [Tharmann et al., 2007].

2.1.2.2 Fascin

Fascin is a monomeric 55 kDa cross-linking protein that in filopodia and filopodia-like structures contributes to the formation of actin bundles [Vignjevic et al., 2006]. *In vitro*, fascin cross-links actin at low concentrations and at higher concentrations induces the formation of polar, hexagonally packed, individual bundles, which are limited to a size of about 20 actin filaments [Claessens et al., 2008]. Here, recombinant human fascin is prepared by a modification of the method of [Ono et al., 1997] as described by [Vignjevic et al., 2003].

2.1.2.3 Filamin

Filamin is a huge actin binding protein (the dimer has a size of $\approx$ 560 kDa) which not only cross-links cortical actin filaments and links them to the cell membrane, but also plays an important role as a signaling molecule [Stossel et al., 2001, Feng and Walsh, 2004]. *In vitro*, filamin induces the formation of kinetically trapped, curved and branched bundle networks [Schmoller et al., 2008b]. Here, muscle filamin is isolated from chicken gizzard and further purified as reported in [Shizuta et al., 1976].

2.1.2.4 α-actinin

α-actinins have multiple functions ranging from anchoring actin filaments in the Z-disc of muscles to the formation of cytoskeletal actin bundles such as stress fibres. *In vitro*, the 215 kDa dimeric α-actinin similar to filamin forms out-of-equilibrium bundle networks [Lieleg et al., 2009b]. Here, α-actinin is isolated from turkey gizzard smooth muscle following [Craig et al., 1982], dialyzed against G-buffer and stored at 4 °C for several weeks.

2.1.2.5 Cortexillin-I

Cortexillin-I forms a dimer (101 kDa) with actin binding sites of the α-actinin/spectrin type, that bundles actin into non-polar bundles and is enriched in the cortex of locomoting cells [Faix et al., 1996]. Recombinant *Dictyostelium discoideum* cortexillin-I (gift from G. Gerisch, Max Planck Institute of Biochemistry, Germany) is purified from *E.coli* BL21-CodonPlus-RP using a C-terminal His_6-Tag [Faix et al., 1996]. Cortexillin-I is stored at -80 °C in cortexillin buffer (pH 8; 20 mM TRIS, 100 mM NaCl, 4 mM $CaCl_2$ and 2 mM DTT).

2.1.2.6 Anillin

In vitro, anillin forms branched bundle networks [Kinoshita et al., 2002]. *In vivo* it serves as a scaffold protein that is able to link myosin and actin [Kinoshita et al., 2002]. Here, an anillin fragment is used, that can be purified in E.coli, but still bundles F-actin and contains the non-muscle myosin II. The fragment of *Xenopus laevis* anillin spanning amino acids 1-428 [Kinoshita et al., 2002] is cloned into pET-28a and purified from *E. coli* with His-tags on both termini. Anillin 1-428 is stored in 25 mM imidazole pH 6, 25 mM KCl, 4 mM $MgCl_2$, 1 mM EGTA, 1 mM DTT) at -80 °C.

2.1.3 Other actin binding molecules

2.1.3.1 Myosin-II

Myosins are a large family of ATP dependent motor proteins, which "walk" along actin filaments. Myosin-II (or conventional myosin) is the most prominent subfamily, with muscle myosin-II being responsible for force generation in muscle cells [Howard, 2001]. Non-muscle myosin-II is essentially involved in fundamental cellular processes, such as cell division and cell migration. Here, muscle myosin-II is purified from rabbit skeletal muscle as reported in [Uhde et al., 2004].

2.1.3.2 Tropomyosin

Tropomyosin is an actin binding protein that decorates actin filaments in muscles by spanning 7 actin subunits. In the absence of calcium, tropomyosin blocks the myosin binding site of actin and by that regulates muscle contraction. Tropomyosin troponin is prepared from the residue of rabbit muscle acetone powder left after the actin extraction [Spudich and Watt, 1971] and separated into tropomyosin and troponin by hydroxyl apatite column chromatography [Eisenberg and Kielley, 1974].

2.1.3.3 Cofilin

Cofilin is a major regulator of actin filament dynamics. By severing actin filaments it can either promote disassembly or assembly (by creating new actin barbed ends) of actin networks. Here, *dictyostelium discoideum* cofilin is expressed as a GST fusion protein in E.Coli DH5alpha cells. The GST tag is removed by cleavage with the factor Xa and cofilin is stored in cofilin buffer (pH 8; 10 mM TRIS, 0.2 mM $CaCl_2$, 0.2 mM DTT).

2.1.3.4 Gelsolin

Gelsolin is an actin binding protein that severs and caps actin filaments. It can be used to control the average length of actin filaments because the ratio of actin monomers to gelsolin monomers scales with the filament length over a wide range of filament lengths [Janmey et al., 1986]. However, this relation obviously holds true only for actin filament lengths shorter than the average filament length in the absence of gelsolin. Gelsolin can therefore not be used to adjust the average actin filament length to a value larger than the average length of pure F-actin, which is in the order of ≈ 5 µm (chapter 3). Gelsolin is obtained from bovine plasma serum following [Kurokawa et al., 1990]. In chapter 5 small amounts of gelsolin (1 gelsolin per 7770 actin molecules) have been added. Representative regions of the actin/filamin phase space have also been tested without gelsolin, but no significant change in the structural state diagram (Fig. 5.3) has been observed.

2.1.3.5 Latrunculin B

Latrunculin B is a small molecule that binds G-actin in a one-to-one stoichiometry and by that prevents polymerization of the sequestered actin monomers. Latrunculin B (Sigma-Aldrich) dissolved in DMSO (5 mM) is stored at -20 °C. Prior to use, it is diluted to 500 µM in G-buffer without ATP.

2.2 Microscopy

While bright field microscopy allows to observe only strongly bundled actin filaments, fluorescence microscopy is ideally suited to visualize reconstituted actin systems. Confocal microscopy can be used to obtain three dimensional information about the network architecture. However, due to thermal fluctuations individual actin filaments in an F-actin solution are hardly observable with a confocal microscope and are therefore better studied with an epifuorescence microscope. Taking time lap videos allows for a distinction between single filaments and bundles. If not stated otherwise, all microscopy experiments are performed at room temperature.

2.2.1 Fluorescence microscopy

Fluorescence microscopy data are acquired on a Zeiss Axiovert 200 inverted microscope using a 100x oil immersion objective with a numerical aperture of 1.4. In chapter 4, for

actin/filamin bundle networks a 25x oil immersion objective with a numerical aperture of 0.8 is used.

2.2.2 Confocal microscopy

Confocal images are taken with a Leica TCS SP5 point-scanning confocal microscope (Leica, Wetzlar, Germany).

2.3 Macrorheology

Macrorheology is well suited to study the mechanical properties of reconstituted actin systems both in the limit of small deformations (i.e the linear regime) as well as in the non-linear regime at high deformations. In contrast to microrheological techniques which measure the mechanical response on a microscopic length scale, macrorheology typically probes on a length scale which is large compared to the characteristic length scales of the sample [Bausch and Kroy, 2006, Kasza et al., 2007]. Yet, in this thesis, in the case of strongly bundled actin networks the characteristic length scales of the sample can exceed the gap distance, which is the smallest dimension in the macrorheology setup and experimentally limited to the order of $\approx$ 100 µm. The persistence length of actin bundles can reach millimeters [Claessens et al., 2006]. In addition, in the case of actin bundled by filamin or α-actinin the network geometry even gives rise to bundles percolating from one plate to the other. Note that the resulting mesoscopic character of the "macrorheology" technique could lead to a dependence of the measured mechanical properties on the gap distance, as already observed for collagen networks [Arevalo et al., 2010].

Here, a stress-controlled rheometer (Physica MCR 301, Anton Paar, Graz, Austria) is used to measure the viscoelastic response of reconstituted actin networks. Actin polymerization is initiated by addition of 10 % volume of the respective 10x polymerization buffer. Approximately 450 µl sample volume is immediately loaded into the rheometer using a 50 mm plate-plate geometry with 160 µm plate separation. Actin polymerization is carried out *in situ* to guarantee the integrity of the network. To ensure a full polymerization of the network, polymerization is followed by recording the elastic modulus over time. To ensure a linear response and avoid mechanical disruption of the network only small torques (0.5 µNm) are applied. The mechanical response in the linear regime is characterized by measuring the frequency dependent viscoelastic moduli $G'(f)$ and $G''(f)$ over three orders of magnitude from 10 mHz to 10 Hz. To obtain a better resolution, measurements are taken in the constant strain mode. A suitable strain, which results in

small torques ($\approx$ 0.5 µNm) is determined from the polymerization curve. The non-linear response is probed by applying a constant shear rate.

2.3.1 Confocal rheology

Whereas macrorheology is perfectly suited to measure the macroscopic mechanical properties of biopolymer systems, it provides no information about their structural properties. Numerous studies have used microscopy techniques to gain structural information in independent experiments and then correlate the structure of the material with its macromechanical response [Lieleg et al., 2009b]. This approach is sufficient in the case of equilibrium structures which are exposed only to small deformations during the macrorheological experiment. However, it has strong limitations in cases where the microscopic structure of the material is expected to change during the experiment – especially if this structural change is induced by the experimental procedure itself, as it can be the case during non-linear rheological experiments. To overcome this dilemma, simple shear cells have been used to obtain structural information of the sheared state [Liu et al., 2007, Kang et al., 2009]. Yet, since the mechanical response of biopolymer networks can be very sensitive to the actual experimental conditions, and large sample to sample variations are possible, it would be ideal to directly visualize a biopolymer network during the macrorheological experiment.

To this end, a confocal rheometer – a setup that combines a commercial macrorheometer with a confocal microscope – has been realized in the lab of Prof. Daniel Blair (Georgetown University, Washington DC) and is used here to obtain the data presented in chapter 6. The confocal rheometer consists of a modified Anton Paar MCR 301 stress-controlled rheometer, which is coupled to a Leica TCS SP5 point-scanning confocal microscope. Here, a 25 mm cone-plate geometry is used. The metal cone is rinsed with H_2O and wiped ten times prior to use. A fresh glass cover slip which has been rinsed with H_2O is used as lower plate. For the cyclic hardening procedures applied to actin bundle networks in chapter 6, strain is controlled. After upward and downward shearing with constant shear rate, strain is kept at 0 % in the pauses between the cycles. Similarly, strain is kept constant in the pauses of stepwise shear experiments. The confocal-rheometer coupling allows to image three-dimensional volumes of the network over time while simultaneously applying a precisely controlled shear strain.

2.3.2 Surface effects in the non-linear rheology of biopolymer networks

In chapter 6 the confocal rheometer will be used to reveal the microscopic origin of the unique response of actin/α-actinin and actin/filamin bundle networks to cyclic shearing.

It will be shown that high strains mainly result in rupturing of actin bundles from the surface – rather than rupturing of the bundle-bundle interconnections. This raises the question whether strain induced rupturing of the network from the surface is a phenomenon which is specific for such bundle networks with a large mesh size, or a generic effect occuring if biopolymer networks are sheared to large strains. In the latter case, it can be expected to have severe implications for our understanding of the non-linear rheology of biopolymer systems. Although for macrorheological experiments the attachment of the network to the surface is typically provided only by unspecific interactions, for the interpretation of the measured mechanical response potential rupture events during nonlinear deformations have been neglected so far.

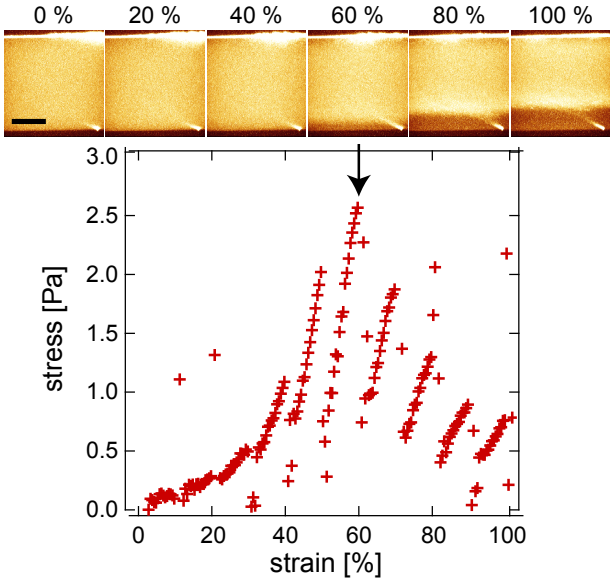

Figure 2.2: Confocal rheology is used to observe the response of an actin solution (c_a = 9.5 µM) at room temperature to a stepwise shearing protocol. A shear rate of 10%/s is used, and between the steps of 10% the strain is kept constant for 120 s. During this waiting times confocal z-stacks are taken. The images shown here are maximum x-projections of 144.6 µm. The scale bar denotes 50 µm. The confocal images reveal that the strain where the maximum stress is reached roughly correlates with the strain where the actin solution ruptures from the (lower) surface.

Confocal rheology can be used to test whether rupturing from the surface is also critically involved in determining the non-linear mechanical response of pure F-actin solutions. A stepwise shearing protocol is applied in order to allow confocal imaging during the waiting times. As shown in Fig. 2.2, the response of the actin solution to stepwise shearing is qualitatively similar to a shear experiment with a constant shear rate [Semmrich et al., 2008]. Although the stress drastically relaxes during the waiting times due to the strong viscoelastic character of the F-actin solution, it demonstrates a clear strain hardening behavior. While the measured stresses are similar to what is observed in a simple shear experiment, the strain where the maximum stress is reached is significantly lower in the stepwise shearing experiment. However, the fact that the

overall response is qualitatively similar suggests that information about the role of the surface obtained from the stepwise shearing protocol can be transfered to experiments with a constant shear rate.

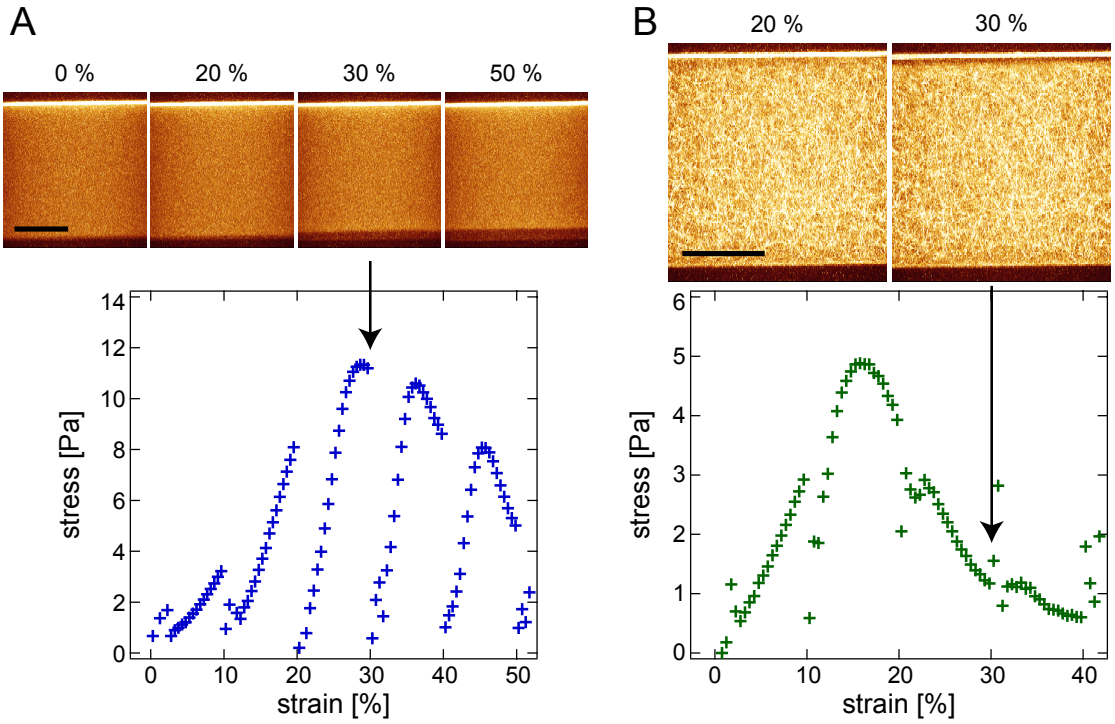

Figure 2.3: Stepwise shearing (protocol as described in Fig. 2.2) of actin networks (c_a = 9.5 µM) at room temperature in the presence of 0.475 µM HMM (A) or 0.95 µM fascin (B). The confocal images are maximum x-projections of 144.6 µm. The scale bars denote 50 µm.(A): In the case of the actin/HMM network, the maximum stress is roughly reached at the strain where the network ruptures from the (lower) surface. (B): In the case of the actin/fascin network, rupturing of the network from the (upper) surface becomes obvious at a strain which is larger than the strain where the maximum stress is reached.

Confocal imaging reveals that roughly at the strain where the maximum stress is reached, the fluorescently labeled actin solution ruptures from the surface. The rupturing occurs collectively at least on the length scale of ≈ 100 µm which is experimentally accessible here. However, since the stress is not drastically decreasing at a distinct strain, it can be expected that the rupturing is not collective on the length scale of the whole sample (centimeters). In contrast, it is likely that at different positions in the sample the rupturing occurs at different strains and either from the upper or the lower surface. Such a step by step rupturing can explain the continuous decrease of the measured stress

over a large range of strain.

As shown in Fig. 2.3A, a similar behavior is also observed for actin networks cross-linked by HMM. Again, the rupturing of the network from the surface correlates with reaching the maximal stress. In the case of the actin/fascin bundle network shown in Fig. 2.3B, rupturing becomes obvious at a strain which is significantly higher than the strain where the maximal stress is reached. However, it is still possible that the network ruptured already at lower strains at other positions in the sample.

Future studies have to address the question how rupturing of the network from the surfaces affects the measured non-linear macrorheological response. This can be achieved by repeating the experiments to obtain statistical information about the distribution of strains at which the network ruptures. Variation of the stepsize would help to get a better strain resolution and to unravel the effect of the exact shearing protocol. However, already the preliminary experiments presented here demonstrate that surface effects play a major role for the non-linear mechanical response of various types of actin networks as measured with macrorheology. The fact that rupturing of the networks has not been observed at lower strains where the maximal stress has not been reached yet, suggests that in this regime rupturing plays a minor role. Interpreting the non-linear response at these lower strains without taking rupturing from the surface into accout – as done by many previous studies [Tharmann et al., 2007, Semmrich et al., 2007, Lieleg and Bausch, 2007, Schmoller et al., 2008a, Kasza et al., 2009] and also in this thesis (in chapter 5 and 7) – is therefore most probably valid. Yet, at higher strains rupturing from the surface might even dominate the mechanical response and account for the decrease of the stress as a function of strain. In this regime surface effects definitely have to be considered.

3 Steady state dynamics of actin filaments: Fragmentation is a crucial process

The dynamics of actin filaments play a crucial role in many cellular processes, including cell motility and cell division [Carlier and Pantaloni, 2007]. *In vivo*, treadmilling of actin filaments – an ATP driven continuous lengthening at one end of the filament which is balanced by a shortening at the other – is utilized by cells for force generation. In *in vitro* experiments, actin-turn-over driven movement of bacteria or beads has been reconstituted using actin and various actin binding proteins [Loisel et al., 1999, Bernheim-Groswasser et al., 2002]. The underlying process – steady state treadmilling of pure actin filaments – has already been suggested more than 30 years ago [Wegner, 1976]. Measurements of the relevant association and dissociation rates at both filament ends have been used to estimate the turn-over rate [Wegner, 1976, Pollard and Mooseker, 1981, Pollard, 1986]. Labeling of actin monomers with radioactive [Wegner and Neuhaus, 1981] or fluorescent dyes [Pardee et al., 1982] as well as isotopic labeling [Simpson, 1980, Pardee et al., 1982] have provided direct evidence for the ATP-dependent exchange of actin monomers in polymerized steady state actin. Additional information has been obtained by measuring the continuous phosphate release during steady state [Asakura and Oosawa, 1960, Korn et al., 1987]. Total internal reflection microscopy allows following the polymerization and depolymerization of single actin filaments [Fujiwara et al., 2002, Kuhn and Pollard, 2005, Fujiwara et al., 2007, Kueh et al., 2008]. Indeed, treadmilling of selected individual filaments has been observed [Fujiwara et al., 2002]. On the other hand, single filament experiments revealed new puzzling features of actin dynamics: unexpected fast diffusive length fluctuations [Fujiwara et al., 2002, Kuhn and Pollard, 2005] as well as switching between different depolymerization rates [Kueh et al., 2008, Kueh and Mitchison, 2009] have been observed. Our understanding of actin dynamics is additionally limited since ATP hydrolysis in actin filaments is still not completely understood [Bugyi and Carlier, 2010] and only little is known about spontaneous fragmentation and annealing [Wegner, 1982, Erickson, 1989, Sept et al., 1999, Fass et al., 2008] – although fragmentation is suggested to be a crucial process for actin turn-over *in vivo* [Berro et al.,

2010].

In this chapter, the steady state dynamics of an ensemble of actin filaments are studied by a novel, but simple approach: Investigating the time evolution of the length distribution of labeled actin reporter filaments in an unlabeled F-actin solution reveals that a process which is dependent on the filament length plays a major role in the dynamics of a steady state F-actin solution. The decay length of the exponential length distribution of visible filaments is found to decrease with time. Since treadmilling or diffusive length fluctuations cannot account for such behavior, spontaneous fragmentation, which can be expected to show at least a linear dependence on the filament length, and annealing are major dynamic processes in pure actin solutions. Nevertheless, the determined ATPase activity indicates the presence of treadmilling dynamics, which influence the steady state dynamics.

3.1 Theoretical background

Although actin filaments are extremely complex polymers, which are still far from understood, already very simple models can help to understand basic features of the internal dynamics of an ensemble of actin filaments.

3.1.1 Single-stranded polymer in thermal equilibrium

3.1.1.1 Length distribution

The simplest model for a polymer of proteins is a single-stranded chain consisting of identical subunits [Howard, 2001], with association and dissociation rates of the monomeric subunits to the polymer that do not depend on the length of the filament (Fig. 3.1). This model obviously does not take into account major features of actin filaments, such as the polarity, the double-stranded helical structure of actin filaments and the fact that association and dissociation rates at both ends depend on the nucleotide state of the G-actin molecule. However, in the following it will be shown that the single-stranded polymer model, also referred to as the Einstein polymer, is sufficient to reproduce the exponential length distribution observed for an ensemble of actin filaments [Kawamura and Maruyama, 1970].

In thermal equilibrium, every chemical reaction is balanced by its reverse reaction. For the addition of a monomer A_1 to a polymer A_N consisting of N subunits,

$$A_N + A_1 \underset{k_{\text{off}}}{\overset{k_{\text{on}}}{\rightleftharpoons}} A_{N+1} \ , \tag{3.1}$$

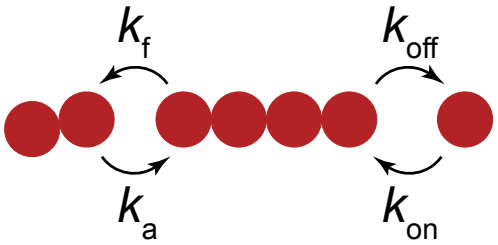

Figure 3.1: The Einstein polymer is a single-stranded chain that consists of identical subunits. The association and dissociation rates k_{on} and k_{off} are assumed to be independent of the filament length.

this gives

$$\frac{[\mathrm{A}_N][\mathrm{A}_1]}{[\mathrm{A}_{N+1}]} = \frac{k_{\text{off}}}{k_{\text{on}}} . \tag{3.2}$$

Here, $[\mathrm{A}_N]$ denotes the concentration of polymers with a length of N subunits. k_{on} and k_{off} denote the association and dissociation rate, respectively. Rewriting equation 3.2 and substituting $N+1$ by N gives

$$[\mathrm{A}_N] = [\mathrm{A}_{N-1}][\mathrm{A}_1]\frac{k_{\text{on}}}{k_{\text{off}}} . \tag{3.3}$$

Equation 3.3 can now be solved by recursive substitution:

$$[\mathrm{A}_N] = [\mathrm{A}_{N-1}][\mathrm{A}_1]\frac{k_{\text{on}}}{k_{\text{off}}} = [\mathrm{A}_{N-2}][\mathrm{A}_1]^2(\frac{k_{\text{on}}}{k_{\text{off}}})^2 = \ldots = [\mathrm{A}_1]^N(\frac{k_{\text{on}}}{k_{\text{off}}})^{N-1} . \tag{3.4}$$

This solution can be rewritten as an exponential length distribution

$$[\mathrm{A}_N] = C\mathrm{e}^{-\frac{N}{N_0}} , \tag{3.5}$$

with $C = \frac{k_{\text{off}}}{k_{\text{on}}}$ and $N_0 = -\frac{1}{\ln(\frac{k_{\text{on}}}{k_{\text{off}}})}$. One main assumption in the simple Einstein polymer model is that the dissociation constant $K_{\text{D}} = \frac{k_{\text{off}}}{k_{\text{on}}}$ is independent of the filament length. Because the entropy loss of a monomer binding to a long polymer is higher than that of a monomer binding to a short polymer, in reality the dissociation constant increases as a function of polymer length. However, this effect is expected to be rather small [Howard, 2001], and the fact that an exponential length distribution is indeed observed for actin filaments suggests that it can be neglected.

3.1.1.2 Fragmentation and annealing

Because in thermal equilibrium every reaction is balanced by its reverse reaction, annealing of two filaments with lengths of N_1 and $N - N_1$ subunits is balanced by spontaneous fragmentation. With the annealing rate k_a and the fragmentation rate k_f (Fig. 3.1), the annealing reaction

$$\mathrm{A}_{N_1} + \mathrm{A}_{N-N_1} \underset{k_\mathrm{f}}{\overset{k_\mathrm{a}}{\rightleftharpoons}} \mathrm{A}_N \tag{3.6}$$

gives

$$\frac{[\mathrm{A}_{N_1}][\mathrm{A}_{N-N_1}]}{[\mathrm{A}_N]} = \frac{k_\mathrm{f}}{k_\mathrm{a}} \,. \tag{3.7}$$

Substituting the concentrations in equation 3.7 with the solution obtained in equation 3.4 directly gives

$$\frac{k_\mathrm{f}}{k_\mathrm{a}} = \frac{k_\mathrm{off}}{k_\mathrm{on}} \,. \tag{3.8}$$

The dissociation constant $K_\mathrm{D} = \frac{k_\mathrm{off}}{k_\mathrm{on}}$ is independent of the filament length. Thus, equation 3.8 implies that the fragmentation constant $K_\mathrm{F} = \frac{k_\mathrm{f}}{k_\mathrm{a}}$ is equal for every position in the polymer and for every polymer length. In the Einstein polymer model, the individual rates in equation 3.8 are constants. Therefore, although equation 3.8 has been derived assuming thermal equilibrium, it holds true also in a non-equilibrium situation. The result obtained here for the Einstein model makes clear that also for more complicated systems, the length dependence of the fragmentation constant will be directly linked to the length dependence of the dissociation constant. As a consequence, for modeling attempts the length dependence of fragmentation and annealing rates should not be chosen seperately, as done e.g. by [Sept et al., 1999], but in addition to a physical motivation of the individual rates it has to be assured that the model is overall consistent.

3.1.2 Single-stranded polar polymer in steady state

In contrast to the Einstein polymer introduced in section 3.1.1, actin filaments are polar filaments with different association and dissociation rates at their two ends. Moreover, these rates depend on the nucleotide state of the actin subunit. In combination with hydrolyzation of ATP-actin to ADP-actin within the filament, this results in the steady state process called treamilling, where the filament preferentially polymerizes ATP-actin at the barbed end, while depolymerizing ADP-actin from the pointed end.

The simplest model for a steady state actin filament is a *polar* Einstein polymer. In steady state, the concentrations of actin monomers with different nucleotide states do not change. As suggested in [Edelstein-Keshet and Ermentrout, 1998], this allows to assume constant effective association and dissociation rates at both ends and define the overall effective rates

$$k_{\text{on}} \;=\; k_{\text{on}}^{\text{barbed}} \;+\; k_{\text{on}}^{\text{pointed}} \tag{3.9}$$

$$k_{\text{off}} \;=\; k_{\text{off}}^{\text{barbed}} \;+\; k_{\text{off}}^{\text{pointed}} \;. \tag{3.10}$$

Assuming that the polymers grow and shrink only by addition or dissociation of monomers (i.e. neglecting annealing and fragmentation events) gives the differential equation

$$\frac{\mathrm{d}[\mathrm{A}_N]}{\mathrm{d}t} \;=\; k_{\text{off}}[\mathrm{A}_{N+1}] \;-\; (k_{\text{off}} \;+\; [\mathrm{A}_1]k_{\text{on}})[\mathrm{A}_N] \;+\; k_{\text{on}}[\mathrm{A}_1][\mathrm{A}_{N-1}] \;. \tag{3.11}$$

In steady state, the length distribution does not change over time, which gives

$$0 \;=\; k_{\text{off}}[\mathrm{A}_{N+1}] \;-\; (k_{\text{off}} \;+\; [\mathrm{A}_1]k_{\text{on}})[\mathrm{A}_N] \;+\; k_{\text{on}}[\mathrm{A}_1][\mathrm{A}_{N-1}] \;. \tag{3.12}$$

It can easily shown that equation 3.12 is solved by

$$[\mathrm{A}_N] \;=\; [\mathrm{A}_1]^N(\frac{k_{\text{on}}}{k_{\text{off}}})^{N-1} \;, \tag{3.13}$$

which is the same exponential length distribution as obtained for the equilibrium Einstein polymer before (equation 3.4).

As shown in this section, simple models are sufficient to rationalize the exponential length distribution observed for F-actin solutions. However, while the models can be used to motivate the physical origin of observed effects, the drastic oversimplifications of the models impedes reliable predictions. As an example, it is still completely unclear how the fragmentation rate depends on the filament length and the position in the filament. While the simple models introduced here suggest a single fragmentation constant $K_{\text{F}} \;=\; \frac{k_{\text{f}}}{k_{\text{a}}}$, the different nucleotide states of the actin subunits in the filament could result in strong dependence on the position in the filament. Since such basic properties of actin filaments are still elusive, experiments are of avail that unravel the fundamental features of actin filaments which have to be known to successfully model their behavior.

3.2 Steady state dynamics of actin filaments directly visualized by fluorescence microscopy

In steady state, the growing of filaments by step by step association of monomers and annealing is balanced by dissociation of protomers and spontaneous fragmentation. Thus, the investigation of the individual effects requires an experimental method which allows for separation of the processes causing filament growth from the ones causing filament shrinkage. One such experiment is mixing covalently labeled actin reporter filaments with an unlabeled F-actin solution and following the apparent length distribution of visible filaments over time via fluorescence microscopy (Fig. 3.2): While the overall length distribution of actin filaments is constant due to steady state, spontaneous fragmentation, length fluctuations as well as treadmilling cause shortening of the visible filaments. Processes which result in lengthening of the filaments are hidden in this approach, as they are dominated by the incorporation of unlabeled monomers into the originally labeled filaments. As spontaneous fragmentation, length fluctuations and treadmilling have qualitatively different effects on the length distribution of visible filaments, such an experiment should reveal the dominating process and therefore provide new insights into the steady state dynamics of an ensemble of actin filaments.

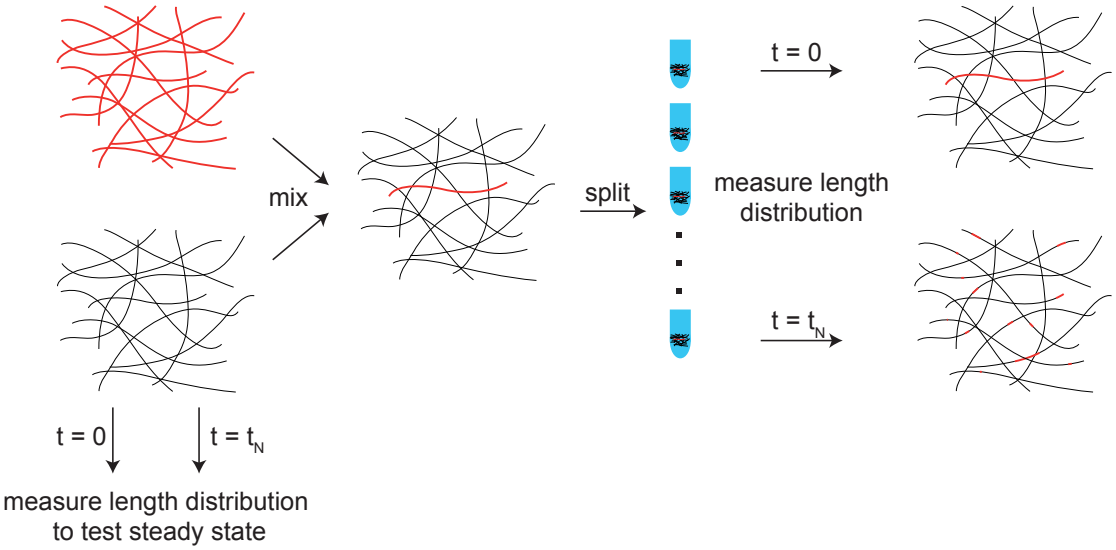

Figure 3.2: (A) Illustration of the experiment: labeled and unlabeled actin filaments are polymerized separately for 3 hours at 10 µM. Labeled actin reporter filaments are mixed with a 300 fold excess of unlabeled F-actin. The sample is splitted each time and a new aliquot is used to measure the length distribution of labeled filament fragments.

Labeled and unlabeled actin filaments are polymerized separately for 3 hours at a total actin concentration of 10 µM. In order to exclude dye specific effects, experiments are performed with Alexa Fluor 555 as well as with Atto 488 labeled actin. As a first control, the length distribution of unlabeled actin filaments is measured after 3 hours of polymerization and 50 hours later by staining with labeled phalloidin directly before observation (Fig. 3.3).

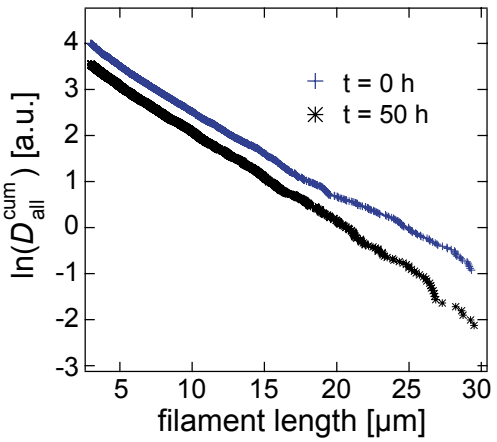

Figure 3.3: The length distribution of unlabeled actin is measured after 3 hours of polymerization and 50 hours later after subsequent labeling with Alexa 488-phalloidin. No significant change can be observed suggesting that the system has reached steady state.

For this purpose, 2 µL of the sample are pipetted on a microscope slide and covered with a cover slip. By this, filaments are roughly oriented in the horizontal plane. Videos are taken above the lower surface. In order to obtain length distributions, a gliding average of 5 images as well as a gaussian blur is applied, background subtraction is done with ImageJ and a treshold which is adjusted globally for the whole time series is used to create a binary image. Using the MATLAB R2007a function *regionprops*, interconnected objects with an area larger than 20 pixels are substituted by an ellipse that has the same normalized second central moments as the region, and the major axis length is used as a measure for filament length. Distributions are obtained from minimal 40 images and are shown only for lengths larger than 20 pixels (3 µm). Qualitatively similar results are obtained if the number of pixels within an interconnected object is used as a measure for filament length. As expected (section 3.1) an exponential length distribution is found at both points of time, which is best seen by computing the complementary cumulative length distribution. The decay length λ_{all} of the complementary cumulative distribution $D^{\mathrm{cum}}_{\mathrm{all}}(x) = \int_x^\infty D_{\mathrm{all}}(x')dx' = A^{\mathrm{cum}}_{\mathrm{all}} \cdot e^{-\frac{x}{\lambda_{\mathrm{all}}}}$ is equal to the decay length of the exponential length distribution $D_{\mathrm{all}}(x) = A_{\mathrm{all}} \cdot e^{-x/\lambda_{\mathrm{all}}}$. The prefactor is given by $A^{\mathrm{cum}}_{\mathrm{all}} = A_{\mathrm{all}} \cdot \lambda_{\mathrm{all}}$. Consistent with [Sept et al., 1999], the length distribution does not significantly change within 50 hours (Fig. 3.3). This indicates that on the experimental time scale all processes

which affect the filament length distribution are balanced and a steady state is reached already during the 3 hours of polymerization.

To visualize the dynamic processes occuring during steady state labeled filaments are mixed with a 300 fold excess of unlabeled filaments after 3 hours of polymerization. The sample is splitted such that for each observation a new aliquot can be used to measure the length distribution of visible filaments $D_{\mathrm{vis}}(x)$ (Fig. 3.2). This procedure guarantees the avoidance of any artifacts by bleaching and filament fragmentation induced by the observation process. Directly prior to observation, actin is stabilized with unlabeled phalloidin.

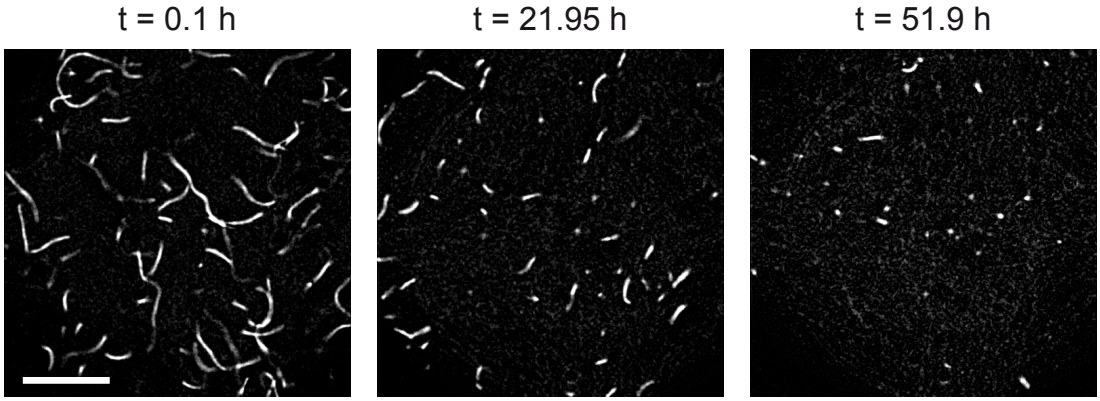

Figure 3.4: Typical fluorescence images (background subtracted, brightness adjusted) of labeled actin filaments mixed with unlabeled filaments are shown for three points of time during the experiment shown in Fig. 3.5A. Each time, a new aliquot of the sample is used in order to avoid artifacts due to observation. Obviously, the lengths of the visible filaments decrease over time. The scale bar denotes 20 µm.

Figure 3.4 shows typical fluorescence images taken during the experiment. Obviously, the length of the visible filaments decreases over time, indicating that a dynamic exchange between the labeled and unlabeled filaments occurs. Over the whole time course of the experiment, the complementary cumulative length distribution of visible filaments is well described by a single exponential, i.e. $D^{\mathrm{cum}}_{\mathrm{vis}}(x,t) = A^{\mathrm{cum}}_{\mathrm{vis}}(t) \cdot e^{-\frac{x}{\lambda_{\mathrm{vis}}(t)}}$ (Fig. 3.5A). The decay length $\lambda_{\mathrm{vis}}(t)$ – and thus the average visible filament length – significantly decreases over time (Fig. 3.5C). The initial decay length is found to be $\lambda_{\mathrm{vis}} \approx 4.3$ µm and it decreases to $\lambda_{\mathrm{vis}} \approx 1.1$ µm after 52 hours. This corresponds to an increase of the prefactor of the non-cumulative length distribution $A_{\mathrm{vis}}(t) = A^{\mathrm{cum}}_{\mathrm{vis}}(t)/\lambda_{\mathrm{vis}}(t)$ over time (Fig. 3.5D).

This finding is in sharp contrast to what would be expected, if treadmilling was the dominant process. For the rather long filaments observed in the experiment, the turn-

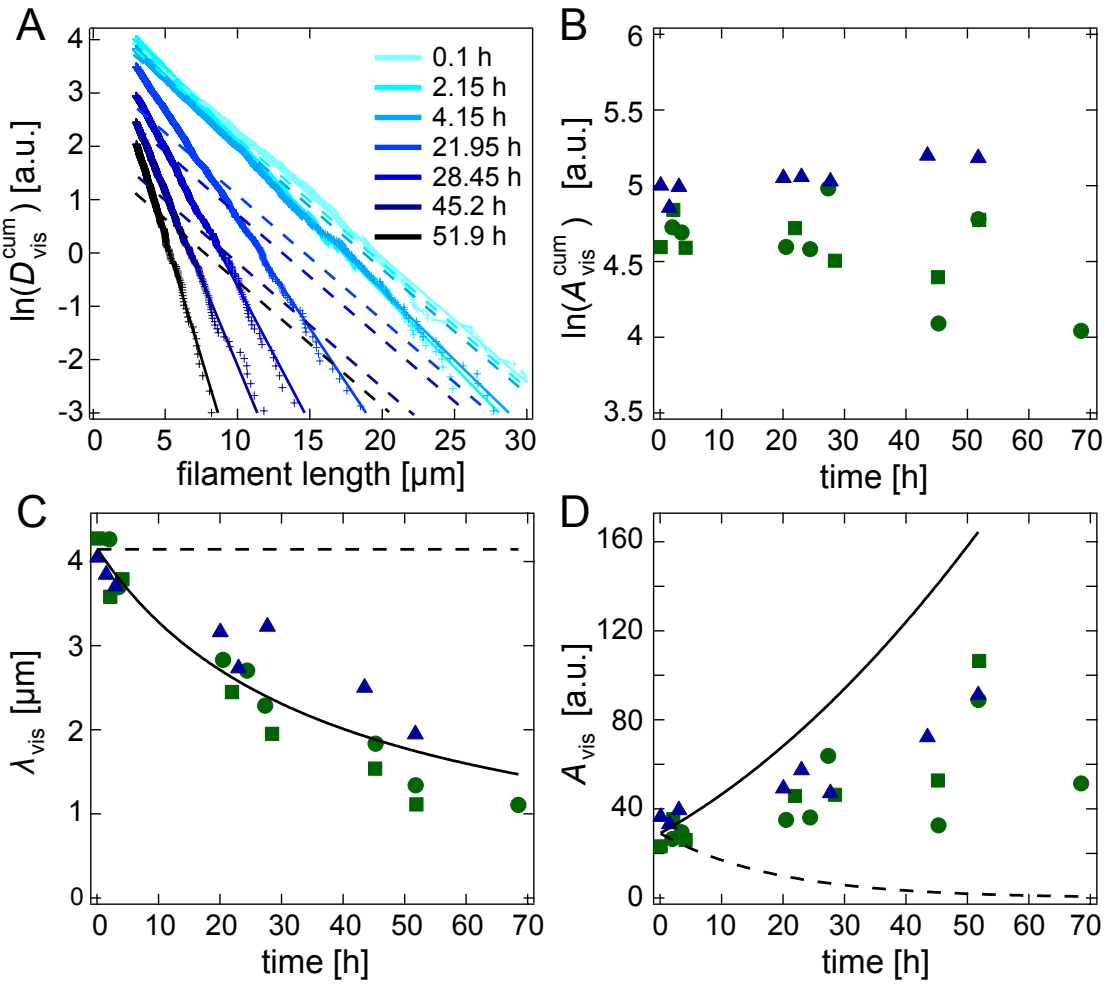

Figure 3.5: (A) The time evolution of the complementary cumulative length distribution $D_{\mathrm{vis}}^{cum}(x,t)$ of Alexa Fluor 555 labeled actin filaments (33 nM) in an unlabeled F-actin solution (10 µM) is shown. Solid lines show exponential fits $D_{\mathrm{vis}}^{cum}(x,t) = A_{\mathrm{vis}}^{cum}(t)e^{-x/\lambda_{\mathrm{vis}}(t)}$. Dashed lines show the evolution of the initial exponential distribution as expected if just treadmilling with a turn-over rate of 0.23 µm/h is considered. The natural logarithm of the prefactor $A_{\mathrm{vis}}^{\mathrm{cum}}(t)$ (B) and the decay length $\lambda_{\mathrm{vis}}(t)$ (C) of the exponential fit functions to the complementary cumulative length distributions as well as the prefactor of the non-cumulative length distribution $A_{\mathrm{vis}}(t) = A_{\mathrm{vis}}^{\mathrm{cum}}(t)/\lambda_{\mathrm{vis}}(t)$ (D) are shown as a function of time for three independent experiments, where actin has been labeled with Alexa Fluor 555 (green, squares and circles) or Atto 488 (blue, triangles). Solid lines in (C) and (D) show a simple fragmentation model assuming a local fragmentation rate k_0 which is independent of the position in the filament and the filament length (equation (3.15)). The value of $k_0 = 6.4 \cdot 10^{-3}$ h^{-1} µm^{-1} is obtained from a best fit to $\lambda_{\mathrm{vis}}(t)$ (C). Dashed lines show the time evolution as expected if just treadmilling with a turn-over rate of 0.23 µm/h is considered.

over rate, as well as diffusive length fluctuations, can be expected to be independent of the filament length. In consequence, the length distribution would be uniformly shifted to shortened filaments, which is manifested in a decrease of the prefactor $A_{\rm vis}(t)$ but a constant decay length $\lambda_{\rm vis}(t)$. Thus, the observation of a decreasing decay length $\lambda_{\rm vis}(t)$ demonstrates that a major process has to depend on the filament length. One such process is spontaneous fragmentation.

In the simplest model, spontaneous fragmentation occurs with the same probability at any site between actin protomers [Wegner, 1982]. This results directly in a linear dependence of the filament fragmentation rate on the filament length. Since filaments consist of many subunits, they can be described as continuous objects, breaking at random positions with the rate $k_0 \mathrm{d}x$. Neglecting in a first approximation association and dissociation of monomers, the length distribution of the visible parts of filaments $D_{\rm vis}(x,t)$ can be described by the master equation

$$\partial_t D_{\rm vis}(x,t) = -k_0 x D_{\rm vis}(x,t) + 2k_0 \int_x^\infty dx' D_{\rm vis}(x',t) \ . \tag{3.14}$$

The first term describes that a visible segment with length x vanishes when it breaks with rate $k_0 x$. The second term describes that additional visible segments with length x are created when longer filaments with length $x' > x$ break into two fragments with lengths x and $x'-x$. With the initial exponential distribution $D_{\rm vis}(x, t=0) = A_0 e^{-x/\lambda_0}$, the solution of this equation is given by

$$D_{\rm vis}(x,t) \ = \ A_0 \cdot (1+k_0\lambda_0 t)^2 \cdot e^{-\frac{x(1+k_0\lambda_0 t)}{\lambda_0}} \ . \tag{3.15}$$

The reverse process, filament annealing, has not to be accounted for, since there is a 300 fold excess of unlabeled filaments and thus annealing events between two labeled filaments are extremly rare. Moreover, in the fragmentation model used here, the total length of the filaments, including invisible parts, does not play a role for the fragmentation rate of the labeled parts. Indeed, the observed decrease of the decay length $\lambda_{\rm vis}(t)$ – which is not affected by length independent processes, not accounted for here – can be fitted by this fragmentation model (Fig. 3.5C). The resulting local rate of spontaneous fragmentation $k_0 \ = \ 6.4 \cdot 10^{-3}$ h^{-1} µm^{-1} – corresponding to $k_0 \ = \ 4.8 \cdot 10^{-9}$s^{-1} per F-actin protomer – is surprisingly similar to the value of $k_0 \ = \ 1 \cdot 10^{-8}$s^{-1} as estimated by [Erickson, 1989] from polymerization experiments performed by [Wegner, 1982] at higher salt concentrations and higher temperature than used in this study. Very similar values are also suggested by other studies [Kinosian et al., 1993b, Sept et al., 1999]. Using the values obtained for k_0 and $\lambda_0 \ = \ 4.2$ µm from the fit of $\lambda_{\rm vis}(t)$ and setting $A_0 \ = \ 29$ a.u.

to calculate the expected time evolution of $A_{\mathrm{vis}}(t)$, shows that the model overestimates the increase of $A_{\mathrm{vis}}(t)$ (Fig. 3.5D). This overestimation can be rationalized by the fact that treadmilling and diffusive length fluctuations have been neglected. These processes result in a decrease of $A_{\mathrm{vis}}(t)$ as long as the ends of the labeled filaments have not annealed with unlabeled filaments. On the other hand, the deviation might also indicate that the local fragmentation rate is not completely independent of the filament length resulting in nonlinear fragmentation and annealing rates.

3.3 Phosphate release of a steady state F-actin ensemble

In order to test if fragmentation is indeed the dominant process accounting for the dynamics of an F-actin solution, an independent estimation of the turn-over rate is of avail. Calculating the turn-over rate from literature values is difficult, since association and dissociation rates for ATP, ADP-Pi and ADP-actin at the barbed and the pointed end have to be known. In addition, most literature values are obtained from polymerization experiments and thus might differ from steady state rates [Kueh et al., 2008]. Therefore a direct measurement of the turn-over rate would be preferable. Protomers involved in treadmilling eventually release their bound γ-phosphate [Melki et al., 1996]. Thus, an upper bound for the turn-over rate of actin filaments can be estimated by measuring the phosphate release of the system. In order to exclude that labeling significantly alters the rate of ATP hydrolysis, both fluorescently labeled actins which are used in this study, namely Alexa Fluor 555 labeled actin and Atto 488 labeled actin are investigated in addition to unlabeled actin. The EnzCheck phosphate assay (Invitrogen) [Webb, 1992] is used to monitor the release of inorganic phosphate by polymerized actin. To measure the phosphate release as a function of time, the desired number of samples equalling the number of data points in the time series are mixed contemporaneously and polymerized for one hour. 0.2 mM MESG substrate and 1 % volume of 100 U/ml stock solution PNP is added and incubated for 30 minutes. A spectrum is recorded at 24°C with a PerkinElmer Lambda 25 spectrometer. The increase of the absorbance at 360 nm as a function of time is translated to the phosphate release using a calibration curve measured in the presence of F-actin. As shown in Fig. 3.6A, for 10 µM actin, phosphate is released with rates between 0.54 µM/h and 0.92 µM/h. The difference of the values obtained for different types of actin is not larger than the difference between two independent measurements of the same type of actin. Thus, within the experimental error, labeling has no influence on the rate of ATP hydrolysis. From the measured phosphate release rate it can be estimated that most G-actin molecules have bound ATP: ADP-actin is expected to exchange its nucleotide to ATP on the timescale of minutes [Kinosian et al., 1993a].

Since the critical concentration is on the order of one µM [Pollard, 1986] and less than one µM phosphate is released per hour, the nucleotide exchange can be expected to be fast enough to guarantee that most G-actin molecules have bound ATP.

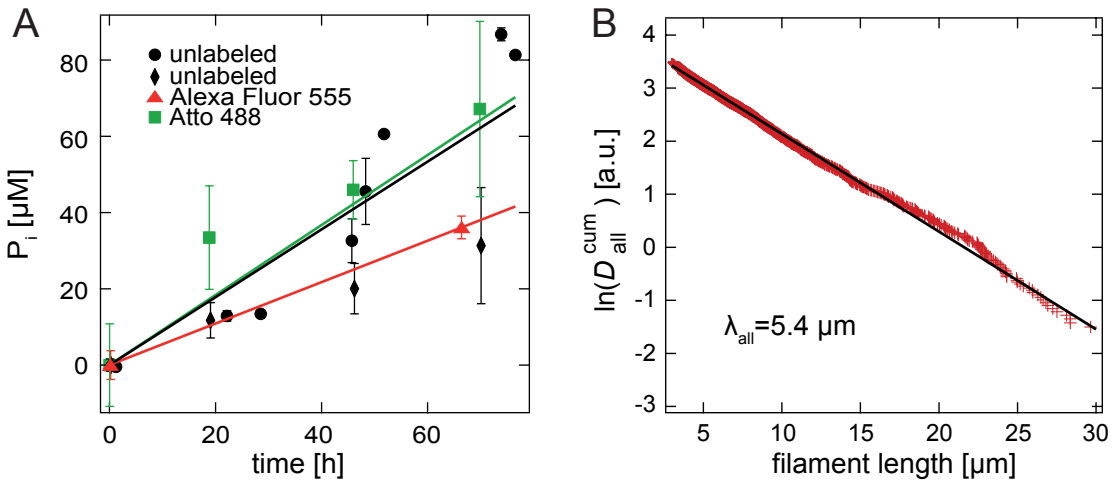

Figure 3.6: (A) The concentration of phosphate released by 10 µM steady state F-actin is shown as a function of time: Two independent series of measurements are performed for unlabeled actin (black circles and diamonds). Actin labeled with Alexa Fluor 555 (red triangles) or Atto 488 (green squares) is tested in order to exclude labeling artifacts. Error bars show the standard deviation for 1 to 6 data points measured at the respective points of time. Solid lines show fits assuming constant phosphate release rates for each type of actin. The two series of experiments with unlabeled actin are fitted globally and a rate of 0.89 µM/h is obtained. 0.54 µM/h and 0.92 µM/h are obtained for Alexa Fluor 555 labeled actin and Atto 488 labeled actin, respectively. (B) In order to correlate the measured phosphate release rate with a turn-over rate, the total number of F-actin filaments is needed. For this purpose, unlabeled F-actin is polymerized and subsequently labeled with Alexa 488-phalloidin, and the complementary cumulative length distribution is measured. In order to minimize the experimental error due to variations between different actin preparations, the same actin preparation as used for one of the phosphate release measurements shown in (A) (black circles) has been used to measure the length distribution of actin filaments.

In order to calculate the ATP hydrolysis rate per filament, the total number of actin filaments has to be determined from the length distribution of filaments and the F-actin concentration. Here, the length distribution of the unlabeled actin used for the phosphate assay is determined with fluorescence microscopy after labeling with Alexa 488-phalloidin (Invitrogen) (Fig. 3.6B), and a similar distribution as shown in Fig. 3.3 is found. If this exponential length distribution $D_{\mathrm{all}}(x) = A_{\mathrm{all}} \cdot e^{-x/\lambda_{\mathrm{all}}}$ with $\lambda_{\mathrm{all}} = 5.4$ µm is assumed to be valid also at filament lengths shorter than 3 µm, the concentration of filaments can be calculated to be $n_{\mathrm{all}} = \int D_{\mathrm{all}}(x)dx = A_{\mathrm{all}} \cdot \lambda_{\mathrm{all}}$. As the critical

concentration is small compared to the total actin concentration, the total length of actin filaments is given by the overall actin concentration times the length per protomer, $\int x \cdot D_{\mathrm{all}}(x)dx = A_{\mathrm{all}} \cdot \lambda_{\mathrm{all}}^2 = 10\ \mu\mathrm{M} \cdot 2.7\mathrm{nm}$, the prefactor A_{all} can be determined and a filament concentration of $n_{\mathrm{all}} = 5$ nM results. As 10 µM actin hydrolyse 0.89 µM ATP per hour (Fig. 3.6), the upper bound for the turn-over rate is 0.48 µm/h which corresponds to 0.05 protomers per second. From analogous calculations using the respective initial decay lengths of the measurements shown before (Fig. 3.5), upper bounds for the turn-over rates of 0.23 µm/h for Alexa Fluor 555 labeled actin and 0.37 µm/h for Atto 488 labeled actin are obtained. Using the turn-over rate obtained for Alexa Fluor 555 labeled actin, the change of the length distribution of visible filaments in an unlabeled network which would be expected if only treadmilling occurs, can be calculated: The exponential fit function of the initial distribution is simply shifted by 0.23 µm/h $\times$ t (dashed lines in Fig. 3.5A). As shown in Fig. 3.5C and D, $\lambda_{\mathrm{vis}}(t)$ would stay constant while $A_{\mathrm{vis}}(t)$ would decrease exponentially. Still the expected effect is in the same order of magnitude as the observed changes attributed to spontaneous fragmentation. Thus, treadmilling could significantly contribute to the time evolution of the labeled filaments and could therefore account for the deviation of the observed increase of $A_{\mathrm{vis}}(t)$ over time from what is expected from the pure fragmentation model.

The assumption of a single exponential length distribution even for short filament lengths below 3 µm is not indisputable: The double exponential decay of depolymerization curves measured with a pyrene assay has been suggested to indicate a double exponential length distribution [Wendel and Dancker, 1986]. A higher number of short filaments than expected from a single exponential length distribution would result in an underestimation of the filament concentration and thus an overestimation of the turn-over rate. Nevertheless, a lower treadmilling rate would also be consistent with the result that spontaneous fragmentation is a crucial process in the dynamics of a steady state F-actin solution. However, in this case other processes have to account for the fact that $A_{\mathrm{vis}}(t)$ increases more slowly than expected from spontaneous fragmentation with a constant local rate of fragmentation.

3.4 Steady state dynamics are even slower at physiological salt concentrations

In this chapter, a low salt polymerization buffer has been used since preliminary experiments with buffers containing additional KCl have shown a drastic slow down of actin dynamics compared to the low salt buffer (Fig. 3.7) as expected from [Pardee et al.,

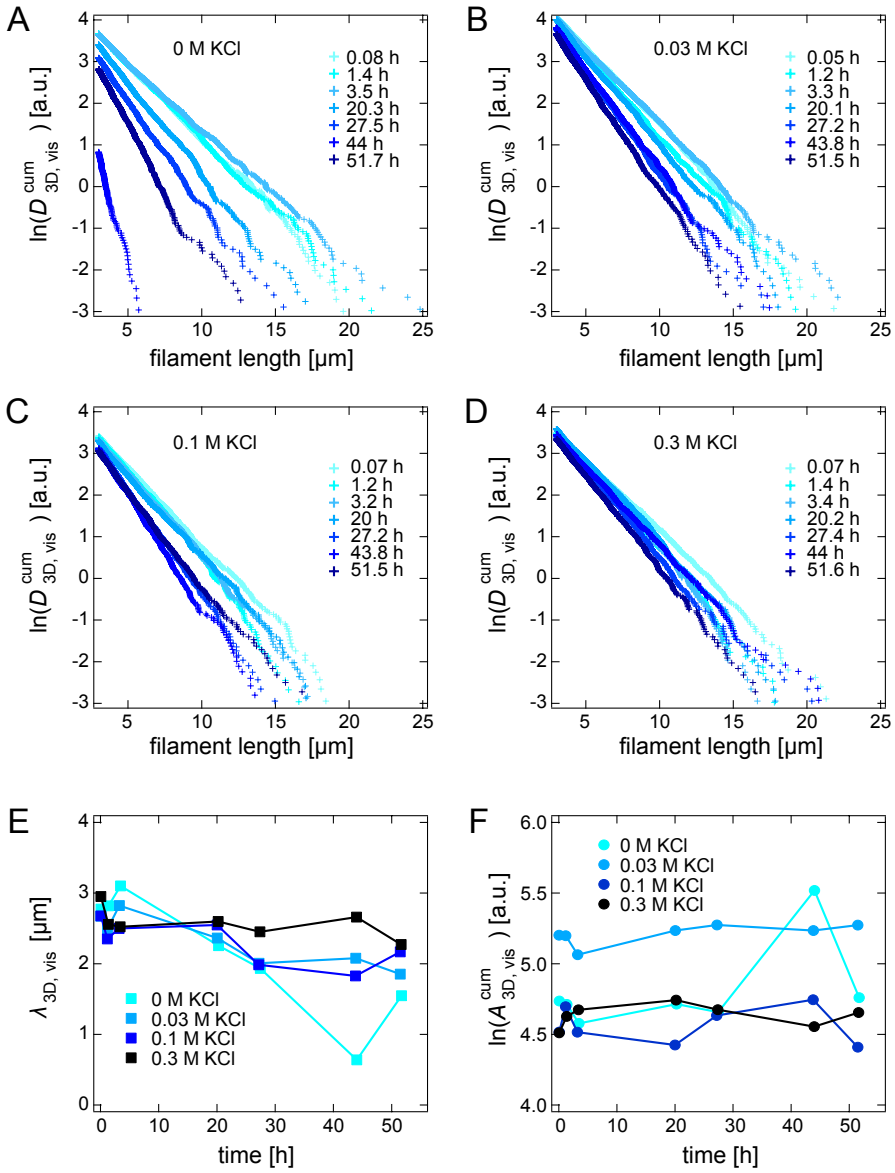

Figure 3.7: (A)-(D): The time evolution of the complementary cumulative length distribution $D^{cum}_{\mathrm{3D,vis}}(x,t)$ of a bulk solution of Alexa Fluor 555 labeled actin filaments (33 nM) in an unlabeled F-actin solution (10 µM) is shown for different KCl concentrations. The decay length $\lambda_{\mathrm{3D,vis}}(t)$ (E) and the logarithm of the prefactor $A^{\mathrm{cum}}_{\mathrm{3D,vis}}(t)$ (F) of the exponential fit functions to the complementary cumulative length distributions are shown as a function of time for different KCl concentrations.

1982]: A change of the length distribution of labeled actin filaments in an unlabeled F-actin solution is hardly resolveable at the more physiological buffer conditions (100 mM KCl), where therefore both treadmilling and spontaneous fragmentation can be expected to occur at slower rates. In contrast to the data shown in Fig. 3.5, where length distributions are obtained from filaments oriented in the xy-plane, the length distributions shown in Fig. 3.7 are obtained from a bulk solution. While 0.2 mM $CaCl_2$ have been used for the measurements shown in Fig. 3.5, 0.07 mM $CaCl_2$ have been used to obtain the data shown in Fig. 3.7.

3.5 Discussion

Following the length distribution of labeled actin filaments in an unlabeled F-actin solution allowed the separation of processes which cause shrinkage of filaments from growth processes, which balance this shrinkage during steady state. It has been shown that, at low salt conditions, treadmilling and diffusive length fluctuations do not dominate the shrinkage of labeled filaments in an unlabeled F-actin solution. In fact, only processes that dependend on filament length – most probably spontaneous fragmentation – can account for the observed decrease of the decay length of the exponential length distribution of visible filaments. Assuming that filaments break with the same probability at any site between actin protomers, the fragmentation rate has been determined to be $k_0 = 4.8 \cdot 10^{-9} \mathrm{s}^{-1}$ per F-actin protomer. As the dynamics of steady state actin are even slowed down at more physiological salt conditions (section 3.4), it can be expected that spontaneous fragmentation does not directly play an important role in *in vivo* processes. However – similar to treadmilling – regulatory proteins can shift the rate of fragmentation to a faster timescale such that it becomes revelant for cytoskeletal processes [Staiger et al., 2009, Berro et al., 2010]. The simple but new experimental approach that has been applied here could also be used to investigate the effect of such regulatory proteins on the steady state dynamics of actin. It might prove useful in future studies due to the fact that e.g. severing rates of proteins such as cofilin [Andrianantoandro and Pollard, 2006] or spire [Sitar et al., 2011] could be determined without inducing artefacts by photodamage or immobilization of filaments to a surface, such as done in a standard TIRF assay.

The results of this chapter highlight that cells need regulatory proteins which accelerate the dynamics of actin filaments to make use of processes such as treamilling and allow for a remodeling of actin networks on reasonable time scales. The effect of proteins which are thought to have their major role as regulators of actin dynamics is in most cases studied in *in vitro* experiments, using only the protein of interest and pure F-actin. However, in

cells actin is typically coexisting with a large number of different actin binding proteins, such as cross-linking proteins. It is thus important to take the next step and use the bottom-up approach to shed light on the interplay of proteins which specifically regulate the actin dynamics and other actin binding proteins which – simply due to their presence – might modify their effect. The following chapter will focus on how cross-linkers affect actin dynamics, and thus alter their steady state.

4 Slow down of actin depolymerization by cross-linking molecules

It is well known that cells make use of actin binding proteins (ABPs) to accelerate the intrinsic dynamics of actin filaments. Considering the extremely slow timescales on which steady state processes such as treadmilling and spontaneous fragmentation play a significant role (see chapter 3), it becomes obvious that an elaborate regulation of actin dynamics is indispensable for cells to harness its inherent potential. While nucleation factors such as the ARP2/3 complex [Mullins et al., 1998] induce the formation of new filaments, capping proteins and actin-depolymerizing factors such as cofilin result in a significant increase of depolymerization and fragmentation dynamics [Carlier, 1998, De La Cruz, 2009]. On the other hand, cells not only need mechanisms to accelerate actin dynamics, but also ways to specifically stabilize certain actin structures against this induced acceleration. One candidate which might fulfill this task are cross-linking proteins: some cross-linking proteins have already been reported to have a stabilizing effect on individual filaments [Zigmond et al., 1992, Cano et al., 1992, Loomis et al., 2003, Lebart et al., 2004]. This seems to be harnessed by cells for the regulation of bundle size *in vivo*: the lack of espin results in inhibition of stereociliary growth followed by progressive degeneration of the hair bundle [Rzadzinska et al., 2005]. Also varying expression levels of fascin in drosophila bristle cells resulted in changes of filament turnover accounting for distinct phenotypes [Tilney et al., 2003]. An overexpression of α-actinin has been shown to cause accumulation of actin filaments and inhibition of actin dynamics [Mukhina et al., 2007]. As such a stabilization of filamentous structures could be an important aspect for cells, it is crucial that filaments are protected against depolymerization factors such as cofilin. Yet, it is still necessary to enable a controlled depolymerization of bundles and filaments, which suggests that additional mechanisms are needed to enable a disintegration of these actin structures.

Despite the importance of the regulation of actin dynamics for many cytoskeletal processes, quantitative investigations of their mediation by cross-linking molecules remain scarce. In this chapter the effect of various cross-linking molecules on actin dynamics will be investigated. Together with Christine Wurm [Wurm, 2011] it is shown that cross-

linking proteins suppress actin depolymerization in a concentration dependent manner. This is a generic effect for all actin binding proteins which simultaneously bind to two F-actin subunits. Moreover, cross-linking proteins even protect actin filaments from disintegration by cofilin. Molecular motors can overcome the stabilization effect: even extremely stable actin bundle structures can be disintegrated by the concerted action of cofilin and myosin-II.

4.1 Fascin and HMM slow down LatB induced depolymerization of actin

Actin depolymerization can be induced by addition of the depolymerization factor latrunculin B (LatB), which sequesters monomeric actin and thus causes a depolymerization at both the barbed and pointed ends. A standard pyrene assay, where the normalized fluorescence intensity $I(t)$ is a measure for the degree of polymerization, allows monitoring of actin depolymerization induced by LatB and is a well established method to study actin depolymerization kinetics [Cooper et al., 1983].

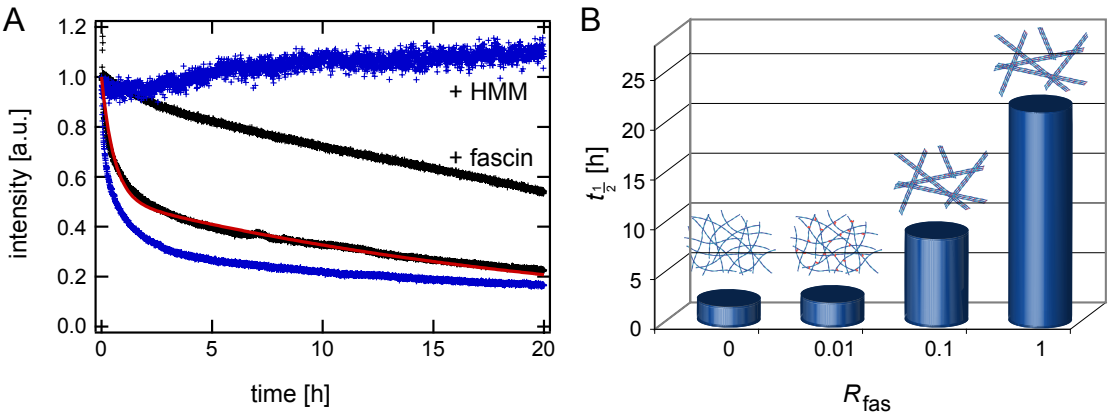

Figure 4.1: A pyrene assay can be used to monitor the depolymerization of cross-linked actin networks induced by LatB: (A): Cross-linking molecules inhibit actin depolymerization. The normalized fluorescence intensity upon addition of 50 µM LatB is shown for actin/fascin ($R_{\mathrm{fas}} = 1$) (black) and actin/rigor-HMM networks ($R_{\mathrm{HMM}} = 1$) (blue) as well as the pure actin solutions in the corresponding buffers (F-buffer with ATP (black); F-buffer without ATP (blue)). The depolymerization of pure actin (F-buffer with ATP) is fitted with a double exponential decay (red). (B): The inhibition of actin depolymerization by fascin is concentration dependent. For actin/fascin networks $t_{\frac{1}{2}}$ is shown as a function of the molar ratio of fascin. The network architectures emerging at the respective fascin concentrations are illustrated.

Here, a total actin concentration $c_a = 3$ µM and a degree of labeling ≈ 11 % is used and the fluorescence intensity is followed using a spectrofluorometer FP-6500 (JASCO). Upon full polymerization, 50 µM LatB is added and thoroughly mixed using a pipette. A normalized fluorescence intensity $I_n = \frac{I-I_0}{I_1-I_0}$ is calculated. Here I_0 is the fluorescence intensity prior to polymerization and I_1 is the fluorescence intensity directly after addition of LatB.

In the case of pure actin solutions, the depolymerization induced by addition of 50 µM LatB (Fig. 4.1A) has been suggested to follow a double exponential decay [Wendel and Dancker, 1986, Kueh et al., 2008]. Interestingly, the depolymerization kinetics are drastically modified in the presence of the actin binding protein fascin, which bundles actin into individual polar bundles [Courson and Rock, 2010]. As depicted in Fig. 4.1B, fascin is slowing down the depolymerization process in a concentration dependent manner: While at a molar ratio between fascin and actin $R_{fas} = c_{fas}/c_a = 0.01$ no effect is resolvable, the time $t_{\frac{1}{2}}$ at which the normalized fluorescence is halved, $I(t_{\frac{1}{2}}) = \frac{1}{2}I(0)$, increases about a factor of ten for $R_{fas} = 1$. In order to test whether bundling accounts for this stabilization, the effect of the ideal cross-linker heavy meromyosin (HMM) in the rigor state is investigated. Rigor-HMM can form cross-links between filamentous actin and can also decorate individual filaments [Tharmann et al., 2007]. As shown in Fig. 4.1A, rigor-HMM completely inhibits actin depolymerization at $R_{HMM} = 1$, even though it does not cause any bundling at all [Tharmann et al., 2007].

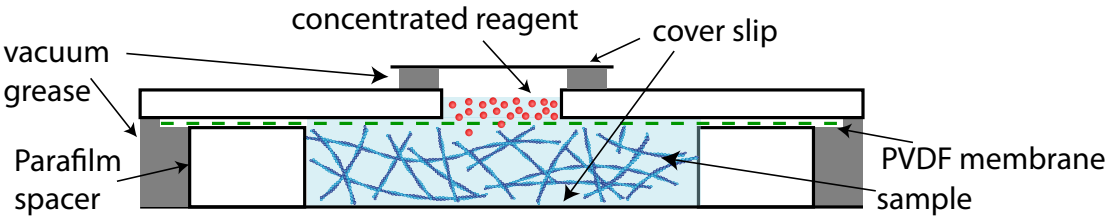

Figure 4.2: To add agents such as LatB, cofilin or ATP to actin networks without a mechanical disruption a diffusion chamber is used. The actin network is polymerized between a cover slip and a 0.1 µm pore size Durapore PVDF filter. Four layers of Parafilm are used as a spacer. A glass slide with a hole is used to fix the membrane. The chamber is sealed with vacuum grease. During polymerization, an additional cover slip is used to close the chamber at the top and prevent it from drying. After addition of the agent, also there vacuum grease is used to completely seal the chamber.

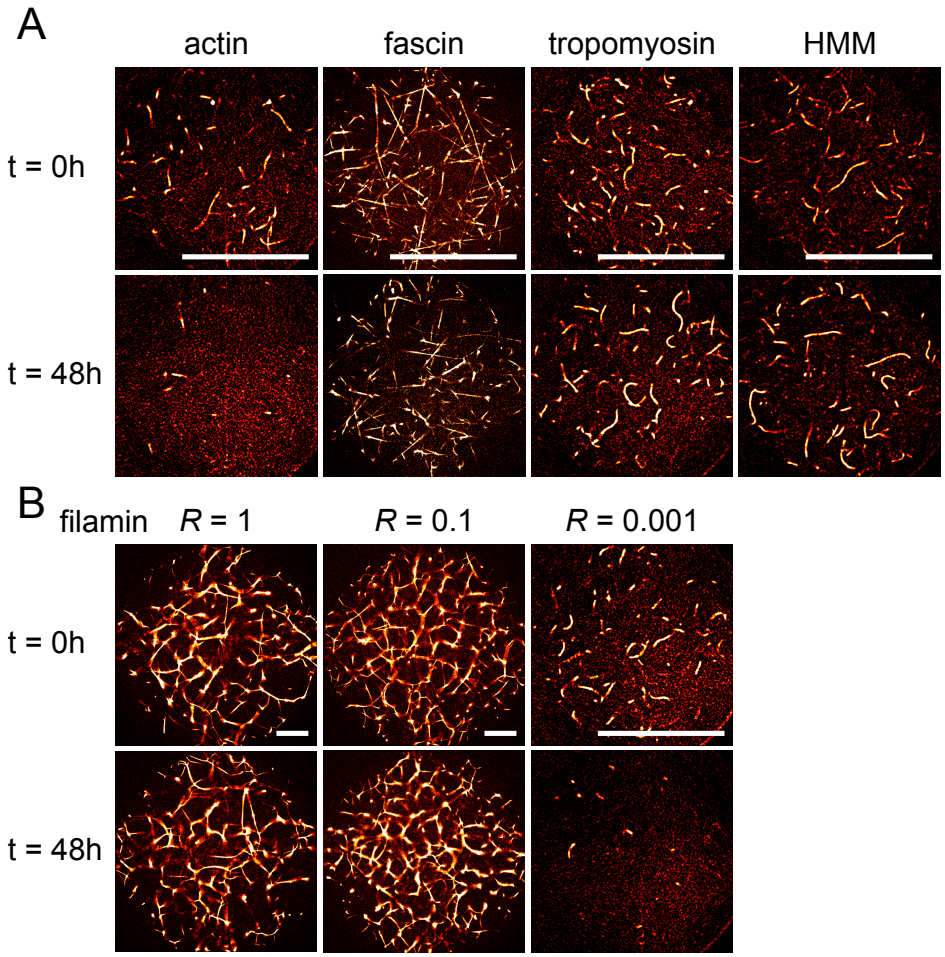

Figure 4.3: Micrographs showing the effective inhibition of depolymerization: Actin networks ($c_a = 3$ µM; for filamentous networks as formed by pure actin and in the presence of HMM or tropomyosin, only 1 % of the actin filaments is labeled) in the presence of various cross-linking proteins are shown before and 48 hours after 50 µM LatB is added via a diffusion chamber. At $R = 1$ all cross-linking proteins effectively inhibit depolymerization (A). As shown for filamin in (B), the slow down of actin depolymerization is concentration dependent. The scale bars denote 50 µm.

4.2 ABPs slow down LatB induced depolymerization

A pyrene assay cannot be used to study the effect of all types of ABPs because it is sensitive to quenching effects and pipetting the polymerized solution is mandatory. This is a problem for networks which – such as actin/filamin bundle networks – are kinetically trapped and show syneresis effects [Schmoller et al., 2008b]. Using a diffusion chamber (Fig. 4.2) allows to add LatB to an actin network without disrupting the network mechanically.

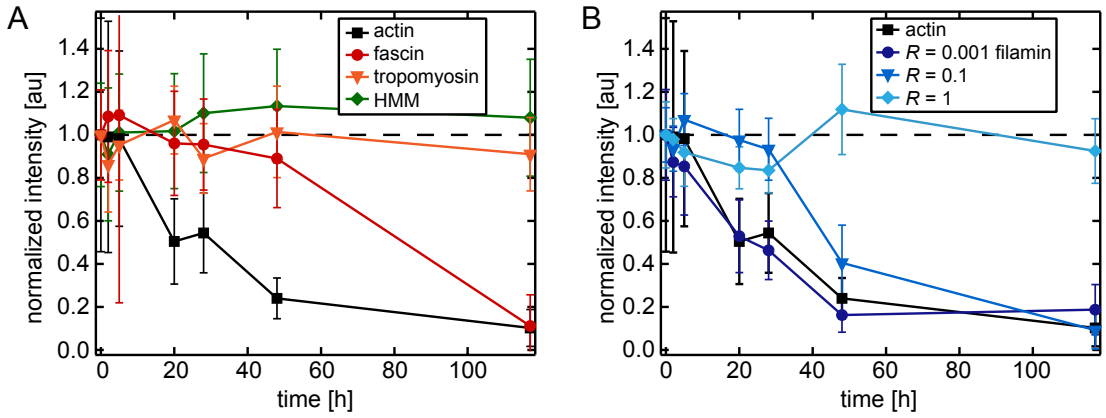

Figure 4.4: Quantitative image analysis allows to extract time courses of depolymerization induced by LatB from fluorescence microscope images as shown in Fig. 4.3. (A): It can be seen that all observed cross-linking proteins slow depolymerization down at $R = 1$ compared to pure actin (squares). While depolymerization is still observed for fascin (circles), no depolymerization can be detected for HMM (diamonds) and tropomyosin (inverted triangles). (B): The slow down caused by filamin is concentration dependent. While no effect compared to pure actin (squares) is observed at $R_{\mathrm{fil}} = 0.001$ (circles), the depolymerization clearly is slowed down at $R_{\mathrm{fil}} = 0.1$ (inverted triangles) and is completely inhibited at $R_{\mathrm{fil}} = 1$ (diamonds).

Fluorescence microscopy experiments confirm the effect of 50 µM LatB on the actin networks as observed using the pyrene assay: While pure actin solutions almost completely depolymerize within 48 hours, only a partial depolymerization is observed for actin/fascin networks at $R_{\mathrm{fas}} = 1$, where even bundles are still present after 48 hours (Fig. 4.3). Quantitative image analysis allows to follow the degree of depolymerization over time (Fig. 4.4). For this purpose, a gaussian blur is applied, background subtraction is done with ImageJ and a treshold which is adjusted for each time point is used to create a binary image. For filamentous networks the number of pixels which are part of filaments is counted and averaged for minimal 30 images. For bundle networks the fluorescence intensity of the bundle structures which are determined by the binarization

is measured to account for bundle thickness. Again, it is averaged over at least 30 images. The time courses over depolymerization are normalized on the initial values.

For pure actin, the time scale of depolymerization obtained from the quantitative image analysis is of the same order of magnitude as the long time scale observed in the pyrene assay (Fig. 4.1). The initial fast decay which is observed in the pyrene assay is not visible in the fluorescence microscopy based assay. This could be explained by the fact that filaments shorter than a cut-off length, which is given by the resolution limit, do not contribute to the decay measured via fluorescence microscopy.

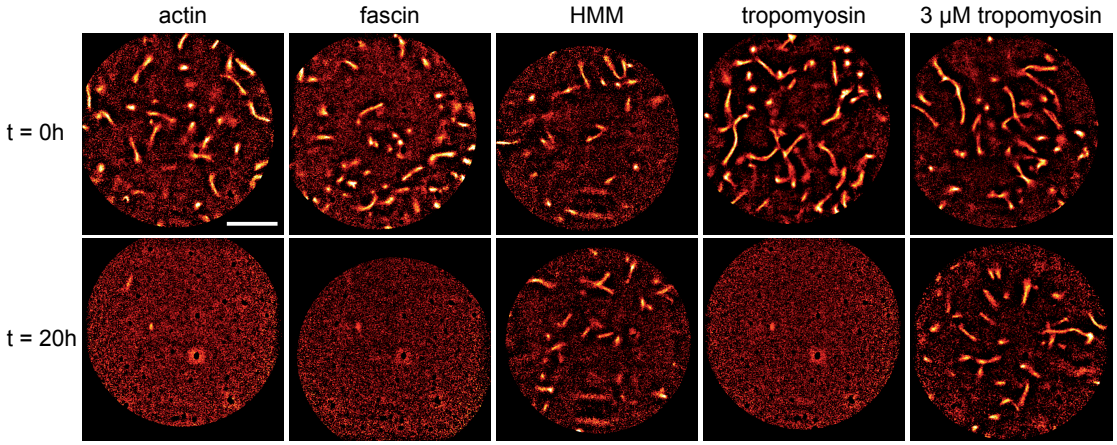

Figure 4.5: Depolymerization induced by dilution is inhibited: Actin networks (polymerized at $c_a = 3$ µM) in the presence of various cross-linking proteins ($R = 1$) are shown directly and 20 hours after 300-fold dilution to $c_a = 0.01$ µM in F-buffer. While pure actin solutions and actin/fascin bundle networks almost completely depolymerize, no depolymerization within 20 hours is observable for actin networks cross-linked by rigor-HMM. Tropomyosin decorated filaments depolymerize but the stabilizing effect can be recovered by addition of 3 µM tropomyosin to the dilution buffer. The scale bar is the same for all images and denotes 20 µm.

In the case of actin networks cross-linked by rigor-HMM at $R_{HMM} = 1$, no depolymerization is observable over the time course of 117 hours (Fig. 4.3 and 4.4A). Although fascin and rigor-HMM arrange actin filaments into significantly different network architectures, both cross-linking proteins suppress the depolymerization of actin filaments quite effectively for 48 hours. This suggests that the stabilization might be a generic effect. Indeed, also the ABP filamin, which induces the formation of curved and branched actin bundle networks [Schmoller et al., 2008b], inhibits actin depolymerization (Fig. 4.3 and 4.4B). Similarly to actin networks cross-linked with rigor-HMM, at $R_{fil} = 1$ actin/filamin networks are completely stable over 117 hours. In the case of filamin, where a pyrene assay cannot be used, this analysis even allows to observe a concentration dependency simi-

lar to that observed for fascin before (Fig. 4.4B). Again, an increase of the cross-linker concentration results in a gradual slow down of the depolymerization dynamics. The stabilizing effect is not restricted to cross-linking ABPs: tropomyosin, which binds to six actin subunits along one filament has been shown to inhibit depolymerization at the pointed end of villin-capped actin filaments [Broschat et al., 1989]. As shown in Fig. 4.3 and 4.4A, tropomyosin even prevents depolymerization of uncapped filaments. An additional advantage of the microscopy based experiments compared to the pyrene assay is that while in both methods the depolymerization curve will depend on the length distribution of the filaments, the relevant part of the length distribution is directly accessible in the microscopy assay. In the case of the pyrene assay, especially the range of short filaments, which is not resolveable with fluorescence microscopy, strongly contributes to the observed behavior. Therefore, a drastic change of the length distribution induced by the presence of the cross-linking molecules could significantly contribute to the observed apparent slow down of the observed depolymerization. In contrast, in the fluorescence microscopy assay only the visible filaments contribute to the analysis. Since in the case of the filamentous systems the visible length distribution is not obviously changed in the presence of the cross-linking proteins, an altered length distribution of filaments can not account for the observed drastic effects.

4.3 ABPs slow down depolymerization induced by dilution

Diluting actin solutions below the critical concentration [Wegner and Isenberg, 1983], which is approximately 0.1 µM at the buffer conditions used here, provides an additional way to induce depolymerization and might give a deeper insight into the principle underlying the stabilization by cross-linking proteins. Upon 300-fold dilution in F-buffer, actin solutions ($c_a = 3$ µM) almost completely depolymerize within 20 hours (Fig. 4.5). Actin/fascin bundles decompose within a few minutes upon dilution, which is followed by a complete depolymerization within 20 hours – comparable to pure actin solutions. However, rigor-HMM at $R_{HMM} = 1$ completely inhibits depolymerization on relevant timescales. While rigor-HMM suppresses depolymerization without bundling filaments, bundling is essential for a slow-down of depolymerization induced by fascin. Both fascin and rigor-HMM form inter-filamental cross-links, but only rigor-HMM can form a high number of intra-filamental cross-links decorating single filaments. This suggests that in the case of rigor-HMM rather intra-filamental cross-links than the comparable small number of inter-filamental cross-links account for the observed stabilization of actin filaments. 300-fold dilution of tropomyosin decorated filaments results in depolymerization (Fig. 4.5). However, this might result from the fact that due to its lower binding affinity

dilution causes a decrease of the molar ratio of bound tropomyosin. While fascin bundles still decompose if 3 µM fascin is added to the dilution buffer, the stabilizing effect of tropomyosin can be indeed recovered by adding 3 µM tropomyosin to the dilution buffer. This again demonstrates the concentration dependency of the stabilizing effect of ABPs.

4.4 ABPs slow down disintegration of actin networks induced by cofilin

The mechanism by which cross-linking proteins affect the depolymerization kinetics of actin filaments is similar if depolymerization is induced by dilution in F-buffer or by addition of LatB. However, different effects can be expected for depolymerization induced by cofilin, which has not only been reported to cause an increase of depolymerization rates [Carlier et al., 1997], but also to sever actin filaments [Moriyama and Yahara, 1999, De La Cruz, 2009, Oser and Condeelis, 2009]. Tropomyosin has been shown to be a physiological inhibitor of cofilin dependent actin dynamics [Ono and Ono, 2002]. As shown in Fig. 4.6A, not only tropomyosin, but also all the cross-linking molecules tested here prevent disintegration of actin networks by cofilin provided that they are present at high concentrations ($R = 1$).

In the case of tropomyosin, HMM and fascin no depolymerization is detectable from the quantitative image analysis (Fig. 4.7A). Although bundles are still visible after more than 20 hours (Fig. 4.6A), a slow disintergration is observed for actin/filamin bundle networks at $R_{\mathrm{fil}} = 1$ (Fig. 4.7A).

Addition of 3 µM cofilin to an actin network cross-linked by rigor-HMM or decorated by tropomyosin at lower concentrations ($R = 0.1$) results in disintegration (Fig. 4.6B) – however, still significantly slower than for pure actin. Suprisingly, actin/filamin bundle networks at $R_{\mathrm{fil}} = 0.1$ are completely stable over 23 hours. The complete stabilization at the low $R_{\mathrm{fil}} = 0.1$ might be explained by an interaction of several actin subunits with a single filamin molecule. The fact that a slow disintegration is observed at the higher cross-linker concentration $R_{\mathrm{fil}} = 1$ might indicate a specific effect that cannot be explained by a simple, general model.

4.5 Simultaneous use of molecular motors and cofilin disrupts bundled actin networks

The insensitivity of actin bundle networks towards the depolymerization methods investigated so far suggests that cells need additional mechanisms to disintegrate such highly

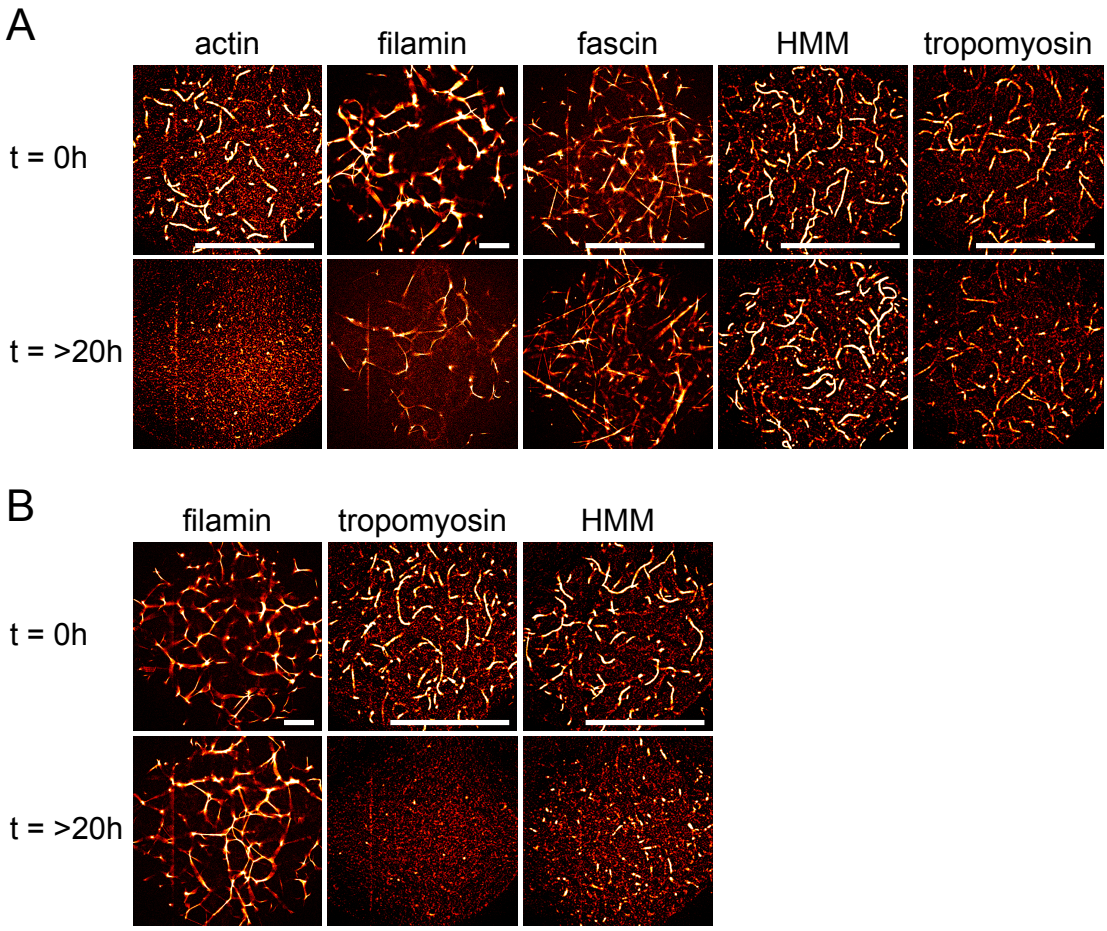

Figure 4.6: Cross-linking molecules inhibit depolymerization induced by cofilin: Actin networks ($c_a = 3$ µM; for filamentous networks as formed by pure actin and in the presence of HMM or tropomyosin, only 1 % of the actin filaments is labeled) in the presence of various cross-linking proteins are shown directly and ≈ 20 hours after addition of 3 µM cofilin. (A): While pure actin solutions completely depolymerize within 2 hours, depolymerization is drastically slowed down for actin networks cross-linked by rigor-HMM, decorated by tropomyosin or bundled by fascin or filamin ($R = 1$). (B): At lower cross-linker concentrations ($R = 0.1$) the slow down of depolymerization is less pronounced than at high concentrations in the case of rigor-HMM and tropomyosin. Only for filamin, the stabilizing effect is even stronger at $R = 0.1$. The scale bars are the same for all images and denote 50 µm.

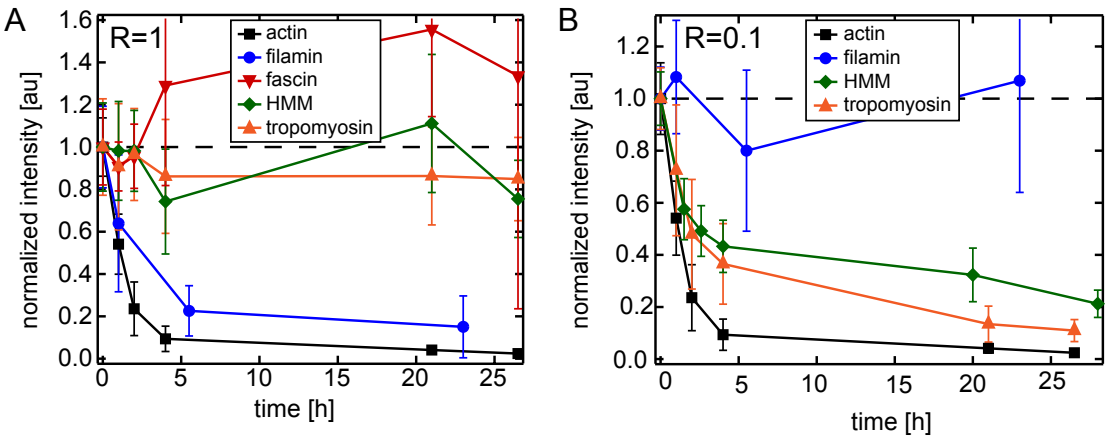

Figure 4.7: Quantitative image analysis allows to extract time courses of depolymerization induced by cofilin from fluorescence microscope images as shown in Fig. 4.6. (A): It can be seen that all observed cross-linking proteins slow depolymerization down at $R = 1$ compared to pure actin (squares). While depolymerization is still observed for filamin (circles), no significant depolymerization can be detected for HMM (diamonds), fascin (inverted triangles) and tropomyosin (upright triangles). (B): At $R = 0.1$, a slow depolymerization is observed for HMM (diamonds) and tropomyosin (upright triangles). No depolymerization is observed for actin/filamin networks.

stabilized actin structures. Molecular motors might help to disrupt even actin networks bundled by filamin. To test this hypothesis, an actin/filamin network ($c_a = 3$ µM, $R_{fil} = 1$) is polymerized in the presence of myosin-II ($c_{myosin} = 0.035$ µM) which has been saturated with a 16-fold excess of the non-hydrolyzable ATP analog AMP-PNP and is therefore not able to bind actin (Fig. 4.8A). As expected, 20 hours after addition of 3 µM cofilin bundles are still present (Fig. 4.8B). Also activation of the molecular motors by addition of 5.4 mM ATP in the absence of cofilin causes only a drastic reorganization (Fig. 4.8C) but not a disintegration of the actin structures. Only if both agents are added simultaneously, the network is completely disintegrated within 20 hours (Fig. 4.8D). Thus, both cofilin and the presence of motor activity is needed to disintegrate actin/filamin bundle networks effectively.

4.6 Stabilization by cross-linking molecules is a generic effect

The effect of cross-linking proteins on the depolymerization behavior of F-actin has been rather unknown. Although an inhibition of actin depolymerization has been reported

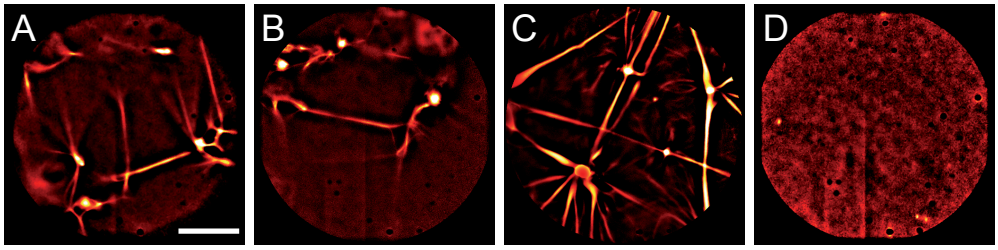

Figure 4.8: Actin/filamin bundle networks can be disintegrated using molecular motors: (A): Actin/filamin networks ($c_a = 3$ µM, $R_{fil} = 1$) are polymerized in the presence of myosin-II ($c_{myosin} = 0.035$ µM), which has been saturated with with a 16-fold excess of AMP-PNP and is therefore unable to bind to actin. (B): Addition of 3 µM cofilin does not result in complete depolymerization within 20 hours. (C): Activation of myosin-II by addition of 5.4 mM ATP causes drastic structural reorganization but actin structures are still present after 20 hours. (D): By addition of both, cofilin and ATP, the networks can be completely disintegrated. The scale bar is the same for all images and denotes 20 µm.

previously for *dictyostelium* 30 kDa actin-bundling protein [Zigmond et al., 1992], α-actinin [Cano et al., 1992], espin [Loomis et al., 2003] and plastin [Lebart et al., 2004] and has been postulated for bundles from *in vivo* experiments [Tilney et al., 2003, Rzadzinska et al., 2005], it has so far not been systematically investigated. Thus, multiple depolymerization assays have been used here to reveal the effect of cross-linking on the kinetics of actin filaments: Depolymerization has been induced by dilution or by addition of latrunculin B and followed by quantitative fluorescence microscopy as well as a pyrene actin assay.

Different cross-linking proteins result in the formation of actin networks with strongly varying network architectures and properties [Bausch and Kroy, 2006, Lieleg et al., 2007, Lieleg et al., 2010]. Yet, all studied cross-linking molecules inhibit depolymerization of F-actin provided that they form a high number of cross-links. This can be achieved either in the case of bundling, where inter-filamental cross-links are formed (Fig. 4.9A), or if ABPs decorate actin filaments with intra-filamental cross-links (Fig. 4.9B). The latter is the mechanism by which the well studied toxin phalloidin stabilizes F-actin [Steinmetz et al., 1998]. Both cases result in an increase of the total binding energy of the cross-linked actin subunits in the filament – which is set by the actin-actin as well as the actin-ABP interaction – due to the additional bonds to the cross-linking molecules. As solely simultaneous unbinding of the actin-actin as well as the actin-cross-linker bond allows for a complete depolymerization event, depolymerization is shifted to slower timescales. Moreover, a concentration dependence of the slow-down is reasonable: At low molar ratios of the cross-linker, such an improbable depolymerization event

may be followed by several actin subunits which can freely depolymerize until the next cross-linking molecule is reached.

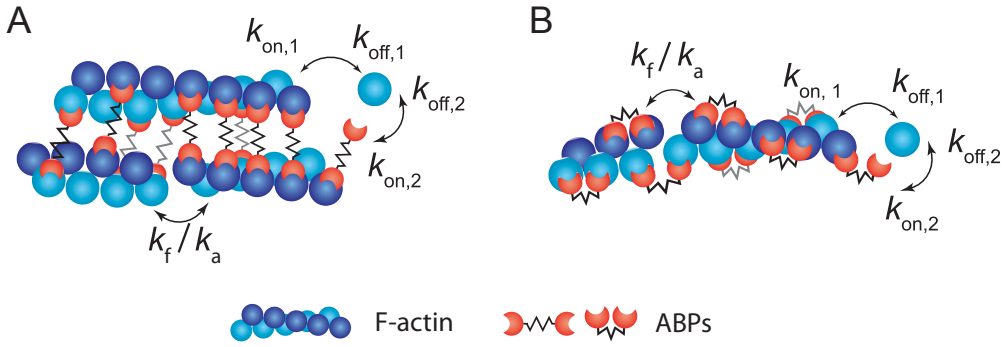

Figure 4.9: Simple model for depolymerization of actin in the presence of cross-linking molecules. (A): Cross-linking molecules which bundle actin filaments prevent potential depolymerization or fragmentation events. (B): A similar effect occurs if cross-linking molecules decorate an individual actin filament.

Since the turn-over rate of a treadmilling actin filament is given by the respective on- and off-rates, the observed cross-linker induced slow down of actin depolymerization has direct consequences on the steady state dynamics of cross-linked actin systems: All cross-linking proteins tested here can be expected to slow down also treamilling processes. Moreover, because cross-linking proteins stabilize actin filaments not only at the ends but wherever they are bound to two actin monomers, also the rate of spontaneous fragmentation as observed in chapter 3 will be decreased by the presence of cross-linking proteins (Fig. 4.9).

The simple model (Fig. 4.9A, B) captures the major effects of cross-linking proteins, but does not account for their specific properties, such as the binding propensity to actin [Lieleg et al., 2010] or the bundle geometry. The fact that no specific properties are needed to rationalize a stabilization effect of cross-linking proteins suggests that a similar behavior can be expected also for other dynamic polymers. In order to test this hypothesis, the depolymerization of microtubules upon dilution is investigated. In analogy to rigor-HMM in the case of actin, kinesins in the rigor state can be used to decorate microtubules with intra-filamental cross-links. Indeed, an obvious slow-down of the depolymerization process upon dilution is observed in the presence of kinesins (Fig. 4.10).

Cross-linking proteins not only inhibit the intrinsic dynamics of actin filaments but all cross-linking proteins tested here also inhibit disintegration of actin filaments by cofilin. Presumably, the cross-linking proteins sterically hinder the access of cofilin to the actin

filament (Fig. 4.11C), inside bundles this access is additionally hampered. As expected from the model, disintregration induced by cofilin is possible at lower cross-linker concentrations (Fig. 4.11D). Such an interpretation agrees with the previous findings that bundling by villin1 [Huang et al., 2005] or nonspecific interactions [Michelot et al., 2007] can prevent depolymerization induced by cofilin. In addition, actin bundles induced by dynamin2 and cortactin are remodeled to a more loosely packed conformation if GTP is added, which in turn causes a higher sensitivity to cofilin [Mooren et al., 2009]. However, cross-linking proteins could not only sterically hinder cofilin binding: In case that cofilin can still bind, cofilin induced breakage of the filament could be inhibited by a cross-linking protein bound at the site where cofilin would induce fragmentation of the filament.

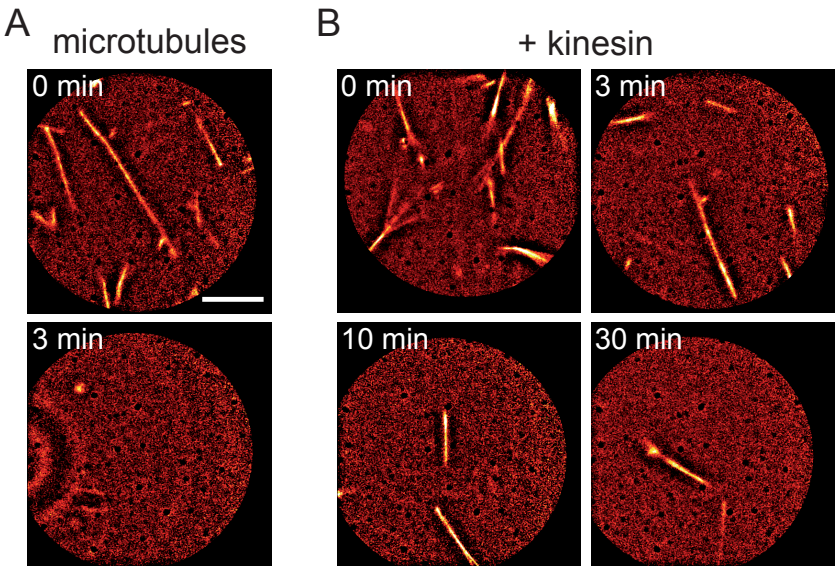

Figure 4.10: Depolymerization of microtubules induced by dilution is slowed down by kinesin. (A): Microtubules (≈ 100 µM) are shown directly after 100-fold dilution. Within 3 minutes, a complete depolymerization is observed. (B): If the microtubules have been decorated with kinesin (KIF5A) in the rigor state previous to dilution, some microtubules are still present even after 30 minutes. The scale bar denotes 20 µm.

4.7 Outlook on quantitative models

It has been demonstrated in this chapter that cross-linking proteins slow down actin depolymerization in a concentration dependent manner. Qualitatively, this generic effect

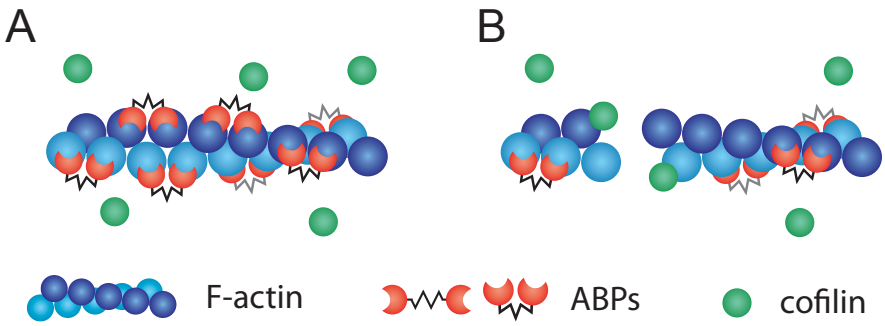

Figure 4.11: Simple model for cofilin induced disintegration of actin in the presence of cross-linking molecules. (A): At high concentrations cross-linking molecules can prevent disintegration of actin filaments induced by cofilin. (B): At lower cross-linker concentrations disintegration induced by cofilin is possible.

can be understood considering that cross-linking proteins stabilize the actin filaments by binding to at least two actin subunits simultaneously and by that prevent their dissociation (Fig. 4.9). Obviously, the next step would be a quantitative model describing the slow down by means of the physical properties of the cross-linking protein and its binding to the actin filament.

Depolymerization of pure actin filaments is dominated by dissociation of monomers from the filament ends: breakage of filaments into long fragments is frozen out because, due to their slow diffusion, long polymer fragments have a high chance of reannealing after their dissociation [Howard, 2001]. In addition, in a multi-stranded polymer such as F-actin, depolymerization by a dissociation of single monomers is significantly more likely than by a dissociation of short oligomers, because less bonds have to broken to remove a subunit from the filament end. Thus, as a first approximation, quantitative models for the depolymerization dynamics of actin filaments can assume a stepwise depolymerization from the filament ends. In contrast, this assumption can be expected to be not valid in the case of cross-linked actin filaments. The dominant depolymerization process for pure actin filaments, dissociation of a single monomer (Fig. 4.12A), is drastically slowed down if the dissociating monomer is bound to a cross-linking protein. Depending on the size of the cross-linking protein, dissociation of the whole monomer-cross-linker complex will be an alternative pathway (Fig. 4.12B). Also dissociation of short oligomers (Fig. 4.12C) can be expected to play an important role, because due the additional bond of the actin monomer at the filament end to the cross-linking protein its dissociation constant might no longer be higher than the fragmentation constant of an oligomer. Additional complications will occur in the case of cross-linked bundles, not only because the filaments

are connected via the cross-linking proteins, but also due to the confinement in the bundle, which will affect the diffusion of dissociated filament fragments. How exactly the different pathways contribute to the overall depolymerization will therefore depend on the binding and diffusion properties of the particular cross-linking protein and the geometry of the system. As a consequence, before a quantitative model for the depolymerization behavior of a cross-linked actin system can be established, the dominant depolymerization pathways have to be identified for this specific system.

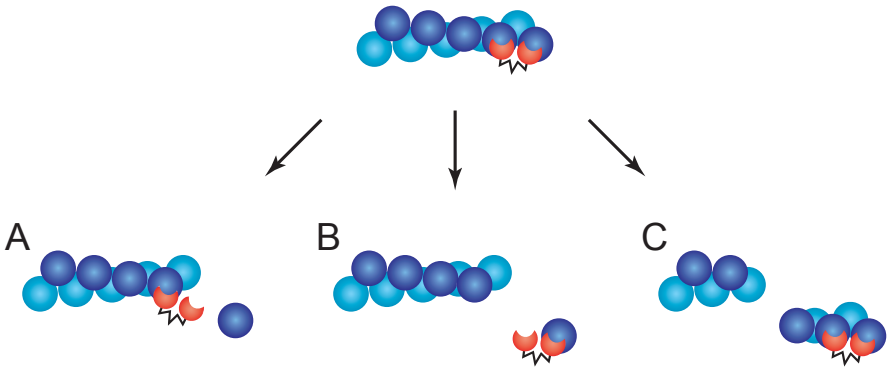

Figure 4.12: Actin filaments decorated with cross-linking proteins can depolymerize via various pathways. Examples are dissociation of a single actin monomer (A), dissociation of a monomer-cross-linker complex (B) or dissociation of an oligomer (C).

4.8 Discussion

The drastic modification of actin kinetics by cross-linking molecules can be expected to have wide-ranging implications for living cells, where cross-linking proteins or ABPs such as tropomyosin, which bind at least two actin subunits simultaneously are omnipresent. Cross-linking ABPs may not only guarantee a mechanical stability and integrity of cytoskeletal actin structures but can also provide a powerful tool for cells to stabilize distinct actin structures against the intrinsic actin dynamics and can therefore fulfill regulatory functions. On the other hand, additional concepts which enable cells to disintegrate cross-linked actin structures or facilitate a continuous turn-over of actin filaments are indispensable. In addition to severing ABPs such as cofilin – which accomplishes a disintegration of moderately cross-linked networks but is not able to destroy most networks cross-linked with a one-to-one stoichiometry – cells may need to deal with the cross-linker induced stabilization of actin filaments using active molecular motors [Ishikawa et al.,

2003, Medeiros et al., 2006, Haviv et al., 2008]. Here, it has been shown that in combination with active myosin-II, cofilin is able to completely disintegrate even actin/filamin networks. Myosin-II activity might partially disrupt actin/filamin bundles by tearing them apart and thereby create free binding sites along the filaments or at the ends of the filaments, where cofilin can have access to. While this study demonstrates that cross-linkers drastically alter the actin dynamics, it is a formidable challenge to address their role on the actin kinetics *in vivo*, where multiple molecules are involved and compete for their effect on the filaments. Future studies on the interplay between the numerous cytoskeletal constituents will eventually enable the reconstitution of *in vitro* modules with controlled properties akin to those of the highly dynamic and complex living cell.

5 Actin/Filamin Networks

In the previous chapter it has been shown that cross-linking proteins drastically slow down the depolymerization of actin filaments. However, cross-linking proteins not only inhibit the internal dynamics of actin filaments, but can also provide a structural stabilization on a larger length scale: Transient cross-links between actin filaments, as they are formed e.g. by HMM in the rigor state [Lieleg et al., 2008, Lieleg et al., 2009a], can be expected to slow down diffusive motion of actin filaments within the network. This effect is even more drastic in the case of bundling: Whereas in networks of individual, transiently cross-linked bundles – as formed e.g. by fascin or espin – reorganizations and thermal fluctuations of the bundle positions within the network are still observable [Schmoller, 2008, Lieleg et al., 2009b], networks which are almost completely static on the timescale of days are formed e.g. by filamin [Schmoller et al., 2008b]. Since bundles in these actin/filamin networks are not interconnected by single cross-linking proteins, but – due to the branched network architecture – by a huge number of cross-links, multiple unbinding events would be necessary to allow for a structural reorganization. Due to this hindrance of structural reorganizations, the architecture of branched bundle networks results in kinetic trapping: Such networks, as they are also formed by α-actinin, can be kinetically trapped in different metastable states which depend on the network history [Schmoller et al., 2008b, Lieleg et al., 2009b]. Moreover, actin/filamin networks exhibit significant internal stresses which are built up during the network formation process.

Cells could make use of the non-equilibrium nature of such highly cross-linked actin systems because it allows to build different metastable structures with different mechanical properties using the same constituents. It is thus important to obtain a deeper understanding of the parameters which set the structure of kinetically trapped actin networks and how their structure correlates with their mechanical properties. The effect of different cross-linking ABPs on the mechanical properties of actin networks has been studied extensively over the last years by both, reconstituting and simulating *in vitro* model systems with varying degree of complexity [Bausch and Kroy, 2006, Kasza et al., 2007, Huisman et al., 2007, Conti and MacKintosh, 2009, Heussinger et al., 2007, Head et al., 2003, Wilhelm and Frey, 2003, Astroem et al., 2008]. It has

turned out, that the high complexity of the cytoskeleton is reflected by the fact that each cross-linking molecule has its own characteristic effect on the structural and mechanical network properties [Bausch and Kroy, 2006, Wagner et al., 2006, Schmoller et al., 2008a, Shin et al., 2004, Tseng et al., 2001, Tseng et al., 2004, Volkmer Ward et al., 2008]. However, until recently it was widely believed that such reconstituted actin networks should be well equilibrated. Thus it remains still an open question, how the non-equilibrium character of kinetically trapped actin bundle networks affects the network mechanics. Especially for systems showing structural polymorphism as a function of both, actin and cross-linker concentration, a thorough investigation of the viscoelastic network response and its correlation with the various microstructures is needed before suitable theoretical models can be developed and tested.

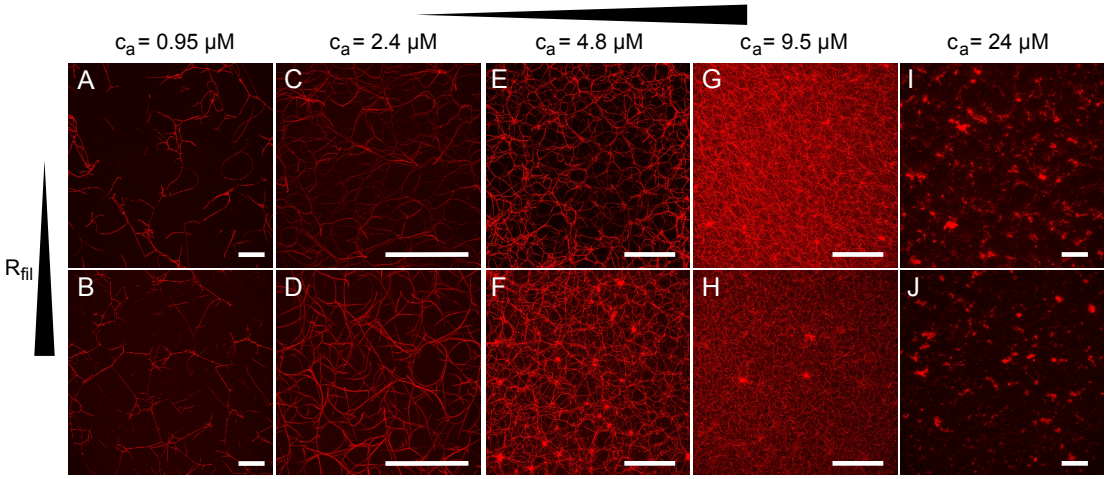

Figure 5.1: Confocal images ((A) and (B): projections of 120 µm height, (C) and (D): projections of 60 µm height, (E)-(J): projections of 100 µm height) of actin/filamin networks are shown for different actin concentrations and molar ratios of filamin. (A): $c_\mathrm{a} = 0.95$ µM, $R_\mathrm{fil} = 0.3$; (B): $c_\mathrm{a} = 0.95$ µM, $R_\mathrm{fil} = 1$; (C): $c_\mathrm{a} = 2.4$ µM, $R_\mathrm{fil} = 0.1$; (D): $c_\mathrm{a} = 2.4$ µM, $R_\mathrm{fil} = 1$; (E): $c_\mathrm{a} = 4.8$ µM, $R_\mathrm{fil} = 0.1$; (F): $c_\mathrm{a} = 4.8$ µM, $R_\mathrm{fil} = 0.4$; (G): $c_\mathrm{a} = 9.5$ µM, $R_\mathrm{fil} = 0.03$; (H): $c_\mathrm{a} = 9.5$ µM, $R_\mathrm{fil} = 0.3$; (I): $c_\mathrm{a} = 24$ µM, $R_\mathrm{fil} = 0.02$; (J): $c_\mathrm{a} = 24$ µM, $R_\mathrm{fil} = 0.1$. The scale bars denote 100 µm. Parts of the data are already shown in [Schmoller, 2008].

In this chapter a detailed characterization of the structural and macromechanical properties of actin/filamin networks will be presented. Depending on the actin and filamin concentrations, two distinct regimes can be distinguished: Within the first concentration regime filamin not only cross-links actin filaments, but also changes the network structure by inducing the formation of bundles, which results in an enhancement of the linear as well as the non-linear network stiffness. At high filamin concentrations, purely

bundled networks emerge, which at high actin concentrations contain bundle clusters. In this bundle regime a structural saturation is observed, which can be explained by the aggregation controlled network formation process and is accompanied by an insensitivity of non-linear viscoelastic network properties with respect to the filamin concentration.

5.1 Structure of actin/filamin networks

Using confocal microscopy, the structure of actin/filamin networks is studied as a function of both the actin concentration c_a and the relative concentration of the ABP filamin, $R_{fil} = c_{fil}/c_a$. The actin concentration is varied from $c_a = 0.95$ µM up to $c_a = 24$ µM. The molar ratio of filamin is varied from $R_{fil} = 0.001$ to $R_{fil} = 1$. Depending on c_a and R_{fil}, different network structures are observed (Fig. 5.1): At low R_{fil}, the network consists of single filaments, which are assumed to be cross-linked [Stossel et al., 2001]. Above a critical ratio R^*_{fil}, filamin induces the formation of bundles. This critical filamin ratio decreases with increasing actin concentrations (Fig. 5.3). At high filamin concentrations, highly static and purely bundled actin/filamin networks are formed. There, no single filaments are detectable using confocal microscopy. Also microrheological experiments indicate that the number of unbundled filaments in the background of the network is very low and can be neglected: While a high number of PEG-coated polystyrene beads of 942 nm size is observered to stick to the bundles many others show very effective and long-ranged diffusion, which makes a tracking of the beads impossible – even for relatively short time intervals such as 50 s.

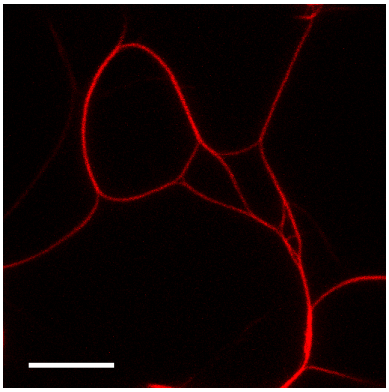

Figure 5.2: Confocal image (projection of 20 µm height) of an actin/filamin network ($c_a = 2.4$ µM, $R_{fil} = 0.1$). Obviously, bundles are interconnected by merged bundle segments. The scale bar denotes 10 µm.

For all actin concentrations investigated here, the purely bundled actin/filamin networks exhibit a common structural feature: Highly curved bundles branch and merge (Fig. 5.2). On the other hand, putative point-to-point cross-links between distinct bundles are hardly observable [Schmoller et al., 2008a]. Moreover, due to the branched

network structure, free bundle ends seem to be absent in these networks. At high actin concentrations, filamin furthermore induces the formation of bundle clusters (Fig. 5.1F-J), which resemble the mesoscopic star-shaped heterogeneities that have been observed in actin/α-actinin networks [Lieleg et al., 2009b].

As significant regions of the phase space of actin/filamin networks have been investigated, the observed network microstructures can be summarized in a schematic structural state diagram as a function of R_{fil} and c_{a} (Fig. 5.3).

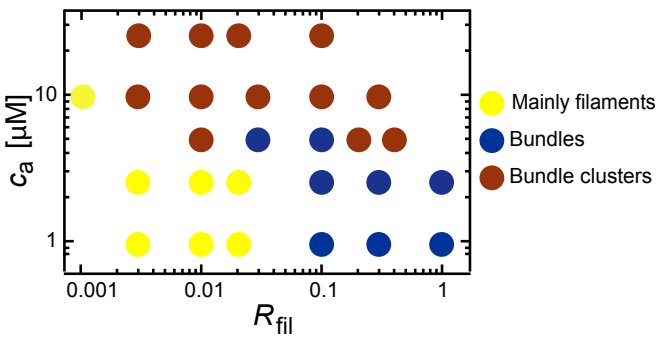

Figure 5.3: (A): The structure of actin/filamin networks is shown as a function of the actin concentration and the molar ratio of filamin. Filamin cross-links actin filaments at low R_{fil} (yellow). A purely bundled network is formed at higher R_{fil} (blue). At high actin concentrations, bundle clusters are formed (red).

Increasing the filamin concentration can induce drastic changes in the network architecture. However, within the purely bundled phase, a critical $R_{\mathrm{fil}}^{\#}$ exists, above which a further increase of the filamin concentration has a surprisingly small effect on the network microstructure: The microstructures of the networks shown Fig. 5.1B,D,H and J are virtually identical to those shown in Fig. 5.1A,C,G and I, respectively. Also the networks shown in Fig. 5.1E and Fig. 5.1F ($c_{\mathrm{a}} = 4.8$ µM) are very similar – only that a small number of clusters is formed at $R_{\mathrm{fil}} = 0.4$. Thus it seems that in the bundle regime the actin concentration has a stronger influence on the network structure than the filamin concentration.

At low actin concentrations, the bundle thickness is experimentally accessible using bright field microscopy and can be used to quantitatively verify the observed insensitivity of the network structure towards high filamin concentrations. The distribution of bundle thicknesses is determined for the actin/filamin networks shown in Fig. 5.1B-D. For this purpose, a Gaussian is fitted to the minima in the intensity profiles perpendicular to the bundles. This method might overestimate the absolute values of the bundle diameters and might also neglect thin bundles, which are not detectable using bright field microscopy. Nevertheless, relative changes in the distribution of bundle thicknesses are resolveable. A variation of the actin concentration ($c_{\mathrm{a}} = 0.95$ µM and $c_{\mathrm{a}} = 2.4$ µM)

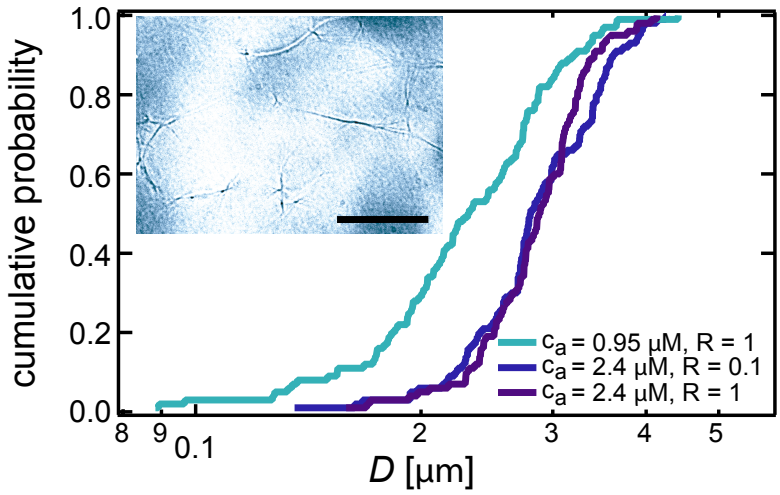

Figure 5.4: Cumulative probabilities of bundle diameters in actin/filamin bundle networks as denoted in the legend. The inset shows an actin/filamin network ($c_a = 2.4$ µM, $R_{fil} = 1$) observed with bright field microscopy. The scale bar denotes 20 µm. The data are obtained from [Schmoller, 2008].

at a given $R_{fil} = 1$ results in different probability distributions of bundle diameters (Fig. 5.4): At the lower actin concentration, a significantly smaller average bundle diameter is observed. Yet, the bundle thickness distribution is independent of R_{fil} for a fixed $c_a = 2.4$ µM (Fig. 5.4). Thus, for a given c_a the actin/filamin bundle thickness is constant for high filamin concentrations. The thickness of actin bundles formed by fascin has been shown to be both limited and well defined by geometric constraints imposed by the helical structure of actin filaments [Claessens et al., 2008]. However, it seems improbable that such intrinsic bundle properties are responsible for the limited size of actin/filamin bundles. Due to the branched network structure, the diameters of actin/filamin bundles are broadly distributed, which is in contrast to the actin bundles formed by fascin. For actin/filamin networks the observed structural saturation might be the consequence of the aggregation controlled growth process, which drives the formation of the kinetically trapped actin/filamin bundle networks [Schmoller et al., 2008b]: In a regime where bundling occurs as soon as filaments or thinner bundles come into contact, it is reasonable that the final distribution of bundle thicknesses does not depend on the filamin concentration – simply because bundles which come into contact fuse anyways. Considering the non-equilibrium character of actin/filamin bundle networks, an insensitivity of structural network parameters towards increasing filamin concentrations is reasonable. Nevertheless, the addition of filamin may still change the properties of the

individual bundles.

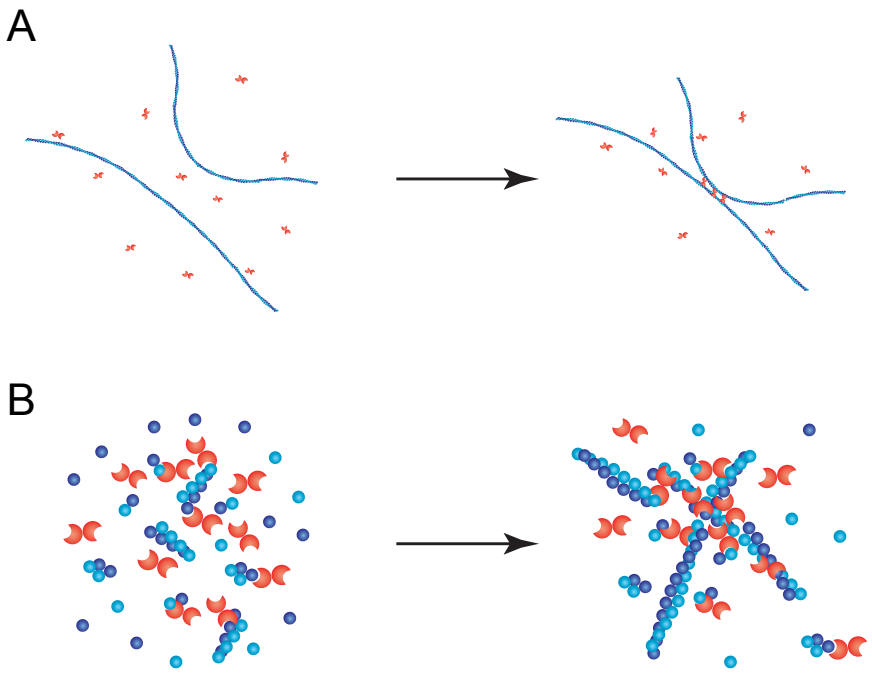

Figure 5.5: Illustration of an aggregation controlled network formation: The final network structure is not only given by the protein concentrations but also by the time scales of filament formation and filament bundling. (A): At lower actin concentrations long filaments can be formed and bundled before they are are kinetically trapped. The final bundle thicknesses decrease with increasing actin concentration. (B): At very high actin concentrations, many short actin filaments are formed simultaneously and trapped in cluster-like structures before they can further elongate and form bundles.

Moreover, considering the aggregation controlled network formation it can also be speculated about the origin of the dependency of the actin/filamin network structure on the actin concentration. An increasing actin concentration can be expected to facilitate the formation of thicker bundles, simply because more material is available. Indeed, at low actin concentrations, the bundle thickness increases with increasing actin concentration (Fig. 5.4). However, at the same time the aggregation controlled network formation imposes the opposite trend. At low actin concentrations, contact events between filaments are rare. Thus, the actin filaments have enough time to freely elongate. Individual contact events between such filaments will result in fusion of these filaments and the formation of long bundles (Fig. 5.5A). Finally, a percolating network will form

in which further bundling events are inhibited [Schmoller et al., 2008b]. The higher the actin concentration is, the faster such a trapped state will be reached. Thus, at higher actin concentrations bundles have less time to form thicker bundles. Therefore, the final bundle thicknesses tends to decrease with increasing actin concentrations. Obviously, this decrease of the bundle thickness with increasing actin concentrations is the dominant effect at high actin concentrations, where the mesh size drastically decreases (Fig. 5.1). It will be shown in chapter 7 that a similar behavior can be observed if the speed of filament formation is varied by a change in pH. In analogy to an increase in actin concentration an acceleration of filament formation results in thinner bundles. At very high actin concentrations, many short filaments are kinetically trapped as soon as they start to polymerize (Fig. 5.5B). This results in the formation of cluster-like structures as observed in (Fig. 5.1F-J).

So far it has been demonstrated that depending on the actin concentration as well as the molar ratio of filamin, strongly different network architectures can be obtained: At low concentrations, filamin cross-links filamentous actin. At high filamin concentrations, bundle networks or even bundle cluster networks are formed, which show a structural saturation with respect to R_{fil}. It remains to be shown how these pronounced differences in the network structure manifest themselves in the viscoelastic network response. In the following section of this chapter, this question is addressed and the macromechanical response of actin/filamin networks is determined using macrorheology.

5.2 Viscoelastic response of actin/filamin networks

To characterize their linear viscoelastic properties, actin/filamin networks are first probed in the limit of small deformations by measuring the frequency-dependent viscoelastic moduli $G'(f)$ and $G''(f)$ over a frequency range of three decades. As the effect of filamin on the linear viscoelastic moduli is extremely small, series of experiments, where the filamin concentration is varied at a fixed actin concentration are conducted with one actin preparation, which guarantees low error bars for the viscoelastic moduli ($\approx$ 30 %) and allows for an accurate investigation of the effect of filamin on the network properties. However, the comparibility of absolute values between different R-series is limited, since different actin preparations had to be used. For the viscoelastic moduli of pure actin solutions, this can result in an error of up to a factor of two – which normally is negligible as the effect of most cross-linking molecules on the linear moduli is much more pronounced [Lieleg et al., 2007, Tharmann et al., 2007, Shin et al., 2004].

Several series of experiments with increasing filamin concentrations are conducted to study the influence of filamin on the viscoelastic response of actin/filamin networks within

this linear regime. All actin concentrations used here are higher than the overlap concentration of actin filaments which can be calculated to be $\approx$ 2.5 µM [Kroy and Frey, 1996]. As an example, the obtained viscoelastic frequency spectra $G'(f)$ and $G''(f)$ of actin/filamin networks with $c_a = 9.5$ µM and varying filamin concentrations R_{fil} are depicted in Fig. 5.6A and B. In contrast to actin networks cross-linked by other ABPs such as HMM [Lieleg et al., 2008] or fascin [Lieleg and Bausch, 2007], these frequency spectra are quite featureless. This indicates that in the linear network response of actin/filamin networks, there is no intrinsic timescale – at least within the exerimentally accesible frequency range. In order to characterize the network stiffness as a function of c_a and R_{fil}, an apparent plateau modulus $G_0 = G'(10\text{ mHz})$ is defined.

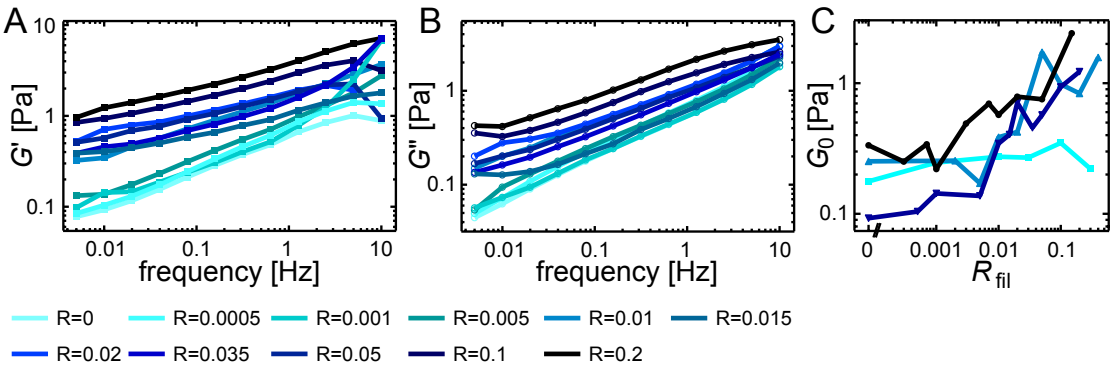

Figure 5.6: Elastic modulus $G'(f)$ (A) and viscous modulus $G''(f)$ (B) of actin/filamin networks ($c_a = 9.5$ µM) are shown for different molar ratios of filamin. The color code depicted in (A) is also valid for (B). (C): The apparent plateau modulus $G_0 = G'(10\text{ mHz})$ is shown as a function of R_{fil} at different actin concentrations (squares: $c_a = 3.6$ µM, upright triangles: $c_a = 4.8$ µM, inverted triangles: $c_a = 9.5$ µM, circles: $c_a = 24$ µM). Parts of the data are already shown in [Schmoller, 2008].

As shown in (Fig. 5.6C), filamin significantly enhances the stiffness of actin networks for $c_a > 3.6$ µM. However, the effect of filamin on the linear stiffness of the actin network is rather weak compared to other actin cross-linking molecules such as HMM [Tharmann et al., 2007], fascin [Lieleg et al., 2007], scruin [Shin et al., 2004] or α-actinin [Tempel et al., 1996]. For all actin concentrations investigated here, even the addition of high filamin concentrations enhances the apparent plateau modulus G_0 by less than one order of magnitude. At least for the filamentous networks this can be rationalized considering the high flexibility of individual filamin molecules [Gardel et al., 2006]. For the bundled networks, the weak increase in the linear network stiffness is rather surprising – especially since actin/filamin bundle networks exhibit internal stresses [Schmoller et al., 2008b], which would be expected to enhance the network elasticity [Gardel et al., 2006, Lieleg

et al., 2009a].

So far the viscoelastic properties of actin/filamin networks have been studied here in the limit of small deformations, i.e. in the linear regime. There, the influence of filamin on the network elasticity is rather small – but not its influence on the network structure. As a consequence, a precise correlation of structural and mechanical network properties is highly difficult. Thus, now the non-linear network properties at high deformations, where the effect of filamin has been reported to be much stronger [Gardel et al., 2006] are addressed. This non-linear regime is investigated best with a constant shear rate $\dot{\gamma}$ to minimize creep artifacts during the measurement. A shear rate $\dot{\gamma} = 20\ \%\mathrm{s}^{-1}$ is used for $c_\mathrm{a} = 4.8\ \mu\mathrm{M}$, $\dot{\gamma} = 12.5\ \%\mathrm{s}^{-1}$ is used for all other actin concentrations. From the recorded stress-strain relation $\sigma(\gamma)$ the differential modulus $K(\gamma) = \frac{\partial\sigma}{\partial\gamma}$ is calculated [Semmrich et al., 2008].

Fig. 5.7A shows the non-linear response for actin/filamin networks with $c_\mathrm{a} = 9.5\ \mu\mathrm{M}$ and varying filamin concentrations. The addition of filamin clearly enhances the strain hardening behavior of actin networks. The dependence of the maximal non-linear network stiffness K_max and the corresponding yield stress σ_max on R_fil is similar for all actin concentrations investigated here (Fig. 5.7B,C): At low molar ratios of filamin, both parameters increase strongly. This trend continues up to filamin concentrations that roughly correspond to the regime where bundle networks are formed. Note that for low actin concentrations ($c_\mathrm{a} = 3.6\ \mu\mathrm{M}$ and $c_\mathrm{a} = 4.8\ \mu\mathrm{M}$) pure actin solutions do not show strain hardening at the experimental conditions used here – but filamin induces strain hardening for $R_\mathrm{fil} \geq 0.01$. At high R_fil, an insensitivity of σ_max and K_max towards the filamin concentration is observed. It can be speculated that the saturation of σ_max and K_max in the bundle regime is directly correlated with the observed insensitivity of the structural network properties with respect to high filamin concentrations. Although the network architecture saturates at high R_fil, an increased filamin concentration may still change the interconnectivity of distinct bundles, which is generated by cross-links formed by filamin, as well as the degree of cross-linking between individual actin filaments within a bundle. This might not only explain the fact that the apparent plateau modulus G_0 is still increasing, but also the observation that the shape of the non-linear response $K(\gamma)$ becomes broader with increasing R_fil.

It has been shown before that the interconnectivity of actin networks, i.e. the presence of transient cross-links, gives rise to a pronounced loading rate dependence of the non-linear response, which is based on forced unbinding events of dinstinct cross-links [Lieleg et al., 2009a]. Thus, shear rate dependent measurements can be performed to address the influence of the filament/filament or bundle/bundle interconnectivity on the non-linear response of actin/filamin networks. Indeed, the non-linear response of actin/filamin bun-

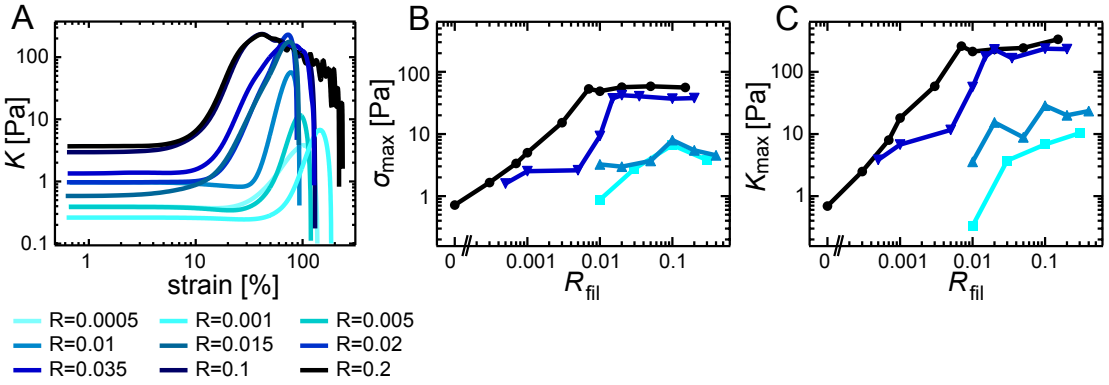

Figure 5.7: (A): The differential modulus K is shown as a function of strain for different molar ratios of filamin (c_a = 9.5 µM). σ_{max} (B) and K_{max} (C) are plotted as a function of R_{fil} for different actin concentrations (squares: c_a = 3.6 µM, upright triangles: c_a = 4.8 µM, inverted triangles: c_a = 9.5 µM, circles: c_a = 24 µM). Parts of the data are already shown in [Schmoller, 2008].

dle networks (c_a = 4.8 µM) strongly depends on the shear rate $\dot{\gamma}$ (Fig. 5.8): With decreasing shear rates the maximum non-linear stiffness K_{max} decreases by more than one order of magnitude; also σ_{max} decreases towards low shear rates. Moreover, for low shear rates K_{max} is reached at higher strains – a reorganization of the actin/filamin network during the shear experiment might be possible due to unbinding events of transient actin/filamin cross-links giving rise to a flow behaviour of the network. The independence of σ_{max} and K_{max} of R_{fil} in the purely bundled regime (Fig. 5.7C) holds true only for shear rates $\dot{\gamma} \gtrsim 10\ \%s^{-1}$. At low shear rates, both parameters depend on the filamin concentration (Fig. 5.8C, D). Although increasing filamin concentrations induce no additional structural changes, they suffice to alter the mechanical properties – most probably by increasing the interconnectivity, i.e. the cross-link density between merged bundle segments or between actin filaments in the bundles. The observed dependence on R_{fil} suggests that for high shear rates the non-linear response is dominated by the network structure. At low $\dot{\gamma}$, however, the interconnectivity – which depends on the filamin concentration – plays a more important role, as σ_{max} and K_{max} depend on R_{fil}. It can be speculated that the critical shear rate $\dot{\gamma} \approx 10\ \%s^{-1}$, below which σ_{max} and K_{max} depend on R_{fil}, corresponds to the time scale which is necessary for sufficient unbinding and rebinding events of filamin molecules to allow for structural reorganizations during the shear experiment.

In conclusion, it has been shown that actin/filamin networks exhibit various network architectures which depend on the concentration of both proteins. In addition to cross-

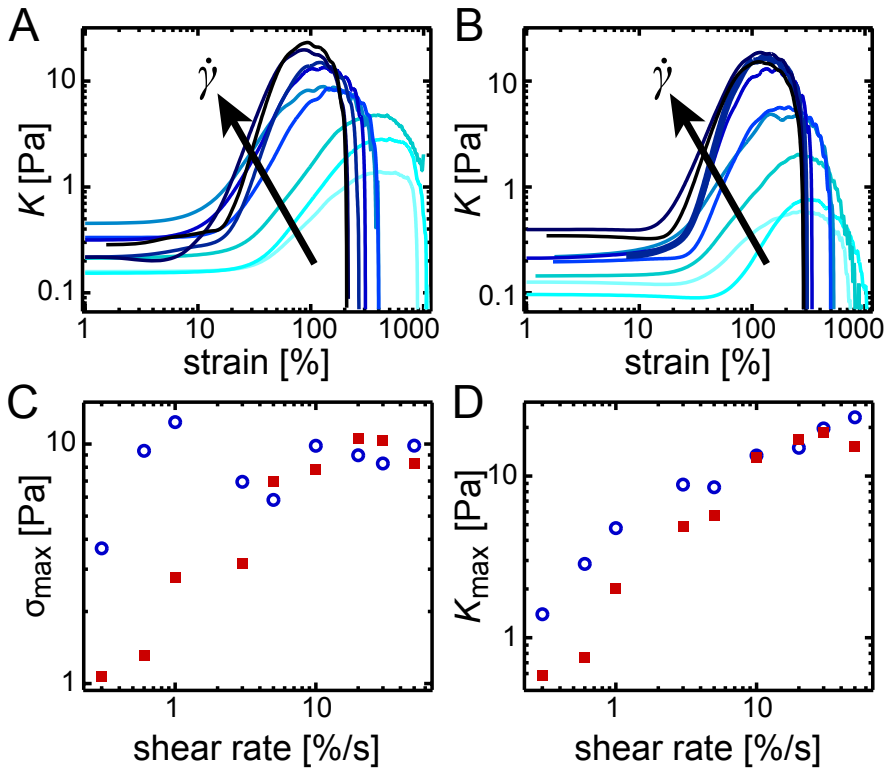

Figure 5.8: The differential modulus K of actin/filamin bundle networks ($c_a = 4.8$ µM) ((A): $R_{fil} = 0.072$, (B): $R_{fil} = 0.216$) is shown as a function of strain for different shear rates. The corresponding σ_{max} (C) and K_{max} (D) are plotted as functions of $\dot{\gamma}$. $R_{fil} = 0.072$ and $R_{fil} = 0.216$ are denoted as cirles and squares, respectively.

linked filamentous networks, bundle networks are observed as well as highly heterogeneous bundle cluster networks. A structural saturation occurs at high filamin concentrations although not all binding sites are occupied. This structural insensitivity towards the molar ratio of filamin manifests itself also in the non-linear viscoelastic network properties. While the transition from a regime of cross-linked filaments to a purely bundled regime is accompanied by a strong increase of the maximal non-linear stiffness K_{max} and the corresponding yield stress σ_{max}, both parameters are constant at higher filamin concentrations. At these high filamin concentrations the structure of actin/filamin networks is rather determined by an aggregation controlled growth process [Schmoller et al., 2008b] than by thermal equilibrium. This may account for the observed structural insensitivity with respect to the filamin concentration. However, the linear network stiffness G_0 still increases as a function of R_{fil} – which is most probably due to an increas-

ing bundle stiffness. The results presented here indicate that the aggregation controlled network formation accounts for a biphasic behavior of the average bundle thickness on the actin concentration. Future studies that focus on the time scales of nucleation, filament elongation, bundling and kinetic arrest are needed to quantitatively understand how the balance of these processes determines the final network structure. The results of this chapter demonstrate that actin/filamin networks exhibit various network structures which entail distinct linear and non-linear viscoelastic properties. Therefore, theoretical descriptions of the mechanical properties of actin/filamin networks must take into account these different network structures. The detailed characterization of actin/filamin networks presented here sets the basis for further studies addressing the microscopic origin of the structural transitions in living cells as well as their consequences on the macromechanical properties of the cytoskeleton.

6 Cyclic hardening in actin bundle networks

In the previous chapter, the structural and mechanical properties of actin/filamin networks have been characterized. It has been shown that in the bundle regime the structure and by that the mechanical properties of the network are determined by the aggregation-controlled growth process rather than equilibrium properties of the cross-linker. The aggregation-controlled growth proccess critically depends on the timescales of nucleation, filament elongation and bundle formation. As a consequence, the final, metastable state should depend on internal parameters which affect these timescales. Indeed, it will be shown in chapter 7 that a variation of pH tunes the speed of actin/filamin bundle network formation and by that results in a drastic change of the mesh size. On the other hand, external stimuli could trigger a structural change of the kinetically trapped networks. By that, the non-equilibrium character of cytoskeletal networks would allow to control their architecture by internal and external stimuli without changing their constituents – a mechanism which provides a powerful tool for the regulation of the cytoskeleton.

As already shown in [Schmoller et al., 2008b], where actin/filamin networks collapse into clusters upon pipetting, mechanical force can result in an irreversible change of the network structure. Mechanical forces can also induce additional bundling in actin/filamin bundle networks: An atomic force microscope (AFM) can be used to bring fully polymerized actin/filamin bundles into contact. Moving the AFM tip in the network to collect material and then pulling the tip in z-direction for several centimeters results in the formation of a macroscopic bundle, which is stable for at least days (Fig. 6.1). Although this experiment is crude, it clearly demonstrates as a proof of principle that the structure of kinetically trapped actin/filamin bundle networks can be irreversibly altered by applying mechanical forces.

In this chapter, a macrorheomter will be used to induce changes in the architecture of actin bundle networks in a precisely controlled way while these structural reorganizations are simultaneously visualized by a confocal microscope. At the same time, the macrorheometer can be used to determine the effect of the induced structural reorganizations on the mechanical network properties. It will be shown that the mechanical

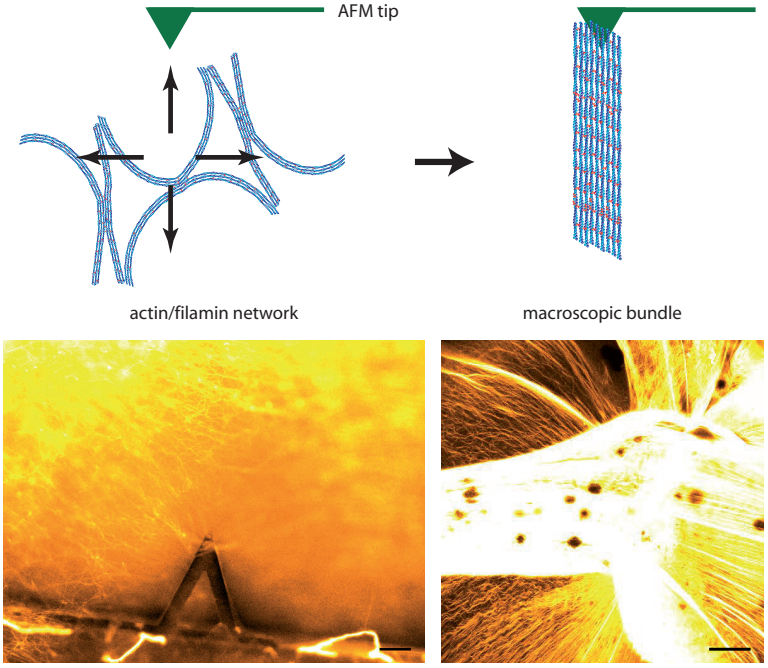

Figure 6.1: Force induced bundling in an actin/filamin bundle network (2.4 µM actin, $R_{\mathrm{fil}} = 0.2$): The tip of an atomic force microscope is moved through a fully polymerized network (left image). By bringing bundles into contact, a macroscopic bundle can be formed, which is stable for at least days (right image). The scale bars denote 100 µm.

response of actin networks bundled by α-actinin or filamin in the irreversible non-linear regime exhibits strong similarities to the so-called Mullins effect (section 6.1). Depending on the concentration of proteins, not only Mullins-like softening is observed, but also cyclic hardening, indicated by an irreversible increase in the nonlinear elasticity as a consequence of repeated loading cycles. Therefore, these networks show a mechano-memory – the maximal applied strain is stored in the network architecture. The simultaneous use of bulk-rheology and confocal microscopy reveals the microscopic origin of the Mullins effect and cyclic work hardening. Specifically it is found that cyclic shearing causes drastic network reorganizations, such as bundling and unbundling of the fibers that is accompanied by the appearance of a negative prestrain.

6.1 Mullins effect

A broad range of materials exhibits dramatic and irreversible changes to their mechanical properties when deformations are applied that are large enough to elicit a nonlinear

response. In many technological applications nonlinear deformations lead to undesirable changes to the material properties. In some instances, irreversible nonlinear deformations provide a simple route to *in situ* alterations of the material properties; as is seen in metals [Polak et al., 2001, Walther and Eifler, 2007] and polymers [Bigg, 2004]. As first reported by Mullins et al. in rubber-like materials [Mullins, 1969], a cyclically applied load can result in an overall softening of the material. Specifically, a lower stress is reached at strains that are lower than the maximum previously applied strain γ_0. The softening is directly dependent on the number of cycles with the most pronounced effect occurring in the first cycle. However, if the system is sheared to a maximum strain $> \gamma_0$, the stress-strain relation exhibits no memory of the previously applied strain (Fig. 6.2).

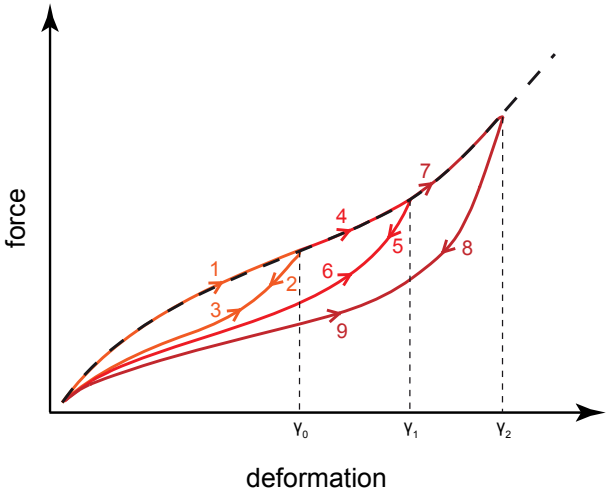

Figure 6.2: Illustration of an ideal Mullins-effect like behavior: Softening occurs if the material is cyclically deformed. A lower force is needed during the second loading cycle to the maximum amplitude γ_0 (path 3 compared to the first loading path 1). If the amplitude is increased beyond γ_0, the loading curve (path 4) follows the path of a single loading experiment (black dashed line). If the material is now cyclically loaded to the new maximal amplitude γ_1, again softening is observed (path 6 compared to path 4).

This type of softening behavior, referred to as the Mullins effect, is observed in pure and filled gums and thermoplastic elastomers [Diani et al., 2009], as well as polymer gels [Webber et al., 2007], living tissues [Rubod et al., 2008, Munoz et al., 2008] and biopolymer networks [Wagenseil et al., 2003]. The microscopic origin of the Mullins effect remains unclear [Diani et al., 2009] in spite of the variety of existing models [Marckmann et al., 2002]. Reconstituted actin networks are ideal candidates for investigating the effect of cyclic loads at the microscopic scale using confocal fluorescence microscopy due to their large mesh sizes, and their propensity to form large bundles (see chapter 5 and [Lieleg et al., 2009b]). Interestingly, bundled actin networks also exhibit strain stiffening (see e.g. chapter 5 and [Kasza et al., 2009]) one hallmark of materials which show the Mullins effect. From a biological perspective, insight into the response of *in vitro* biopolymer networks to cyclic loads may be important, as a passive reorganization

induced by external mechanical stimuli should prove to be a powerful tool to facilitate the high adaptability of living materials.

6.2 Cyclic hardening in actin networks bundled by α-actinin

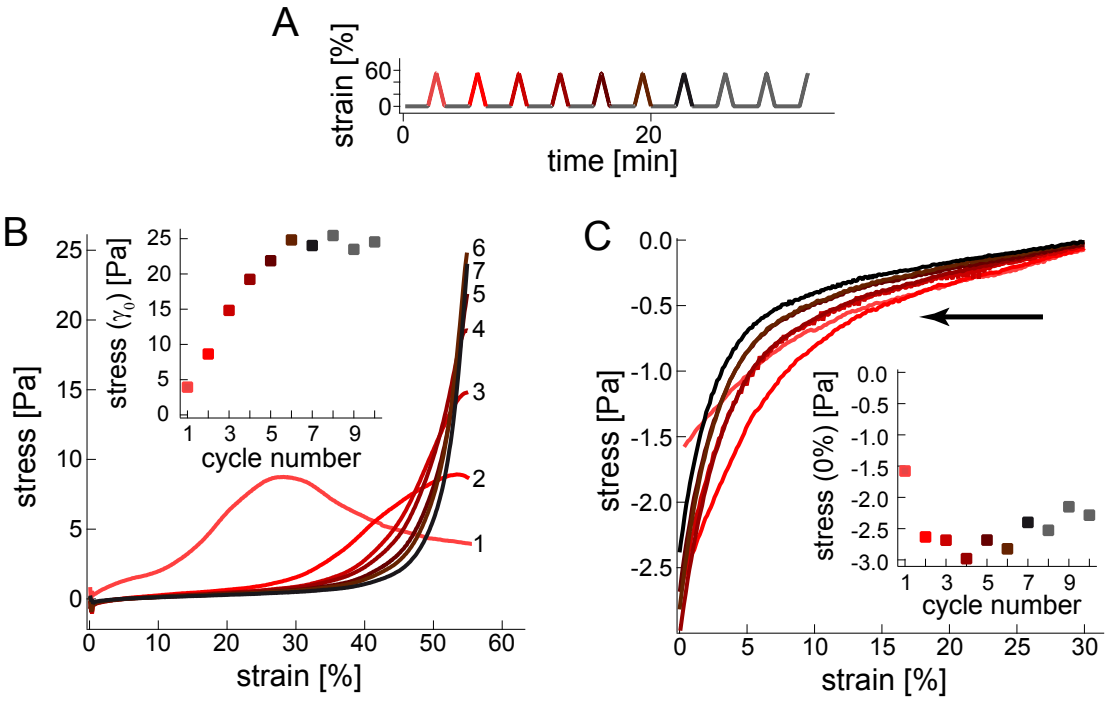

Figure 6.3: (A): The protocol shows the cyclic shearing procedure applied to actin/α-actinin networks at $c_a = 4.75$ µM, $R_{\alpha-\mathrm{act}} = 1$ at 18 °C. The response is shown in (B) and (C). The networks are sheared with 1.4 %/s. The responses to upward (B) and downward shearing (zoom-in shown in (C)) are shown for the first seven cycles in the color denoted in (A), respectively. The arrow in (C) denotes the direction of shear. The stress σ_0 which is reached at the maximal cyclically applied strain γ_0 increases as a function of cycle number (shown in the inset of (B)). The negative stress which is necessary to shear the network back to its initial position saturates after the second cycle and slightly decreases afterwards (shown in the inset of (C)).

Actin networks bundled by α-actinin show a pronounced nonlinear mechanical response to external shear strains. The dependence of the differential modulus on strain in the nonlinear regime can be determined by applying a constant shear rate to the network. Above a certain strain, which is dependent on network parameters as well as external parameters like the shear rate, the network strain hardens (Fig. 6.3); increasingly higher

applied stresses are required to increase the strain. For the network with an actin concentration $c_a = 4.75$ µM and a molar ratio of cross-linking molecules to actin, $R_{\alpha-\mathrm{act}} = 1$, at 18 °C shown in Figure 6.3 a continuous shear strain γ at a rate of $\dot{\gamma} \sim 1.4\ \%\,\mathrm{s}^{-1}$ is applied, the strain hardening response begins at $\gamma \approx 10$ % and the network withstands a maximal stress of $\sigma_{\max} \sim 10$ Pa at $\gamma \approx 25 - 30$ %, after which a decrease of the stress is observed. Repeating the deformation a second time (according to the protocol shown in Fig. 6.3A) results in a significantly different response of the network; the linear stiffness – given by the slope in the stress strain relation – decreases from ≈ 12 Pa to less than ≈ 4 Pa and the strain stiffening response starts not below $\gamma \approx 20$ % (Fig. 6.3B). Each repetition of this deformation protocol results in an increasingly larger linear regime, a continuous decrease of the linear stiffness to ≈ 2 Pa, an increasingly larger differential modulus in the nonlinear regime, higher maximal stresses at the strain amplitude γ_0 and a sharper increase of the modulus in the nonlinear regime (Fig. 6.3B and inset). Thus the cyclic mechanical loading results in networks that can withstand much higher stresses. A result that is in sharp contrast to the Mullins effect, which is accompanied by softening in rubber-like materials.

6.3 Memory effect in actin networks bundled by α-actinin

Interestingly, the actin/α-actinin networks exhibit a history dependence demonstrated by shearing to strains higher than $\gamma_1 > \gamma_0$ after such a cyclic hardening procedure (Fig. 6.4). A sharp peak in the stress-strain relation is observed when γ is slightly above the previously applied maximum strain γ_0. By performing additional cycles up to the new maximal strain γ_1, the network is further cyclically work hardened; concomitantly the previous stress barrier at γ_0 is erased. As shown in Fig. 6.5, the cyclic hardening behavior is qualitatively independent of the strain amplitudes – as long as they are far in the non-linear regime and a significant part of the network is still connected to the surface. However, the saturation value of the stress at γ_0 depends on γ_0 (Fig. 6.5C). The fact that the strain memory is located at the previous maximum strain and not at the maximum stress indicates that the deformation history is coded into a geometrical rearrangement of the network architecture.

6.4 Structural reorganizations account for cyclic hardening

To test this, a simultaneous observation of the structure and the mechanical response is required as a way to pinpoint the microscopic origins of the cyclic hardening behavior. Using the confocal-rheometer a three dimensional structural information is provided while

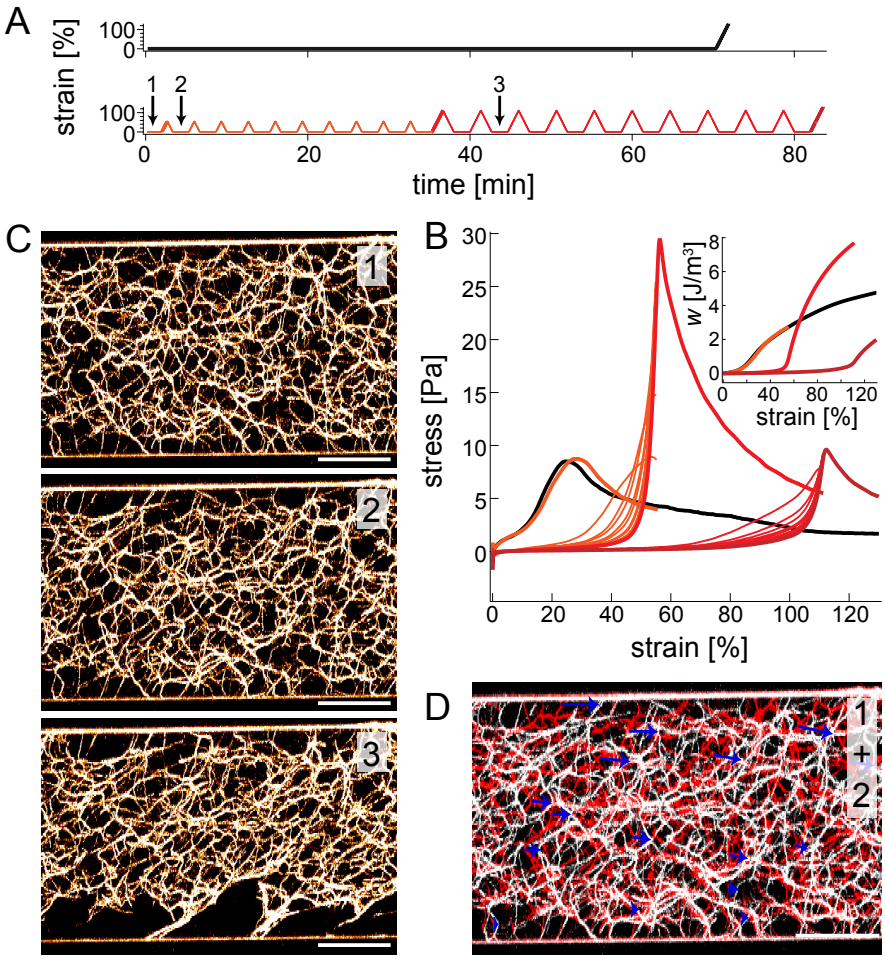

Figure 6.4: The cyclic shearing procedure applied to an actin/α-actinin network at $c_a = 4.75$ µM, $R_{\alpha-\mathrm{act}} = 1$ at 18 °C as shown in Fig. 6.3 is extended by additional cycles at a higher amplitude and a final shearing to a third amplitude. Each color corresponds to a certain strain amplitude. Thick lines mark the first upward shearing to the respective maximum strain. (A): The complete cyclic shearing procedure as well as the control protocol (black) corresponding to the experiments shown in (B) are shown. The networks are sheared with 1.4 %/s. Confocal z-stacks are taken in between the cycles, where the strain is fixed to 0 %. (B): Only the response to upward shearing is shown. Inset: The total energy density necessary to shear the network up to a certain strain is shown as a function of strain. Only the first cycles to a certain strain are shown for simplicity. (C): Confocal images (x-projections of 15 µm are shown for the time points indicated in (A). (D): From the overlay image of the pictures 1 (red) and 2 (white) it can be seen that cyclic shearing causes a negative prestrain of the network. Arrows indicate the displacement of prominent structures to the right. The network has been sheared to the left side. Shearing to the higher strain obviously causes the formation of thicker bundles (3) in (C). The scale bars denote 50 µm.

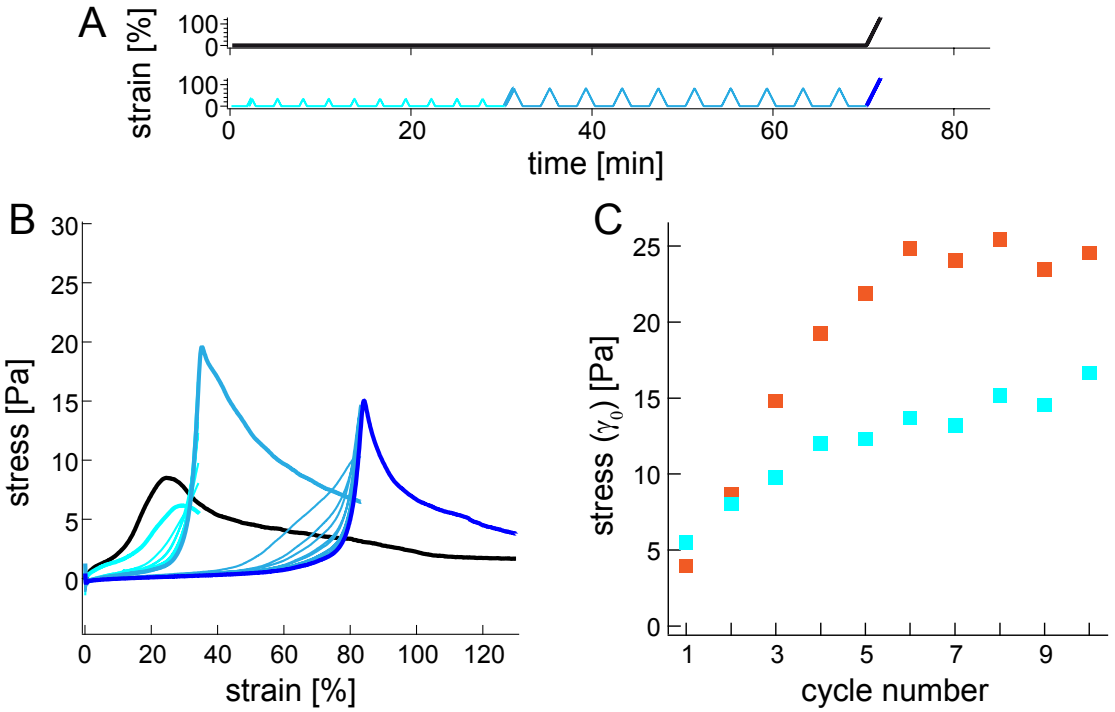

Figure 6.5: The protocol and stress as a function of strain for an experiment analogous to the experiment shown in Fig. 6.4A and B with different strain amplitudes is shown in (A) and (B). The control experiment is shown in black. Again, cyclic hardening is observed: In (C) the stress at $\gamma_0 = 35$ % as a function of cycle number (blue) is compared to cyclic hardening at $\gamma_0 = 56$ % (orange) as shown the inset of Fig. 6.3B.

simultaneously the mechanical response to applied shear strains is measured. First a cyclic deformation protocol is applied to the network while acquiring confocal z-stacks after each cycle at strain $\gamma = 0$ (see Fig. 6.4C).

Initially, the bundled network shown in Figure 6.4 appears homogeneous. The mesh size of the network can be characterized by quantifying the spatial separation between filaments extracted along horizontal and vertical lines within thresholded z-resolved planar confocal images. The distribution of filament spacing is fitted to an exponential decay to obtain an estimate of the characteristic length scale describing the network mesh or pore size [Kaufman et al., 2005]. For the initial network, a mesh size of $\xi \approx 12.5$ µm is obtained. The number of attachment sites of the bundles to the glass substrate is determined to be $\rho \approx 5000$ mm^{-2} by counting within a representative area.

A clear structural reorganization of the network after the first deformation cycle is observed. Indeed, the upper surface has been sheared to the left side and the attachment

points of the network at the upper surface are shifted to the right side (Fig.6.4C). The entire network structure appears as though a negative strain of roughly $\gamma \approx -15$ % was applied (Fig. 6.4D). This observation is verified by the rheology. Focusing on low strains reveals that negative stresses of up to $\sigma \approx 3$ Pa are required to drive the system back to its initial $\gamma = 0$ position (Fig. 6.3C).

In subsequent shear cycles, the network orientation no longer opposes the applied deformations. Most fibers become reorganized into structures that correspond to the spanning distance set by the previously applied strain amplitude. Therefore, the network only bears significant forces when the fibers are strongly stretched. During the subsequent cycles up to γ_0 the shear induced network reorganization becomes increasingly diminished consistent with the observation that the maximal stress reached at γ_0 is saturating with increasing cycle number (Fig. 6.3B, inset) and that the necessary negative strain is saturating and decreasing with cycle number (Fig. 6.3C, inset).

The reorganization described above, taken together with the resulting negative prestrain, provides insights into the physical mechanism of the extended linear regime with lower stresses, and the sharp increase of the modulus near γ_0. In addition, increasingly higher stresses $\sigma_{\max}$ at γ_0 are obtained and also the total energy which is necessary to deform the network up to its complete failure is increased after the cyclic hardening procedure is performed (Fig. 6.4B, inset). Due to the viscoelastic character of the network, the reorganization of attachment points could account for this effect. However, it might also indicate that a wholesale reorganization of the network constituents occurs; this is directly observed in cycles with strains to $\gamma = 112$ %. The cyclic shearing results in drastic bundle fusion and reorganizations while attachment points to the surface are lost thus lowering the density of attachment sites from $\rho \approx 5000$ mm^{-2} to only $\rho \approx 500$ mm^{-2}.

6.5 Stepwise shearing of actin networks bundled by α-actinin

To better understand the process of network reorganization a stepwise shear is applied while visualizing the network response (Fig. 6.6). Stepwise shearing to $\gamma_0 = 56$ % results in continuous rupture of attachment points and an overall contraction of the network with increasing strain. The detachment from the glass appears to be cooperative; on a length scale on the order of the field of view, bonds break only at one surface while all bonds on the opposing surface remain unaffected. The observed network contraction correlates with a decrease in the measured stress (Fig. 6.6C). Shearing back to $\gamma = 0$ results only in a partial relaxation of the network contraction (Fig. 6.6). Some of the detached bundles

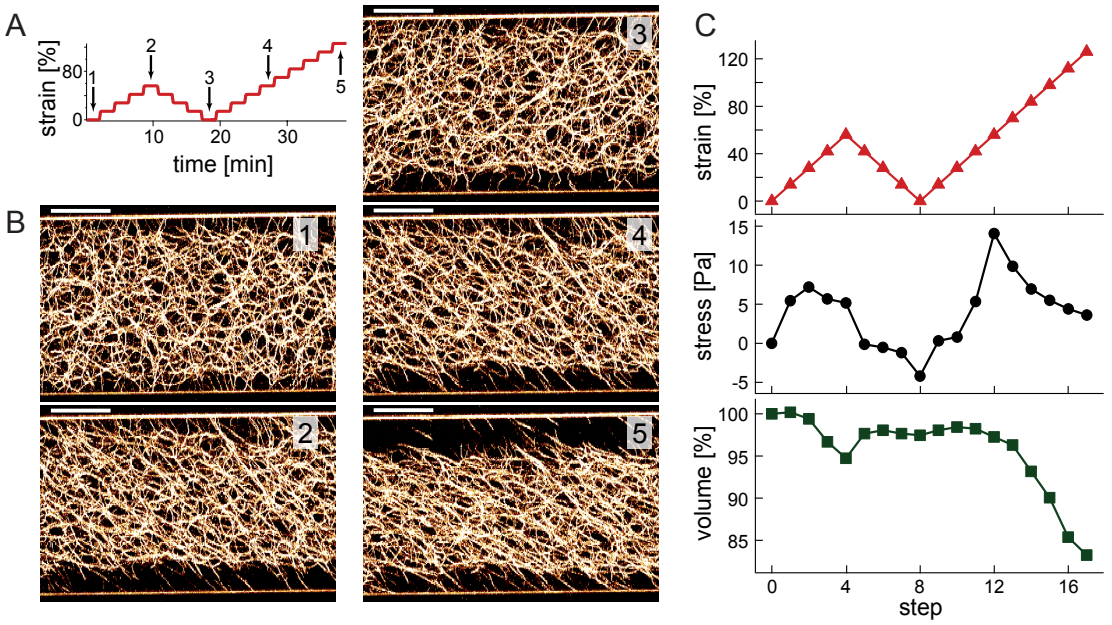

Figure 6.6: Shearing an actin/α-actinin network at $c_a = 4.75$ µM, $R_{\alpha-\mathrm{act}} = 1$ at 18 °C stepwise allows to image the network with a confocal microscopic during cyclic loading. Indeed cyclic hardening can be observed if the network is sheared up to 56 % then back to 0 % and then up to a higher strain (Fig. 6.7). In between the steps of 14 % the strain is hold fixed for 2 minutes and a confocal z-stack is taken. The time points where the micrographs 1-5 have been taken are indicated in the protocol (A). (B): During the shearing of the network to 56 % many bundles loose contact to the lower surface (confocal images 1 and 2). An irreversible reorganization is observed when the network is sheared back (3). If the network is sheared up again, distinctly higher stresses are reached. Shearing to a higher stress results in a peak in the stress-strain relation roughly at the previous maximum strain 56 %. Interestingly the network now looses contact mainly from the upper surface (5). Confocal images are x-projections of 35 µm. The scale bars denote 50 µm. (C): Strain, stress and the network volume normalized on the initial value are shown as a function of step number. As the network shrinks only in z-direction, the volume is proportional to the thickness of the network. The thickness is obtained from an intensity line profile along the z-direction and averaged over ≈ 250 µm in x and y direction, respectively. The position where the fluorescence intensity reaches half of the maximum value is defined as the boundary of the network.

find new contact points at the glass surface in locations where rupturing occurred. After establishing a new connection, a negative prestrain returns when the strain direction is reversed. In the subsequent deformation cycle, very few dramatic reorganization events occur. The reestablished attachment points remain in place and the network volume is almost constant and only excess lengths are extended when $\gamma_0 = 56$ %. Above γ_0, rupturing, shrinkage, and reorganizations of the network are once again observed. This time most rupture events occur at the opposite – in this case the upper surface; suggesting that the reformed attachment sites at the lower surface are strengthened during the first cycles and demonstrating the cooperative nature of detachment.

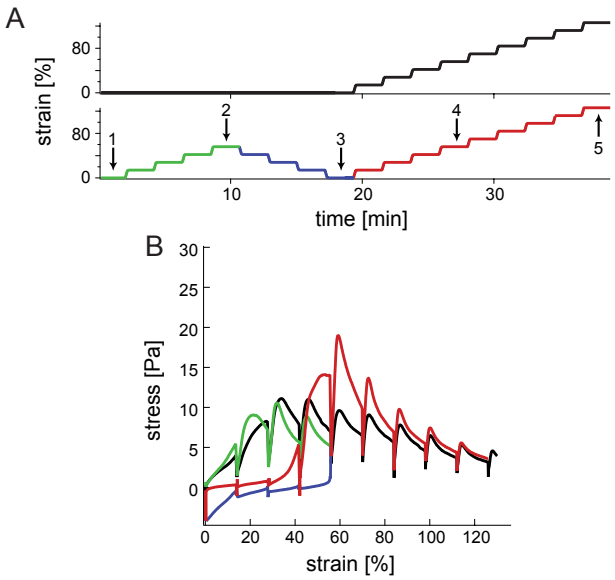

Figure 6.7: The response of an actin/α-actinin network at $c_a = 4.75$ µM, $R_{\alpha-\mathrm{act}} = 1$ at 18 °C to stepwise shearing protocols (A) with a shear rate of 1.4 %/s as shown in (B) is shown. Colors are used to indicate different sections of the stepwise shearing protocol. Cyclic hardening can be observed if the network is sheared up to 56 % then back to 0 % and then up to a higher strain.

6.6 Cyclic hardening is sensitive to network architecture

To confirm that the observed network reorganizations are a necessary precondition for the measured strain hardening effect, a system with comparable microstructure that lacks the cyclic hardening response (Fig. 6.8) can be tested. Networks with a lower effective α-actinin concentration exhibit a cyclic softening in accordance with the classic Mullins effect (Fig. 6.8B, F) and do not show dramatic reorganizations with an encoding of a prestrain (Fig. 6.8G). However, through the cyclic shearing process, some attachments to the surface are lost, which may explain the observed similarity to the Mullins effect. The stress necessary to shear the network back to its initial position is compared with that of a network with an effectively higher α-actinin concentration, which shows the cyclic

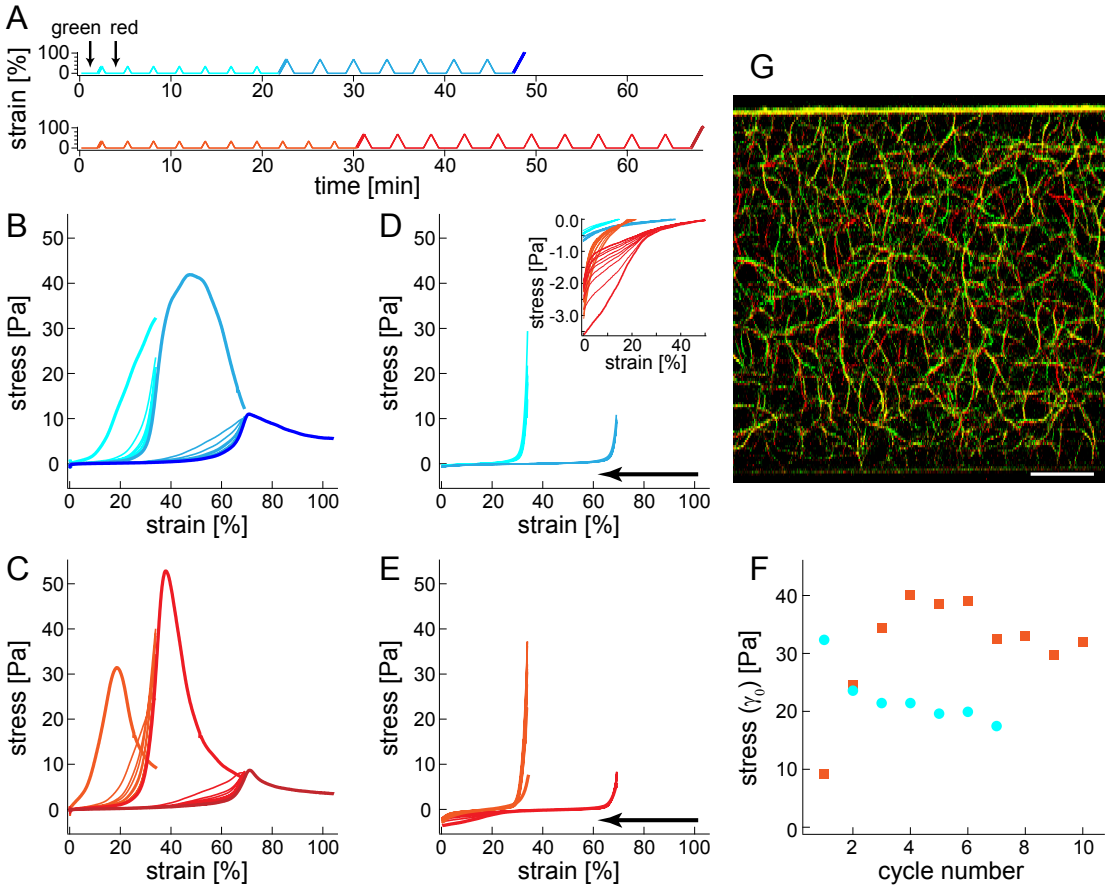

Figure 6.8: The cyclic hardening behavior is very sensitive to protein concentrations. Actin/α-actinin networks at $c_a = 9.5$ µM, $R_{\alpha-\mathrm{act}} = 1$ at 18 °C show a clear cyclic hardening (red – different strain amplitudes are indicated by different red colors) while it is hardly observable for actin/α-actinin networks at $c_a = 9.5$ µM, $R_{\alpha-\mathrm{act}} = 0.5$ at 21 °C (blue – different strain amplitudes are indicated by different blue colors). Thick lines mark the first upward shearing to the respective maximum strain. The responses corresponding to the protocols shown in (A) to upward and downward shearing (indicated by an arrow) are shown in (B, C) and (D, E; the inset in D shows a zoom in at low strains), respectively. A shear rate of 1.4 %/s and pauses of 120 s are used for both experiments. It can be seen in D and E that for the network showing the strong cyclic hardening, distinctly higher negative stresses are reached during the downward shearing. (F): The stress at the lower cyclically applied strain 35 % as a function of cycle number is shown for both networks. (G): For $c_a = 9.5$ µM, $R_{\alpha-\mathrm{act}} = 0.5$ at 21 °C no negative prestrain results if the network is cyclically sheared to 35 %/s. The micrograph shows an overlay of confocal images (x projections 21 µm before (green) and after (red) the first cycle). The scale bar denotes 25 µm.

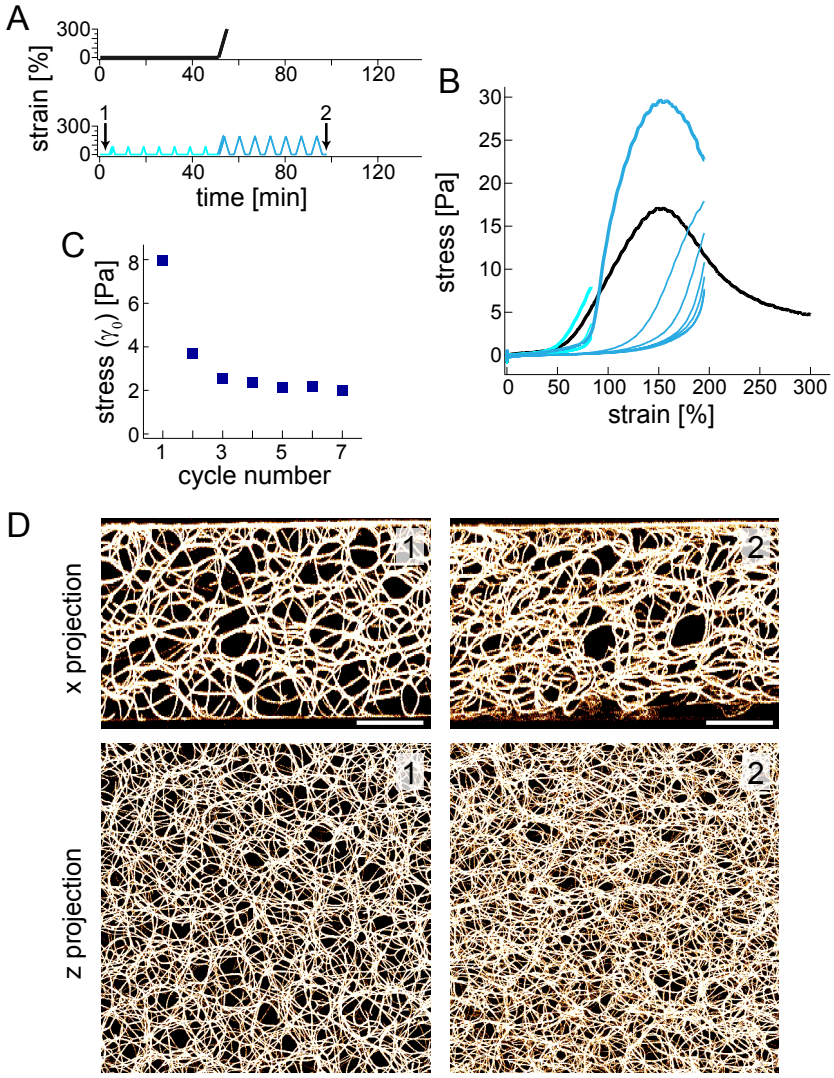

Figure 6.9: Actin/filamin networks at $c_a = 9.5$ µM, $R_{\text{fil}} = 0.1$ at 21 °C show cyclic hardening. (A): The protocol for the control experiment (black) and the cyclic shearing procedure (blue – different strain amplitudes are indicated by different blue colors) are shown. Thick lines mark the first upward shearing to the respective maximum strain. (B): The black line shows the network response to a constant shear rate 1.4 $\%/s$. Blue colors show the response to the cyclic shearing procedure shown in (A). Thick lines show the response to the first cycle applied up to the respective maximum strain. Only the response to upward shearing is shown. At the maximal cyclically applied strain the stress decreases as a function of cycle number (C). Higher stresses are reached beyond this strain (B). Confocal images (x projection of 63 µm; z projection of 130 µm - surface near regions are not shown in order to reduce the background fluorescence) which are taken during the experiment (time points where the images are taken are indicated in the protocol (A)) reveal that cyclic shearing causes unbundling. A larger number of thin bundles appears and the mesh size decreases. The scale bars denote 50 µm and are also valid for z-projections.

hardening effect. For the network that hardens, the negative stresses reached at $\gamma = 0$ are far higher than for the network with the lower α-actinin concentration (Fig. 6.8D, E) – although the maximum positive stresses which are reached during the cyclic shearing procedure are comparable in magnitude for both networks (Fig. 6.8B, C). This supports that the negative prestrain observed with confocal microscopy accounts for the negative stresses and contributes to the cyclic hardening effect.

6.7 Cyclic hardening in actin networks bundled by filamin

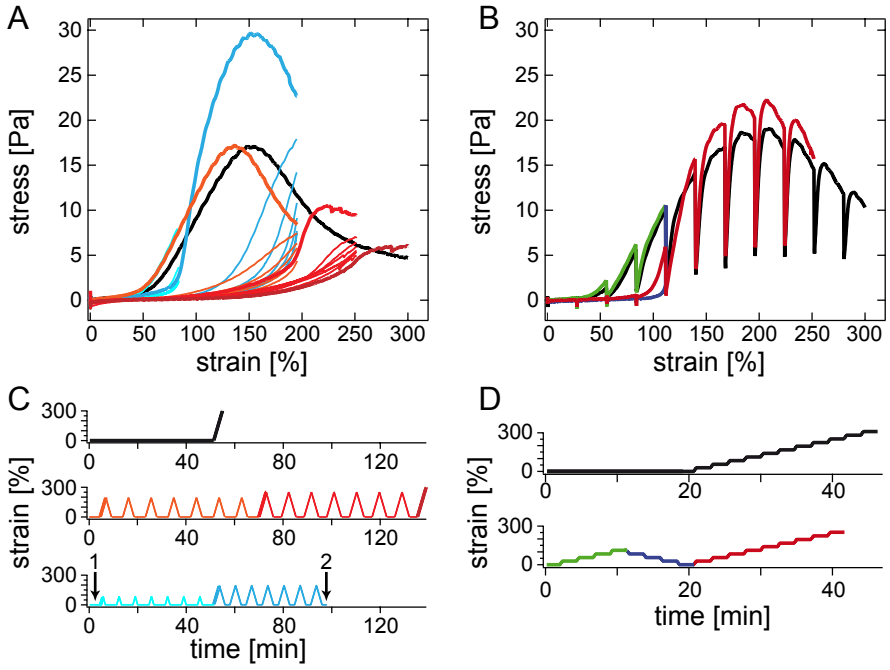

Figure 6.10: Actin/filamin networks at $c_a = 9.5$ µM, $R_{\text{fil}} = 0.1$ at 21 °C show cyclic hardening. At the cyclically applied maximum strain the stress decreases as a function of cycle number. Higher stresses are reached beyond this strain. (A): The black line shows the network response to a constant shear rate 1.4 $\%/s$. Blue and red show the responses to the cyclic shearing procedures shown in (C). Thick lines show the response to the first cycle applied up to the respective maximum strain. Only the response to upward shearing is shown. (B): The black line shows the response to stepwise shearing protocols as shown in (D). A shear rate of 1.4 %/s is used. Also this stepwise protocol causes strain hardening. During the second cylce (red line) higher strains than in the control experiment (black line) are reached.

To test if the high binding propensity of α-actinin is a precondition for the observed reorganization and cyclic hardening behavior [Lieleg et al., 2009b, Lieleg et al., 2010],

the actin bundling protein filamin is utilized, which similar to α-actinin kinetically traps actin networks (chapter 5). The architecture of the bundled actin/filamin networks, at the concentrations chosen, resembles that of actin/α-actinin networks. Interestingly, cyclic shearing of actin/filamin networks also results in hardening (Fig. 6.9): In contrast to the response of actin/α-actinin networks, the stress reached at the maximal cyclically applied strain γ_0 decreases as a function of the cycle number (Fig. 6.9C) – in accordance with the classic Mullins effect. However, if the network is sheared to larger strains, significantly higher stresses than in the control measurement are obtained. Also, stepwise shearing of the network results in a higher maximum stress if a single stepwise cycle to a lower strain is previously applied (Fig. 6.10). Confocal imaging reveals that cyclic shearing not only results in a negative prestrain, but in addition the actin/filamin bundles are partially unbundled. As shown in Figure 6.9D, a larger number of thin bundles is observed after the cyclic shearing procedure resulting in a decrease in the mesh size. Quantitative image analysis reveals that the mesh size of the network shown in Figure 6.9 decreases from initially 34.3 µm to 27.4 µm at time point 2 (see Fig. 6.9). One potential consequence of the unbundling is an increase in the length of bundle-paths percolating between the surfaces. Thus, the cyclic training results in bundles, which are longer than the maximal cyclically applied strain would imply. In this scenario, higher strains have to be applied to fully stretch bundles and detach them from the surface. This causes that the sharp increase of stress is seen at higher strains, while the stress reached at γ_0 decreases.

The fact that also for actin/filamin bundle networks cyclic loads result in irreversible structural reorganizations which manifest themselves in the non-linear mechanical response, suggests that this might be a typical feature of kinetically trapped actin bundle networks.

6.8 Cyclic hardening – a unique property of actin bundle networks

Using confocal-rheology revealed that bundled actin networks demonstrate a significant mechanical history dependence, which is encoded into the network architecture as a strain memory. This sets the mechanical response of these biopolymer networks. At low concentrations of the crosslinking protein α-actinin, a cyclic softening is observed, similar to the classic Mullins effect – previously observed in rubber-like polymer networks [Diani et al., 2009]. By simultaneously recording the rheology while visualizing the mechanical response of bundled actin networks, the classic Mullins effect is traced back

to detachments of bundles. In contrast, strongly crosslinked α-actinin networks show a pronounced cyclic hardening behavior. Cyclic shearing results in a reorganization of the network architecture, accompanied by the development of a negative prestrain, and a reorganization of the network constituents. Shearing enables a reorganization of the bundles through a disruption of network structures, that leads to new contacts being formed between bundles. The surface-network interface seems to play an important role for the shear induced network reorganization. The most drastic rupture events occur at the surface – this is presumably the case because these links are the weakest in the system. A remaining challenge is understanding the intricate balance between rupturing events, reorganization and prestrain and their combined consequence for the mechanical response. The high binding propensity of the α-actinin and filamin coupled with their tendency to kinetically trap actin networks seem to be a prerequisite for the observed effects; actin networks cross-linked by other cross-linking proteins, such as fascin or HMM do not cyclically harden at the conditions tested.

Cyclic work hardening is not expected for flexible polymers [Rabinowitz and Beardmore, 1974]. However, it has been shown in this chapter that semi-flexible polymers bundled by transient cross-links provides a material that demonstrates work hardening and mechano-memory. Such a smart material may be interesting for the ability to adapt to repeated deformations. The experiments presented here demonstrate that rather simple composite biological systems consisting of solely actin and cross-linking proteins passively adapt their structural and mechanical properties upon external mechanical stimuli. Living cells may make use of such mechanisms to adapt or reorganize cytoskeletal structures through external mechanical stimuli. It can be speculated that a strain memory effect, where the material drastically softens within an applied strain range, but exhibits a high stress barrier at higher strains, might be utilized in biological systems to allow for movement in a certain but adaptable range while maintaining mechanical stability.

6.9 Analogy to shape memory alloys

The classic Mullins effect like response to cyclic shearing, which has been observed here also for certain actin bundle networks (see chapter 6.6), is a generic behavior which occurs for a broad range of polymer materials. On the other hand, cyclic hardening is a unique response, which has never been shown for any polymer system before. However, a surprisingly similar response to cyclic loading has been observed for a very different kind of material, namely shape memory alloys. In the following, a phenomenological analogy will be drawn, between the cyclic deformation behavior of shape memory alloys and both the Mullins effect and the cyclic hardening response in actin bundle networks.

6.9.1 Shape memory alloys

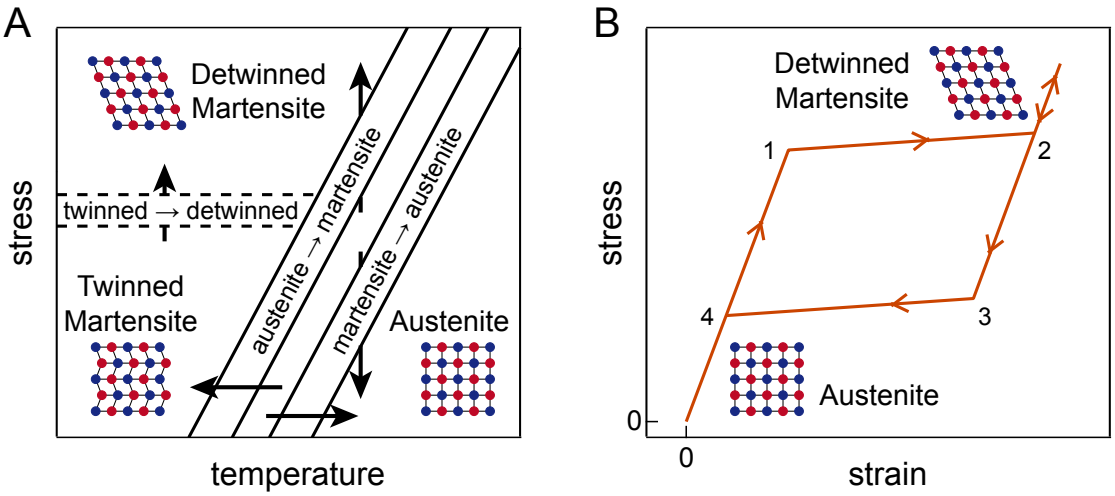

Figure 6.11: (A): Stress-temperature phase diagram of shape memory alloys. Depending on the temperature, SMA exist as martensite or austenite. Applying a critical stress results in the formation of detwinned martensite. (B): Idealized pseudoelastic response of shape memory alloys. The stress induced transition from austenite to detwinned martensite occurs during loading between point 1 and 2. The reverse transition during unloading occurs between 3 and 4. Both illustrations are adapted from [Kumar and Lagoudas, 2008].

Shape memory alloys (SMA) have the ability to recover their shape when the temperature is increased [Otsuka and Ren, 1999, Kumar and Lagoudas, 2008]. This shape memory effect is based on the fact that, depending on the temperature, SMA exhibit two different crystal structures (Fig. 6.11A). The cubic high temperature phase is called *austenite*, whereas the tetragonal, orthorhombic or monoclinic low temperature phase is called *martensite*. The transition from one phase to the other occurs by shear lattice distortion, which means that during this transformation each lattice point maintains its neighbor sites. The martensitic crytals can have different orientations. Depending on their orientation, they are classified into different so-called *variants*. An assembly of martensitic crystals can therefore either exist in the *twinned* state, where the variants "self-accomodate", or in a *detwinned* state, which is dominated by a specific variant. Applying stress to twinned martensite causes a gradual transformation to detwinned martensite (Fig. 6.11A), which results in a macroscopic shape change. The stress induced transformation of twinned to detwinned martensite at low temperature is irreversible even after unloading – resulting in a plastic deformation of the material.

However, increasing the temperature after unloading results in a transition to austenite and goes along with a recovery of the initial shape (*shape memory effect*).

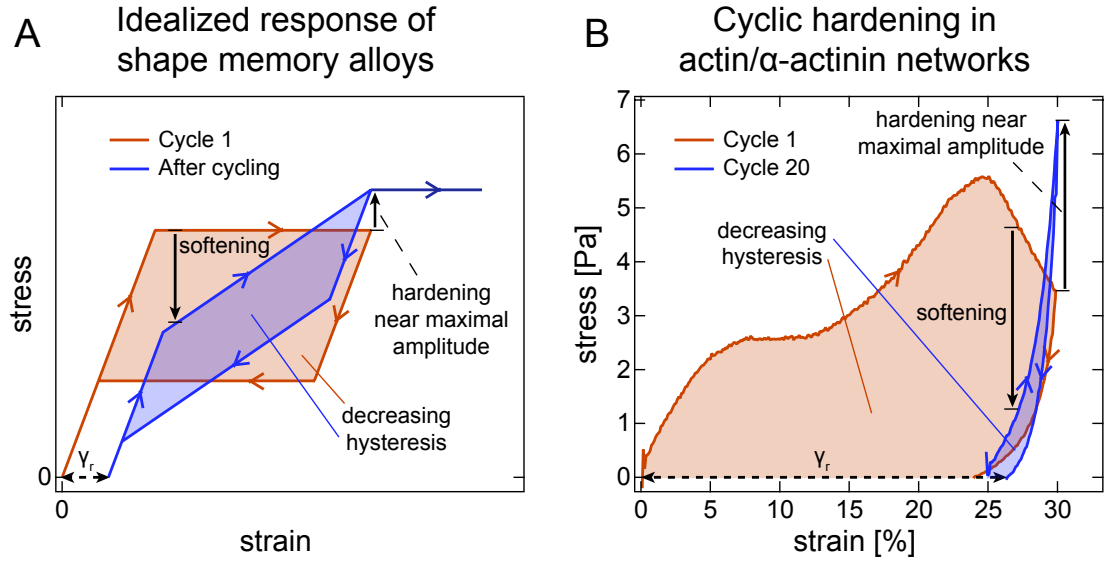

Figure 6.12: (A): shows the idealized response of shape memory alloys to cyclic loading as proposed by [Lim and McDowell, 1995]. (B): Response of an actin/α-actinin network at $c_a = 4.75$ µM, $R_{\alpha-\text{act}} = 1$ at 18 °C to a modified cyclic hardening procedure. The network is sheared with 1 %/s to 30 % and the backward shearing is stopped as soon as zero stress is reached. Between the cycles, the sample is allowed to relax for two minutes at zero stress. The observed response to cyclic deformations is qualitatively similar to that of shape memory alloys.

Also the high temperature austenite is transformed to detwinned martensite if a critical stress is applied (Fig. 6.11A). In contrast to the transition from twinned to detwinned martensite, the stress-induced transition from austenite to detwinned martensite is reversible upon unloading. An idealized stress-strain response is shown in Fig. 6.11B [Huo and Müller, 1993, Kumar and Lagoudas, 2008]. During loading, an elastic response is observed until at a critical stress the transition to detwinned martensite starts (point 1 in Fig. 6.11B), which results in a drastic decrease of the non-linear elastic modulus. As soon as the transformation to martensite is complete (point 2), the elastic modulus increases again, and the elastic response of the martensite is observed. During unloading, the stress at which the reverse transition to austenite occurs is lower than the transition stress to martensite during loading (point 3 to 4), demonstrating that the transition is a non-equilibrium process. As a consequence of this hysteresis, energy is dissipated during the loading-unloading cycle (Fig. 6.11B). Therefore, such behavior is referred to as *pseudoelasticity*.

6.9.2 Cyclic hardening in actin bundle networks and shape memory alloys

The idealized response of SMA to cyclic loading which is shown in Fig. 6.11B does not take into account any changes of this response that might occur if the cycle is repeated. Yet, it has been demonstrated that SMA can show a pronounced change of the stress-strain response during repeated cyclic loading [Miyazaki et al., 1986, Lim and McDowell, 1995, Tahara et al., 2009]. Fig. 6.12A depicts an idealized response of a SMA to a cyclic loading procedure, where the SMA is repeatedly loaded to a certain amplitude – which is within the strain range where the austenite to martensite transformation occurs – and subsequently unloaded to zero stress. Comparing this response to that of an actin/α-actinin bundle network to a similar cyclic loading procedure (Fig. 6.12B), reveals a striking analogy of the phenomenological features:

(i) The response is not ideally elastic – energy is dissipated during each loading cycle.

(ii) The hysteresis energy continuously decreases with the cycle number.

(iii) A residual strain accumulates in the direction of the applied strain.

(iv) The material softens at strains which are small compared to the maximal applied strain.

(v) The maximal stress which is reached at the maximal applied strain eventually increases with the cycle number [Lim and McDowell, 1995] – or the stress which is reached slightly beyond the previously maximal strain if the amplitude is increased, as it is the case for actin/filamin bundle networks and certain SMA [Ma et al., 2010]. In the case where the stress at the maximal strain does not increase but is rather constant (e.g. [Tahara et al., 2009]), the behavior of SMA resembles that of the classic Mullins effect.

(vi) Increasing the maximal amplitude after repeated cyclic loads results in a peak or kink roughly at the previously applied maximal strain. Cyclic loading to the new maximal amplitude erazes this memory (see [Lim and McDowell, 1995] for SMA; chapter 6.3 for actin/α-actinin networks). The material memorizes the largest amplitude that has been applied (see e.g. [Ma et al., 2010] for SMA).

Obviously, SMA and actin bundle networks show a phenomenologically strongly analogous response to cyclic loads. For the actin bundle system the observed behavior has been traced back to strain induced reorganizations of the bundle architecture. In the case of SMA, cyclic loading has been proposed to cause the gener-

ation of heterogeneous internal stress fields, which are probably mainly based on point defects [Ma et al., 2010], which stabilize the martensitic inclusions [Miyazaki et al., 1986, Lim and McDowell, 1995, Ma et al., 2010]. This results in residual martensites at zero stress, which together with the generation of dislocations in the austenite phase accounts for the accumulation of residual strain [Miyazaki et al., 1986, Lim and McDowell, 1995, Tahara et al., 2009]. Moreover, the oriented internal stresses facilitate the reformation of martensite during the following cycles in the same strain range and thereby result in a decrease of the stress which is required to induce martensitic transformation.

In addition to the surpisingly similar phenomenological behavior of actin bundle networks and SMA, to a certain degree an analogy can be drawn even for their microscopic origins. In both materials, the maximal applied strain is encoded into the microstructure of the initially isotropic material. The structural reorganization during deformation results in a metastable state with an anisotropy that correlates with the applied strain range and ensures that a repeated deformation is energetically more favorable – resulting in lower stresses at small strains. Increasing the amplitude results in new, irreversible structural reorganizations, which are similar to the reorganizations which would occur in juvenile samples. This analogy holds true not only for actin bundle networks, but also for the much more generic Mullins effect [Diani et al., 2009]. Since in most cases the structural reorganizations which give rise to Mullins effect like behavior are not unambiguously identified, the mechanical response is often described by phenomenological models [Diani et al., 2009]. Although it is strongly suggested by the analogous mechanical behavior, future studies have to clarify whether such modeling efforts can be further extended to a generic model, which even includes SMA.

In actin bundle networks as well as in SMA cyclic loading can – under certain conditions – result in an increase of the stress at the maximal applied strain. However, for both materials it is still not clear which parameters determine whether cyclic hardening occurs. Setting cytoskeletal networks in the general context of materials which show strain induced structural reorganizations might not only help to qualitatively model their behavior but might also help to gain insights into the physical principles which determine their macroscopic response.

7 pH modulates actin network mechanics in multiple ways

It has been shown in chapter 5.1 that the final architecture of actin/filamin bundle networks is hardly dependent on the filamin concentration but can be sensitively tuned by the actin concentration. This can be explained by the aggregation controlled network formation, which is critically dependent on the time scales of filament formation and bundling. In order to further confirm this hypothesis it would be ideal to tune one of the timescales without changing the protein concentrations of the system. In this chapter it will be shown that this can be achieved by a variation of pH. Increasing the pH causes a slow down of the actin/filamin bundle network formation. As expected from chapter 5.1, this results in a larger mesh size of the final network. The fact that actin/filamin networks can be strongly modified by a variation of pH suggests that tuning the local pH might be a elegant way for cells to regulate cross-linked cytoskeletal structures. In order to test whether the strong pH dependence is unique for the kinetically trapped actin networks as they are formed by filamin, also other cross-linking proteins – namely cortexillin and fascin – are investigated. It will be shown that the effect of pH on the structural and mechanical properties of actin systems is strongly dependent on the cross-linking protein. A variation of pH strongly tunes the bundling activity of cortexillin. On the other hand, the bundling protein fascin – which forms more equilibrated networks – almost completely suppresses the intrinsic pH dependence of pure actin solutions. Together with Simone Köhler [Köhler, 2012] it is shown that the molecular motor myosin-II shows a pH dependent cross-bridge strength to actin, which results in a pH dependence of the macroscopic contractility of actomyosin gels. The distinct pH dependencies of the different cross-linking protein can be employed to tune this pH dependent contractility of cross-linked active actin networks.

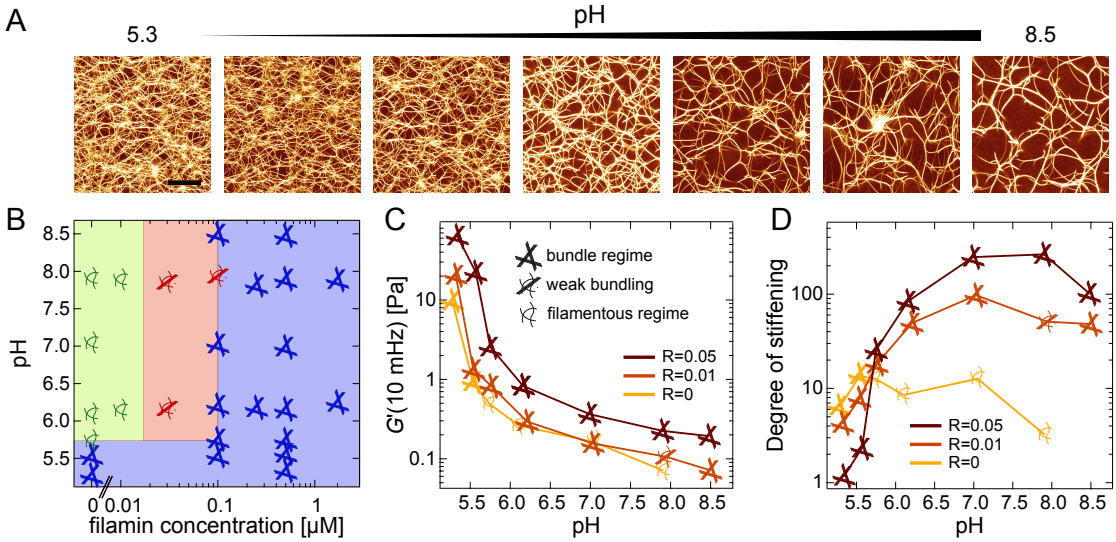

Figure 7.1: (A): Confocal images (maximum projection of 20 µm stacks) of actin/filamin networks (10 µM actin, 0.5 µM filamin): A clear increase of the mesh size is observed with increasing pH. The scale bar denotes 20 µm. Images correspond to the data points ($R = 0.05$, dark red) shown in C and D. (B): Structural state diagram of actin/filamin networks (10 µM actin) as determined from confocal images as a function of pH and filamin concentration. Green symbols denote filamentous networks, red symbols denote weak bundling, blue symbols denote the bundle regime. The elastic modulus $G'(10\ \mathrm{mHz})$ (C) and the degree of stiffening (D) are shown as a function of pH for F-actin (10 µM) in the presence of different concentrations of filamin (0, 0.1 and 0.5 µM). The symbols in (C) and (D) denote the structure of the corresponding network as determined from confocal images.

7.1 Actin/filamin networks exhibit a complex pH dependence

In order to characterize the pH dependence of actin/filamin networks, confocal imaging is used to determine their structure as a function of filamin concentration and pH. As summarized in the structural state diagram shown in Fig. 7.1B, the critical filamin concentration which is needed for bundle formation does not significantly change with pH. Yet, the structure of the actin/filamin bundle networks strongly depends on pH: It is obvious from the confocal images shown in Fig. 7.1A that the mesh size of the networks increases with pH. In chapter 5.1 it has been proposed that due to the aggregation controlled growth process, the final network structure of actin/filamin bundle networks is given by the interplay of the timescales of filament formation, elongation and bundling. Considering this non-equilibrium nature of actin/filamin networks, the pH dependence

of their mesh size can be can be rationalized from the pH-dependent kinetics of both actin nucleation and actin filament elongation [Zimmerle and Frieden, 1988, Wang et al., 1989]. At a lower pH, actin filaments are formed faster, which in turn accelerates the formation of an interconnected actin/filamin network. This can directly be seen by following the network formation using macrorheology: The faster formation of the network at low pH is manifested in a faster saturation of the network elasticity (Fig. 7.2). As a consequence, the filaments have less time to fuse into large bundles before a further reorganization of the network constituents is hindered. Thus, at low pH the network ends up with thinner bundles and a smaller mesh size.

It remains to be shown whether the pH dependence of the network architecture, which originates in the network formation process, is also reflected in the mechanical properties. As shown in Fig. 7.1C, the elastic modulus of actin/filamin networks can indeed be significantly tuned by pH. However, for both filamin concentrations tested, this pH dependence is surprisingly almost identical to that of pure F-actin - only shifted to higher values. This is remarkable considering the completely different network geometries: While filamin induces bundle networks with varying mesh size over the whole range of pH, the pure actin solutions are filamentous except for very low pH (≤ 5.54), where spontaneous bundling is observed (Fig. 7.1B). Note that this pH is close to the isoelectric point of actin of 5.4, which could explain the spontaneous bundling.

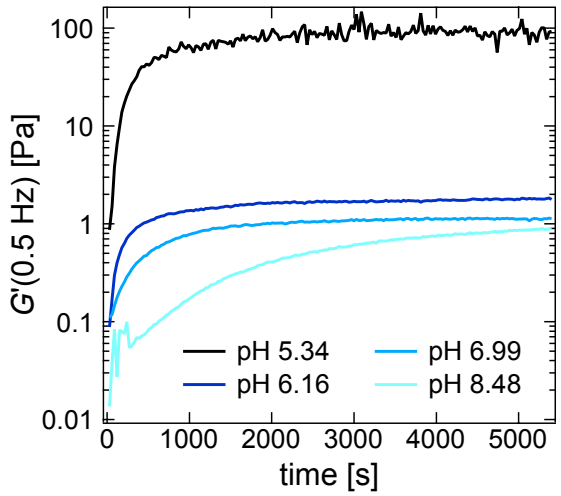

Figure 7.2: The formation of actin/filamin networks (10 µM actin, 0.5 µM filamin) is followed by recording the elastic modulus G' at 0.5 Hz. While the speed of network formation is rather constant at low pH, it obviously slows down above pH 6.

It has been shown in chapter 5.2, that filamin has a surprisingly low effect on the elastic modulus at low deformations, i.e. in the linear regime. Thus, the fact that a variation of pH strongly modifies the mesh size of the actin/filamin bundle networks might only be hidden in the linear regime and might be reflected in the non-linear response to high

deformations. Fig. 7.1D shows the pH dependence of a characteristic parameter, the degree of stiffening, which is defined here as the ratio of the maximal reached differential modulus over the differential modulus at small deformations. For pure F-actin solutions the degree of stiffening slightly increases with decreasing pH - until at very low pH spontaneous bundling occurs. A much stronger pH dependence is observed for actin/filamin bundle networks: By a variation of pH the degree of stiffening can be tuned over more than two orders of magnitude. Thus, while addition of filamin to actin networks does not significantly change the qualitative pH dependence of the elastic modulus in the linear regime, it allows to sensitively tune the pH dependence of the non-linear network response.

In summary, it has been demonstrated that the structural and mechanical properties of actin/filamin networks show a strong but complex pH dependence, which cannot be simply explained by a pH dependence of the actin/filamin interaction but originates in the process of network formation. In the case of actin/filamin networks pH provides a simple parameter to tune the speed of network formation without changing the network constituents. This allowed to confirm that the structure of actin/filamin bundle networks is given by the interplay of filament nucleation, elongation and bundle formation, as proposed in chapter 5.

7.2 The bundling activity of cortexillin is pH dependent

Cortexillin-I is an actin bundling protein, which is enriched in the cortical region of locomoting cells and plays a crucial role for cell shape regulation during cytokinesis and mechanosensation [Faix et al., 1996, Ren et al., 2009]. Cosedimentation experiments already indicated that binding of cortexillin-I to actin is pH dependent [Faix et al., 1996]. This raises the question, how the bundling activity of cortexillin is modified by a variation of pH. As summarized in the structural diagram shown in Fig. 7.3A, the bundling activity of cortexillin is indeed strongly dependent on pH. Whereas at pH 6 strong bundling is observed already at a rather low cortexillin concentration of 0.25 µM, for increasing pH the onset of bundling continuously shifts to higher cortexillin concentrations. Finally, at pH 8.5 no bundles are observable even at the highest cortexillin concentration tested (2.5 µM). Thus, a transition from a filamentous, cross-linked actin/cortexillin network to a bundle network can be achieved either by an increase of the cortexillin concentration or by a decrease of pH (Fig. 7.3B).

As shown in Fig. 7.3C, the pH dependent bundling transition of actin/cortexillin networks is reflected in their mechanical response: While only a weak increase of the elastic modulus is observed at low concentrations of cortexillin, the elastic modulus strongly

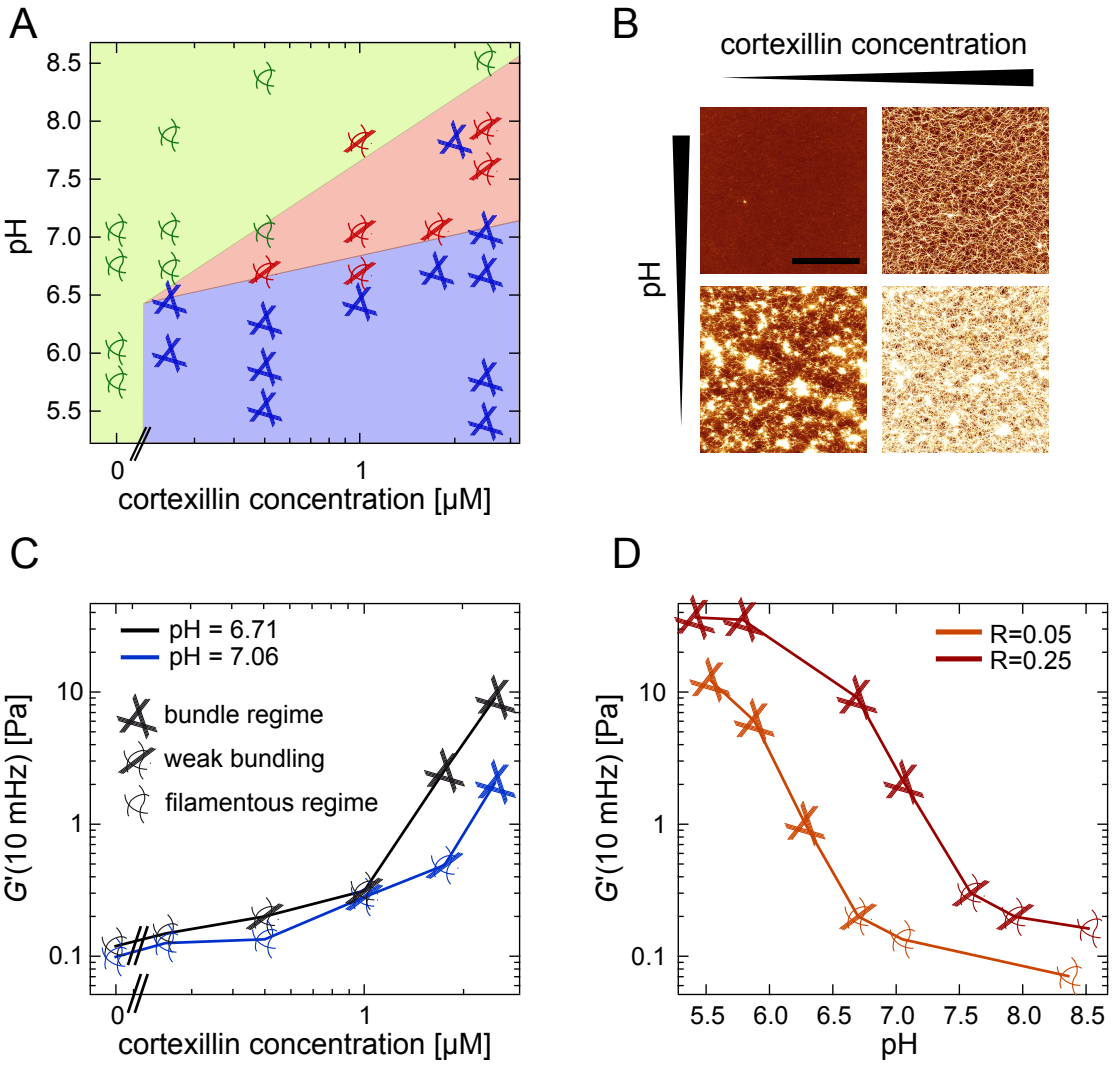

Figure 7.3: (A): Structure of actin/cortexillin networks as determined from confocal images as a function of pH and cortexillin concentration. (B): Confocal images (maximum projection of 50 µm stacks) of actin/cortexillin networks at different pH values ($\approx$ 5.75 and $\approx$ 6.63) and cortexillin concentrations (0.5 µM and 2.5 µM). The scale bar denotes 100 µm. Bundling can be induced either by an increase of cortexillin concentration or a decrease of pH. (C): Elastic modulus $G'(10\ \text{mHz})$ as a function of the cortexillin concentration for F-actin (10 µM) at different pH values (6.71 and 7.06). (D): Elastic modulus $G'(10\ \text{mHz})$ as a function of pH for F-actin (10 µM) in the presence of different concentrations of the cross-linking protein cortexillin (0.5 and 2.5 µM). The symbols in (C) and (D) denote the structure of the corresponding network as determined from confocal images.

increases above a concentration of 1 µM cortexillin (dimer) at pH 6.7. Comparing this concentration dependence to the network structures reveals that the increase of the elastic modulus correlates with the formation of a strongly bundled network. If a slightly higher pH of 7.1 is used, a qualitatively similar behavior is observed. However, since the bundling transition is shifted (Fig. 7.3A), also the strong increase of the elastic modulus is shifted to a significantly higher cortexillin concentration (Fig. 7.3C). The fact that the bundling transition can be tuned by pH directly results in a complex dependence of the elastic modulus on pH: At low concentrations of cortexillin the elastic modulus is hardly dependent on pH. In contrast, in the bundle regime already a decrease from pH 7.1 to pH 6.7 causes a fivefold increase of the elastic modulus (Fig. 7.3C). The correlation of the pH dependence of the elastic modulus with the network architecture can be directly seen in Fig. 7.3D, where the elastic modulus is shown as a function of pH for two different cortexillin concentrations. Whereas only a slight dependence is observed at high pH, where the network is filamentous or only weakly bundled, the elastic modulus increases over more than two orders of magnitude at lower pH, where a bundle network is formed. In analogy to Fig. 7.3C, where an increase of pH has shifted the bundling transition to higher cortexillin concentrations, increasing the cortexillin concentration considerably increases the critical pH at which the bundling transition occurs.

7.3 Fascin suppresses the pH dependence of F-actin solutions

Both cross-linking proteins tested so far, filamin and cortexillin, form complicated networks of branched actin bundles with a heterogenous bundle size. On the contrary, if present at sufficiently high concentrations fascin organizes actin into networks of individual straight and polar bundles with a defined thickness [Claessens et al., 2008, Lieleg et al., 2007]. As shown in Fig. 7.4A, the elasticity of actin/fascin bundle networks is suprisingly constant over a wide range of pH: Above pH 6 even the intrinsic pH dependence of the elasticity of pure actin solutions is completely suppressed by the presence of fascin. Only at a very low pH, in the regime where even pure actin solutions form bundles, a slight increase of the elastic modulus is observed. Moreover, also the nonlinear response of actin/fascin bundle networks to large deformations is almost independent of pH: While pure actin solutions show a pH dependent strain stiffening behavior (Fig. 7.5A), actin/fascin networks show a similar strain weakening response over the whole range of pH (Fig. 7.5B). Consistently, also the structure of bundle networks formed in the presence of fascin is not significantly affected by a variation of pH – except for very low pH, where

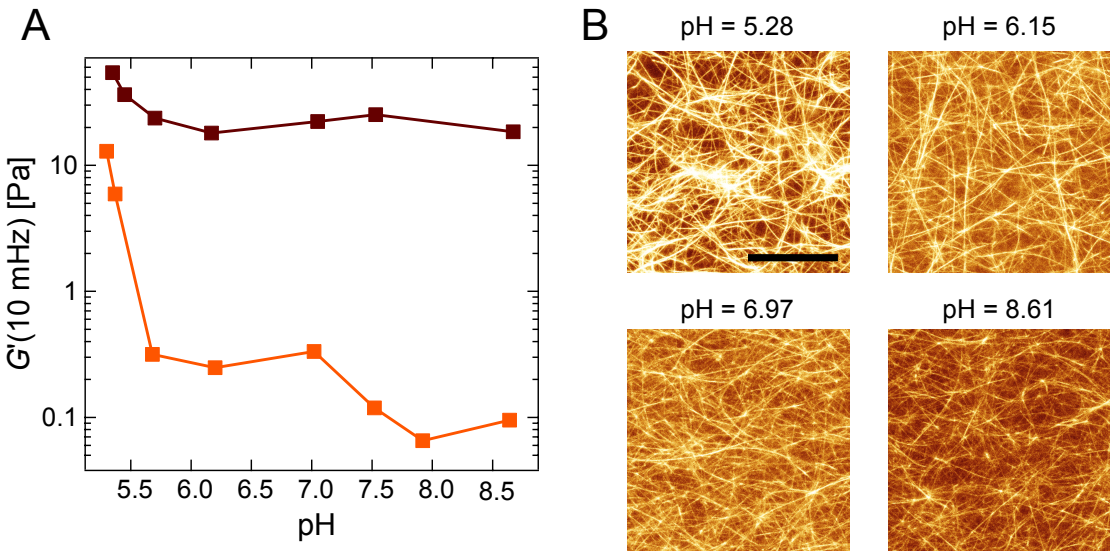

Figure 7.4: (A): Elastic modulus $G'(10\ \text{mHz})$ as a function of pH for pure actin solutions (10 µM) and in the presence of 0.76 µM fascin. (B): Confocal images (maximum projection of a 10 µm stack) of actin/fascin networks at different pH values. The scale bar denotes 20 µm.

actin/fascin bundles seem to form larger aggregates (Fig. 7.4B), which could account for the comparably weak increase in the elastic modulus.

7.4 HMM shows a pH dependent cross-linking activity

While myosin-II motor filaments generate force which moves actin filaments with respect to each other, at least two myosin-II heads need to be attached simultaneously to different actin filaments. By that, myosin-II filaments themselves become effectively transient cross-linkers for a short period of time. Recently, it has been suggested that this dwell time of myosin-II in the actin bound state increases with decreasing pH [Debold et al., 2008], which accounts for the early finding that the speed of actin filaments in a gliding assay decreases with decreasing pH [Kron and Spudich, 1986]. This increased dwell time could result in a significant cross-linking activity of myosin-II at low pH. In order to prevent any network contractions during rheological measurements, the non filamentous heavy meromyosin (HMM) is used here to investigate the pH dependent cross-linking activity of myosin-II. As expected, the presence of HMM does not change the elastic modulus of F-actin solutions at high pH and excess of ATP (Fig. 7.6A). However, below a pH of 6, a sharp increase of the elasticity of actin/HMM networks compared to pure

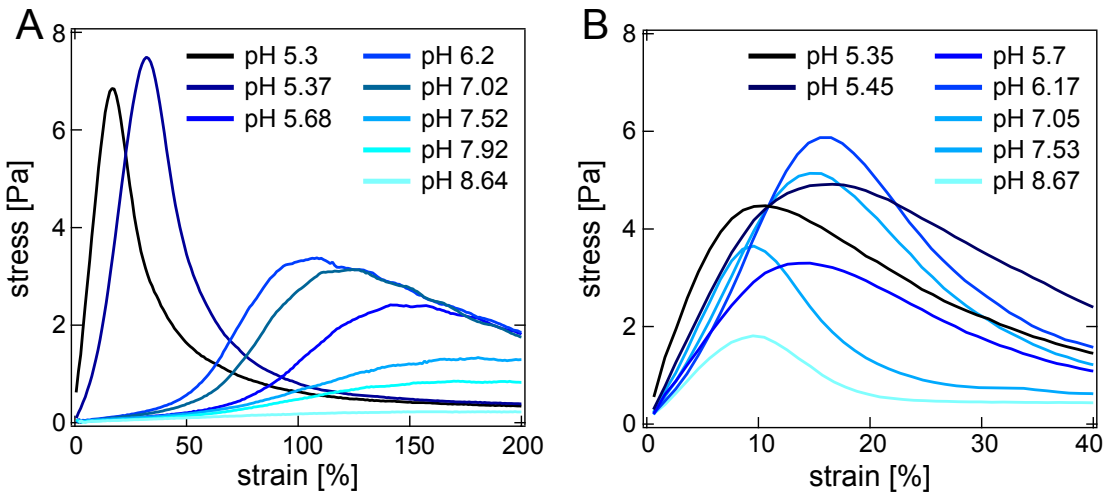

Figure 7.5: Non-linear response as obtained from constant shear experiments ($\dot{\gamma} = 0.125\ \mathrm{s}^{-1}$) for pure actin solutions (10 µM actin) (A) and actin/fascin networks (10 µM actin, 0.76 µM fascin) (B) is shown for different pH values. While the non-linear response of pure actin solutions strongly depends on pH, the response of actin/fascin networks is almost independent of pH.

actin solutions is observed. This demonstrates that low pH indeed results in a very strong cross-linking activity of HMM – and thus myosin-II. Remarkably, the elastic modulus that is reached at a pH of 5.5 is even higher than what is obtained at higher pH after depletion of ATP, when HMM is in the rigor state [Tharmann et al., 2007].

7.5 Contractility of cross-linked active actin systems can be tuned via pH

Contraction of cytoskeletal structures driven by the movement of myosin-II motors along actin filaments is broadly used by cells [Vavylonis et al., 2008, Cai et al., 2010, Martin et al., 2009, Kasza and Zallen, 2011]. *In vitro* macroscopic contraction assays provide a powerful tool to gain insights into microscopic mechanisms of actomyosin contractility [Bendix et al., 2008]. It has been shown that in addition to the ATP dependent motor activity of myosin, a certain degree of network elasticity is crucial for contraction. On the other hand, contraction can also be suppressed if the concentration of cross-linkers is too high [Bendix et al., 2008]. The fact that the contractile behavior of actomyosin gels critically depends on the amount of cross-links in the system, strongly suggests that the pH dependent cross-linking activity of both myosin-II and cross-linking proteins described above should allow to adjust the contractility of actomyosin systems via pH.

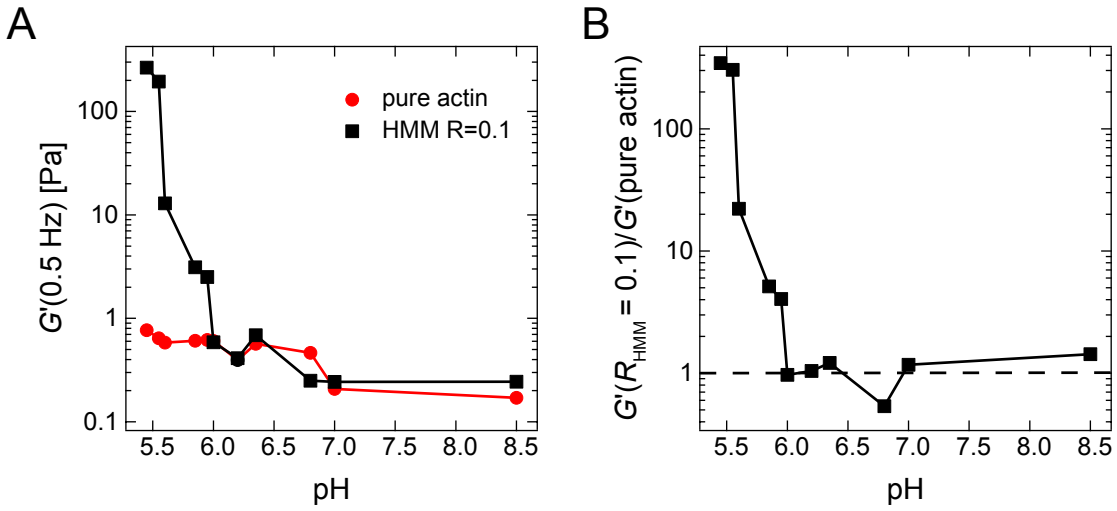

Figure 7.6: (A): Elastic modulus $G'(0.5\ \text{Hz})$ of actin networks (10 µM) in the presence of 1 µM HMM prior to ATP depletion and network contraction (squares) and without HMM after 1.5 hour of polymerization (circles). (B): Ratio of the elastic modulus $G'(0.5\ \text{Hz})$ of an actin/HMM network and of pure actin. A sharp transition to strong cross-linking activity is observed below pH 6.

To test this hypothesis, macroscopic contraction assays are performed. To this end, 1.5 µL of the actin solution (10 µM actin, 0.1 µM myosin-II and the respective cross-linker concentration) is put in a dodecane phase immediately after initiation of polymerization and observed over time with fluorescence microscopy. As expected from literature [Bendix et al., 2008], at neutral pH $\approx$ 7 no contraction is observed for a pure actin/myosin-II system (Fig. 7.7A). However, contraction is enabled if pH is decreased below pH 6, where also the strong increase of the network elasticity in actin/HMM networks has been observed (Fig. 7.6). This strongly suggests that it is indeed the pH dependent cross-linking activity of myosin-II, which accounts for the pH dependent contractility.

Instead of decreasing the pH, the critical network elasticity which is needed for contraction can also be provided by additional cross-linking proteins. All types of cross-linking proteins tested enable contraction at neutral pH, if added at a sufficiently high concentration (Fig. 7.7). All of these cross-linked systems become non-contractile, if the pH is lowered so that myosin-II itself contributes significantly to the network connectivity. There, the motor activity is not sufficient to work against the overall network elasticity, which is given by the cross-linking activity of the cross-linking protein and myosin-II itself.

In the case of cross-linking proteins which, such as fascin, do not show a pH dependent

cross-linking activity, only the single transition from non-contractile at low pH to contractile at high pH is observed. Interestingly, this generic behavior observed for cross-linked active actin networks is also found for mitotic *Xenopus laevis* oocyte extract (Fig. 7.7A) (Mitotic *Xenopus laevis* oocyte extracts prepared as described in [Field et al., 2011] were a kind gift from I. Mattaj, EMBL Heidelberg, Germany). This suggests that also in mitotic oocyte extract, the pH dependence of myosin-II determines the observed pH dependent contractility.

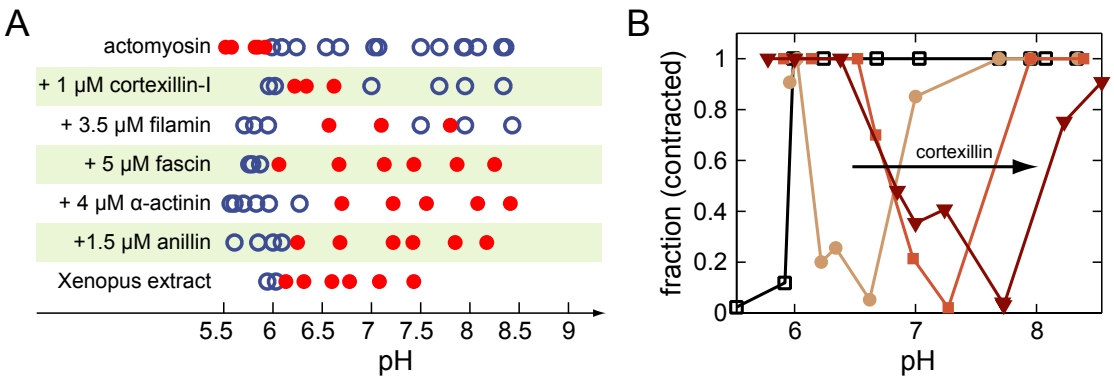

Figure 7.7: (A): The contractility of reconstituted actin/myosin-II systems (10 µM actin, 0.1 µM myosin) is shown as a function of pH (closed circles correspond to contractile systems, open circles correspond to non-contractile systems). In the presence of cross-linking proteins the pH dependence of contractility resembles that of mitotic *Xenopus laevis* oocyte extract. (B): The fraction of the initial area which is still covered by the fluorescent gel after 32 min of contraction is shown for varying cortexillin concentrations (0 µM (open squares), 1 µM (circles), 5 µM (closed squares), 10 µM (triangles) as a function of pH.

However, a more complicated pH dependence can be expected e.g. for actin/cortexillin-I/myosin-II networks, where also the activity of the cross-linking protein is highly sensitive to pH. Indeed, these networks show a second transition at very high pH, where the system gets non-contractile again (Fig. 7.7). Moreover, contraction is not only limited to a certain range of pH, but for increasing cortexillin concentrations this range is significantly shifted to higher pH (Fig. 7.7B). Both effects can be explained considering that the cross-linking activity of cortexillin continuously decreases with increasing pH (section 7.2). The window of contractility is given by the balance of motor activity and the network elasticity, which is set by the pH dependence of both the myosin-II crossbridge strength and the cross-linking activity of cortexillin. For increasing cortexillin concentrations, the window of contractility shifts to higher pH (Fig. 7.7B), as the effective cross-linker activity decreases with increasing pH.

Surprisingly, also the active systems with filamin as cross-linking protein show the second transition at high pH, where the system becomes non-contractile again. In contrast to cortexillin-I, the bundling activity of filamin has been shown to be rather insensitive to pH (section 7.1). Therefore, this behavior cannot simply be explained by a decreased effective filamin activity at high pH, but most probably originates in the complex pH dependence of the non-equilibrium actin/filamin networks described above (section 7.1).

7.6 pH as a potential regulator of cross-linked actin structures in cells

Although recent studies suggest that pH might play an important role in the regulation of cellular processes [Casey et al., 2010], little is known about the mechanisms by which a variation of pH affects the actin cytoskeleton. It has been demonstrated in *in vitro* experiments that cofilin activity [Hawkins et al., 1993, Chen et al., 2004] as well as binding of phosphoinositide, which inhibts cofilin activity, is sensitive to pH [Frantz et al., 2008]. In cells, an increase in intracellular pH (pH_i) due to NHE1 activity has been shown to promote an increase of free actin barbed ends in a cofilin dependent manner [Frantz et al., 2008]. Moreover, cortactin phosphorylation mediates the recruitment of NHE1 to invadopodia, resulting in a local increase of internal pH. This in turn releases the inhibitory binding of cortactin to cofilin [Magalhaes et al., 2011].

Here it has been shown that the effect of varying pH on the structure and mechanics of actin networks qualitatively depends on the present cross-linking protein. How changes in intracellular pH will therefore affect actin structures in cells will critically depend on the particular cross-linking proteins present. As a consequence, even global changes of pH_i could allow cells to locally regulate cytoskeletal structures. Vice versa, the properties of a structure with a homogeneous distribution of cytoskeletal proteins can be tuned in a spatially confined way by a local variation of pH_i. For example, a migrating cell has a pH_i gradient of 0.2 units [Martin et al., 2011]. Therefore, the mechanical response of a cytoskeletal structure will differ depending on where it is located along that gradient, i.e. the leading edge will be mechanically different from the retracting end. Especially if the cytoskeletal structure is in a state near a phase transition - such as the bundling transition in the case of actin/cortexillin networks or the contractile to non-contractile transition in active actin networks - even small variations of pH_i in space or time will have strong effects.

The pH dependent contractility of cross-linked active actin networks directly demostrates that the distinct pH dependencies of cross-linking proteins are a powerful tool for the reg-

ulation of the cytoskeleton: While the pH dependent contractility occurs independently of the present type of cross-linking protein, the specific properties and concentrations of the different cross-linking proteins allow to sensitively fine-tune the pH where the transitions occur. Vice versa, pH modulation allows to adjust the actomyosin system such that a small variation of the concentration of active cross-linking proteins, e.g. induced via biochemical pathways, can also trigger the contraction.

The results presented in this chapter suggest that the distinct pH dependencies of cross-linking proteins could help cells to orchestrate cytoskeletal processes. On the other hand, malfunction of the intracellular pH homeostasis can be expected to have severe consequences.

One of the landmarks of oncogenic transformation is an increase in pH_i [Srivastava et al., 2007, Stock and Schwab, 2009, Webb et al., 2011]. How could the results of this chapter help to understand the increased capacity of cancer cells for migration and invasion? Cytoskeletal structures play an important as mechanical sensors [Wang et al., 2009, Howard, 2009], which strongly suggests that a change of pH_i will modulate mechanotransduction. Although many other proteins are involved in regulating the cytoskeleton, the observed pH dependence of cross-linked actin systems provides clues for understanding overall cellular behavior. For example, in addition to down-regulation of cross-linking proteins [Xu et al., 2010], the increased pH_i may contribute to the reduced stiffness of cancer cells [Guck et al., 2005, Cross et al., 2007], which alters their ability to mechanically sense their environment and leads to substrate-independent growth and suppression of apoptosis [Wang et al., 2000]. This would be in conjunction with the reduced focal adhesion strength, since talin binding to actin is also pH-sensitive [Srivastava et al., 2008]. Surprisingly, although cellular H^+-translocation is not necessary for stress-fiber formation [Denker et al., 2000] it is important for their growth factor-induced disassembly [Meima et al., 2009]. Since cross-linking proteins stabilize actin filaments (chapter 4), a decreased cross-linking activity at high pH_i together with the pH-sensitive activity of cofilin might help the disassembly of stress-fibers. In conclusion, pH might not only play a role in triggering certain cytoskeletal responses but also provides the necessary conditions to make many processes run smoothly.

8 Outlook

During the last decades, *in vitro* studies have provided insights into the fundamental principles that underlie many cytoskeletal processes by identifying basic functions of many actin binding proteins. Although only a small selection of actin binding proteins has already been studied thoroughly, these actin binding proteins provide a toolbox for the reconstitution of many basic mechanisms occuring in the actin cytoskeleton. Processes such as *bundling* [Lieleg et al., 2007, Claessens et al., 2008], *formation of a branched actin network* [Loisel et al., 1999] or *formation of a contractile element* [Thoresen et al., 2011] are to a large extent qualitatively understood and can be reconstituted *in vitro*. However, it is still a mystery how cells manage to orchestrate these processes in space and time. In *in vitro* experiments, they are "initiated" by the experimenter. In cells, it has to be guaranteed that an adaption of the cytoskeleton is initiated at the right time and at the right position in the cell. Therefore, the consequence of a certain signal on the cytoskeletal organization is not only given by the signal itself, but also by the overall state of the cell. Upon detection of an external or internal stimulus, cells have to process this information in order to "decide" whether a reorganization of the cytoskeleton is needed (Fig. 8.1). This information processing can be decoupled from the cytoskeleton, as it is the case if signal cascades of proteins which are not direct components of the cytoskeleton determine the outcome of the initial stimulus. On the other hand, also the cytoskeleton itself can participate in the information processing by directly adapting as a consequence of the stimulus. As an example, external mechanical forces acting on the cell could directly cause a reorganization of the cytoskeleton, similar to the strain induced bundling observed *in vitro* in chapter 6.

In the case of decoupled information processing, cells have different possibilities to finally trigger the desired cytoskeletal response:

(i) A (local) change in the concentration of cytoskeletal proteins.

(ii) Specific biochemical modifications of cytoskeletal proteins that alter their activity (e.g. by phosphorylation, or different nucleotide states as in the case of the Rho GTPases [Jaffe and Hall, 2005]).

(iii) Variation of physical or chemical parameters, such as salt concentrations or pH.

Synthesis or degradation of proteins (i) is an expensive and slow way to modify the cytoskeleton. A controlled transcription of cytoskeletal proteins is definitely important, and even actin itself contributes to the regulation of transcriptional activity [Olson and Nordheim, 2010]). However, it can be expected to be only suitable for long-term adaptions as occuring e.g. upon progression in the cell cycle or permanent changes of the cellular environment. Reversible modulation of the properties of the individual proteins (ii) is a fast and economic alternative that is commonly used by cells. In contrast to these very specific processes such as phosphorylation, changes in the intracellular environment (iii) will tend to affect a high number of proteins. While this certainly limits the applicability of e.g. variation of intracellular pH, it at the same time increases its potential by allowing to regulate several cytoskeletal components simultaneously. Using only minimal variations (of e.g. pH) to modify systems that are near a phase transition, can help to avoid unwanted side effects.

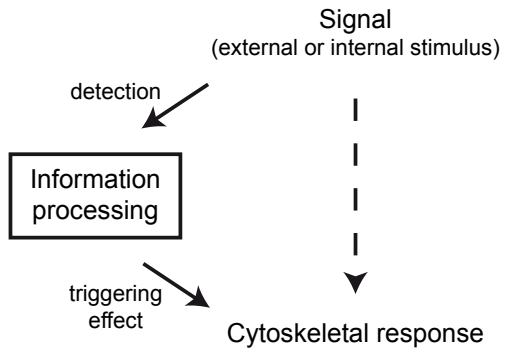

Figure 8.1: Schematic illustration of cytoskeletal regulation: After detection of a signal, cells have to process this information to determine their response to the signal. Subsequently, the cytoskeletal reorganization has to be triggered. As an alternative, the signal itself can cause a reorganization of the cytoskeleton (dashed line).

Not only the accurate timing of a modification of the cytoskeleton is of essential importance, but it also has to be ensured that only distinct structures are specifically addressed. One important feature that can distinguish a cytoskeletal structure from others is its position within the cell. For example, proximity to the cell membrane imposes geometrical constraints and can also result in a specific environment, such as a locally different pH [Casey et al., 2010]. In addition to its location, a particular component of the cytoskeleton is characterized by its constituents: E.g., the presence of certain cross-linking proteins is essential for the formation of distinct cytoskeletal structures (e.g. fascin is essential for the formation of filopodia [Vignjevic et al., 2006]). The results of this thesis indicate that cross-linking proteins are not only needed to maintain the structural integrity of the cytoskeleton but also play an additional important role in the regulation of the actin cytoskeleton. Simply the distinctive presence of particular cross-linking pro-

teins in cytoskeletal structures provides a mechanism which allows cells to address only specific actin structures, even using a homogeneous signal. It has been shown in chapter 4 that cross-linking proteins modify the intrinsic dynamics of actin filaments and can even inhibit the activity of cofilin. A global, homogeneous increase of the concentration of active cofilin would therefore affect actin filaments in different structures differently – depending on the local type and concentration of cross-linking proteins. Similarly, also the effect of a homogeneous change of intracellular pH on a certain structure will be co-determined by the cross-linking proteins which at the same time define the structure itself (chapter 7). The change in pH can thus induce distinct structural changes in different components of the cytoskeleton. In turn, the modified geometry in combination with potential changes in the binding affinity of the cross-linking proteins will go along wih an adaption of the internal dynamics of the actin filaments. This highlights that the interplay of cross-linking proteins with other actin binding proteins such as cofilin is a powerful mechanism, that enables extensive changes of the cytoskeleton upon a single triggering effect.

In this thesis it has been demonstrated that *in vitro* experiments with reconstituted actin systems are ideally suited to investigate mechanisms that are involved in the regulation of the actin cytoskeleton. Future studies will have to pursue this strategy: As a first step, *in vitro* studies can be used to identify parameters that tune the properties of various actin systems. Similar to pH, e.g. salt concentrations can alter the dynamics of actin filaments [Wegner and Neuhaus, 1981] and specifically modify the activity of cross-linking proteins [Burridge and Feramisco, 1981]. In addition, the interplay of different actin binding proteins – especially of ABPs that colocalize in the same cytoskeletal structures – has to be addressed. Presumably not only the effect of cofilin but also of many other proteins that regulate actin dynamics is drastically dependent on the presence of other actin binding proteins. First results suggest that also the activity of motor proteins can be regulated by cross-linking proteins [Elkhatib et al., 2012].

After identifying parameters that affect the properties of steady state actin systems – or the effect of a certain protein on a steady state actin system – future studies have to aim for actually reconstituting regulation processes *in vitro*. To this end, parameters such as pH have to be changed in a steady state actin network, instead of already polymerizing actin networks at the different conditions. This could be done using a diffusion chamber as introduced in section 4.2 or caged compounds such as caged protons or ions. Encapsulation of actin networks in vesicles [Abkarian et al., 2011] would even allow to study regulation processes in a closed system. There, buffer conditions could be changed via the membrane, e.g. by using ionophores which allow to change the salt concentrations. To mimic the specific activiation of a protein, e.g. by phosphorylation, the active

concentration of this protein needs to be increased. While adding the protein via the diffusion chamber allows to globally increase the concentration, photoactivatable protein constructs could be used to locally mimic biochemical activation [Mayer and Heckel, 2006, Lemke et al., 2007, Wu et al., 2009], even within vesicles.

Already very simple switchable *in vitro* systems, such as a homogeneous actin network cross-linked by a single type of ABP, that can be switched between a filamentous and a bundled state, can be expected to give new insights into the regulation processes occuring in the cytoskeleton. Once such a switchable system is established, its complexity can be gradually increased, for example by the addition of a second type of cross-linking protein [Schmoller et al., 2008a, Tseng et al., 2005]. Such composite actin networks could be an ideal model system to investigate regulation processes that specifically target structures dominated by a certain cross-linking protein.

In addition to *in vitro* experiments that identify potential regulation mechanisms, *in vivo* experiments are needed at the same time to directly test which of these mechanisms are actually employed by cells. Indirect evidence can be obtained by correlating precise measurements of local protein concentrations and variations of physical parameters with reorganizations of the cytoskeleton, such as done for the role of pH in the maturation of invadopodia [Magalhaes et al., 2011]. Moreover, changes of parameters can be induced that can similarly also be investigated *in vitro*: *In vivo*, this can be achieved using microinjection techniques, as e.g. already done to study the role of the ABP ezrin during cell blebbing [Charras et al., 2006]), or photoactivatable constructs, such as photoactivatable Rac that allowed to induce cell motility in a controlled direction [Wu et al., 2009]. The resulting cytoskeletal response can then be compared with the effect that is observed *in vitro* for the same parameter change. By that, it can be revealed whether the respective reconstituted model system captures the dominating features of the cytoskeletal structure of interest. If this is the case, the mechanistic insights obtained from the *in vitro* experiments can be transferred to the *in vivo* situation and can thereby help to understand cytoskeletal regulation processes.

In conclusion, the bottom-up approach with well defined reconstituted systems has been proven a powerful tool to unravel the function of cytoskeletal proteins and reconstitute fundamental processes occuring in living cells. The results of this thesis indicate that future studies that combine the *in vitro* approach with the proper *in vivo* experiments will significantly contribute to our understanding of the cytoskeletal regulation mechanisms that underlie the amazing complexity of living cells.

Bibliography

[Abkarian et al., 2011] Abkarian, M., E. Loiseau and G. Massiera (2011). *Continuous droplet interface crossing encapsulation (cDICE) for high throughput monodisperse vesicle design*. Soft Matter, 7:4610–4614.

[Andrianantoandro and Pollard, 2006] Andrianantoandro, E. and T. D. Pollard (2006). *Mechanism of Actin Filament Turnover by Severing and Nucleation at Different Concentrations of ADF/Cofilin*. Mol. Cell, 24:13–23.

[Arevalo et al., 2010] Arevalo, R. C., J. S. Urbach and D. L. Blair (2010). *Size-Dependent Rheology of Type-I Collagen Networks*. Biophys. J., 99:L65–L67.

[Asakura and Oosawa, 1960] Asakura, S. and F. Oosawa (1960). *Dephosphorylation of Adenosine Triphosphate in Actin Solutions at Low Concentrations of Magnesium*. Arch. Bichem. Biophys., 87:273–280.

[Astroem et al., 2008] Astroem, P., B. S. Kumar, I. Vattulainen and M. Karttunen (2008). *Strain hardening, avalanches, and strain softening in dense cross-linked actin networks*. Phys. Rev. E, 77:051913.

[Bausch and Kroy, 2006] Bausch, A. R. and K. Kroy (2006). *A bottom-up approach to cell mechanics*. Nature Phys., 2:231–238.

[Bendix et al., 2008] Bendix, P.M., G. Koenderink, D. Cuvelier, Z. Dogic, B. Koeleman, W. Brieher, C. Field, L. Mahadevan and D. Weitz (2008). *A Quantitative Analysis of Contractility in Active Cytoskeletal Protein Networks*. Biophys. J., 94:3126–3136.

[Bernheim-Groswasser et al., 2002] Bernheim-Groswasser, A., R. M. Wiesner, S. Golsteyn, M. F. Carlier and C. Sykes (2002). *The dynamics of actin-based motility depend on surface parameters*. Nature, 417:308–311.

[Berro et al., 2010] Berro, J., V. Sirotkin and T. D. Pollard (2010). *Mathematical Modeling of Endocytic Actin Patch Kinetics in Fission Yeast: Disassembly Requires Release of Actin Filament Fragments*. Mol. Biol. Cell, 21:2905–2915.

[Bigg, 2004] Bigg, D. M. (2004). *A review of techniques for processing ultra-high modulus polymers*. Polymer Engineering and Science, 16:725–734.

[Broschat et al., 1989] Broschat, K. O., A. Weber and D. R. Burgess (1989). *Tropomyosin Stabilizes the Pointed End of Actin Filaments by Slowing Depolymerization*. Biochemistry, 28:8501–8506.

[Bugyi and Carlier, 2010] Bugyi, B. and M.-F. Carlier (2010). *Control of Actin Filament Treadmilling in Cell Motility*. Annu. Rev. Biophys., 39:449–470.

[Burridge and Feramisco, 1981] Burridge, K. and J. R. Feramisco (1981). *Non-muscle α-actinins are calcium-sensitive actin-binding proteins*. Nature, 294:565–567.

[Cai et al., 2010] Cai, Y., O. Rossier, N. C. Gauthier, N. Biais, M.-A. Fardin, X. Zhang, L. W. Miller, B. Ladoux, V. W. Cornish and M. P. Sheetz (2010). *Cytoskeletal coherence requires myosin-IIA contractility*. J. Cell Sci., 123:413–423.

[Cano et al., 1992] Cano, M. L., L. Cassimeris, M. Fechheimer and S. H. Zigmond (1992). *Mechanisms Responsible for F-actin Stabilization after Lysis of Polymorphonuclear Leukocytes*. J. Cell Biol., 116:1123–1134.

[Carlier, 1998] Carlier, M. F. (1998). *Control of actin dynamics*. Curr. Opin. Cell Biol., 10:45–51.

[Carlier et al., 1997] Carlier, M.-F., V. Laurent, J. Santolini, R. Melki, D. Didry, G.-X. Xia, Y. Hong, N.-H. Chua and D. Pantaloni (1997). *Actin Depolymerizing Factor (ADF/Cofilin) Enhances the Rate of Filament Turnover: Implication in Actin-based Motility*. J. Cell Biol., 136:1307–1322.

[Carlier and Pantaloni, 2007] Carlier, M. F. and D. Pantaloni (2007). *Control of Actin Assembly Dynamics in Cell Mobiltity*. J. Biol. Chem., 282:23005–23009.

[Casey et al., 2010] Casey, J. R., S. Grinstein and J. Orlowski (2010). *Sensors and regulators of intracellular pH*. Nat. Rev. Mol. Cell. Biol., 11:50–61.

[Charras et al., 2006] Charras, G. T., C.-K. Hu, M. Coughlin and T. J. Mitchison (2006). *Reassembly of contractile actin cortex in cell blebs*. J. Cell Biol., 175:477–490.

[Chen et al., 2004] Chen, H., B. W. Bernstein, J. M. Sneider, J. A. Boyle, L. S. Minamide and J. R. Bamburg (2004). *In Vitro Activity Differences between Proteins of the ADF/Cofilin Family Define Two Distinct Subgroups*. Biochemistry, 43:7127–7142.

[Claessens et al., 2006] Claessens, M. M. A. E., M. Bathe, E. Frey and A. R. Bausch (2006). *Actin-binding proteins sensitively mediate F-actin bundle stiffness*. Nature Mat., 5:748–753.

[Claessens et al., 2008] Claessens, M. M. A. E., C. Semmrich, L. Ramos and A. R. Bausch (2008). *Helical twist controls the thickness of F-actin bundles*. Proc. Natl. Acad. Sci. USA, 105 (26):8819–8822.

[Conti and MacKintosh, 2009] Conti, E. and F. C. MacKintosh (2009). *Cross-linked networks of stiff filaments exhibit negative normal stress*. Phys. Rev. Lett., 102:088102.

[Cooper et al., 1983] Cooper, J. A., S. B. Walker and T. D. Pollard (1983). *Pyrene actin: documentation of the validity of a sensitive assay for actin polymerization*. J. Muscle Res. Cell M., 4:253–262.

[Courson and Rock, 2010] Courson, D. S. and R. S. Rock (2010). *Actin Cross-link Assembly and Disassembly Mechanics for α-Actinin and Fascin*. J. Biol. Chem., 285:26350–26357.

[Craig et al., 1982] Craig, S. W., C. L. Lancashire and J. A. Cooper (1982). *Preparation of smooth muscle α-actinin*. Methods Enzymol., 85:316–321.

[Cross et al., 2007] Cross, S. E., Y.-S. Jin, J. Rao and J. K. Gimzewski (2007). *Nanomechanical analysis of cells from cancer patients*. Nature Nanotech., 2:780–783.

[De La Cruz, 2009] De La Cruz, E. M. (2009). *How cofilin severs an actin filament*. Biophys. Rev., 1:51–59.

[Debold et al., 2008] Debold, E. P., S. E. Beck and D. M. Warshaw (2008). *Effect of low pH on single skeletal muscle myosin mechanics and kinetics*. Am. J. Physiol. Cell. Physiol., 295:C173–C179.

[Denker et al., 2000] Denker, S. P., D. C. Huang, J. Orlowski, H. Furthmayr and D. L. Barber (2000). *Direct Binding of Na-H Exchanger NHE1 to ERM Proteins Regulates the Cortical Cytoskeleton and Cell Shape Independently of* H^+ *Translocation*. Mol. Cell, 6:1425–1436.

[Diani et al., 2009] Diani, J., B. Fayolle and P. Gilormini (2009). *A review on the Mullins effect*. Eur. Polym. J., 45:601–612.

[Edelstein-Keshet and Ermentrout, 1998] Edelstein-Keshet, L. and G. B. Ermentrout (1998). *Models for the Length Distributions of Actin Filaments: I. Simple Polymerization and Fragmentation*. B. Math. Biol., 60:449–475.

[Eisenberg and Kielley, 1974] Eisenberg, E. and W. W. Kielley (1974). *Troponin-tropomyosin complex column chromatographic separation and activity of the three active troponin components with and without tropomyosin present*. J. Biol. Chem., 249:4742.

[Elkhatib et al., 2012] Elkhatib, N., M. Neu, C. Zensen, K. M. Schmoller, D. Louvard, A. R. Bausch and D. M. Vignjevic (2012). *Turnover of focal adhesions required for efficient cell migration is regulated by parallel actin bundles*. submitted.

[Erickson, 1989] Erickson, H. P. (1989). *Co-operativity in Protein-Protein Association*. J. Mol. Biol., 206:465–474.

[Faix et al., 1996] Faix, J., M. Steinmetz, H. Boves, R. Kammerer, F. Lottspeich, U. Mintert, J. Murphy, A. Stock, U. Aebi and G. Gerisch (1996). *Cortexillins, Major Determinants of Cell Shape and Size, Are Actin-Bundling Proteins with a Parallel Coiled-Coil Tail*. Cell, 86:631–642.

[Fass et al., 2008] Fass, J., C. Pak, J. Bamburg and A. Mogilner (2008). *Stochastic simulation of actin dynamics reveals the role of annealing and fragmentation*. J. Theor. Biol., 252:173–183.

[Feng and Walsh, 2004] Feng, Y. and C. A. Walsh (2004). *The many faces of filamin: A versatile molecular scaffold for cell motility and signalling*. Nat. Cell Biol., 6:1034–1038.

[Field et al., 2011] Field, C. M., M. Wühr, G. A. Anderson, H. Y. Kueh, D. Strickland and T. J. Mitchison (2011). *Actin behavior in bulk cytoplasm is cell cycle regulated in early vertebrate embryos*. J. Cell Sci., 124:2086–2095.

[Frantz et al., 2008] Frantz, C., G. Barreiro, L. Dominguez, X. Chen, R. Eddy, J. Condeelis, M. J. S. Kelly, M. P. Jacobson and D. L. Barber (2008). *Cofilin is a pH sensor for actin free barbed end formation: role of phosphoinositide binding*. J. Cell Biol., 183:865–879.

[Fujiwara et al., 2002] Fujiwara, I., S. Takahashi, H. Tadakuma, T. Funatsu and S. Ishiwata (2002). *Microscopic analysis of polymerization dynamics with individual actin filaments*. Nat. Cell Biol., 4:666–673.

[Fujiwara et al., 2007] Fujiwara, I., D. Vavylonis and T. D. Pollard (2007). *Polymerization kinetics of ADP- and ADP-Pi-actin determined by fluorescence microscopy*. Proc. Natl. Acad. Sci. USA, 104:8827–8832.

[Gardel et al., 2006] Gardel, M. L., F. Nakamura, J. H. Hartwig, J. C. Crocker, T. P. Stossel and D. A. Weitz (2006). *Prestressed F-actin networks cross-linked by hinged filamins replicate mechanical properties of cells*. Proc. Natl. Acad. Sci. USA, 103:1762–1767.

[Guck et al., 2005] Guck, J., S. Schinkinger, B. Lincoln, F. Wottawah, S. Ebert, M. Romeyke, D. Lenz, H. M. Erickson, R. Ananthakrishnan, D. Mitchell, J. Käs, S. Ulvick and C. Bilby (2005). *Optical Deformability as an Inherent Cell Marker for Testing Malignant Transformation and Metastatic Competence*. Biophys. J., 88:3689–3698.

[Haviv et al., 2008] Haviv, L., D. Gillo, F. Backouche and A. Bernheim-Groswasser (2008). *A Cytoskeletal Demolition Worker: Myosin II Acts as an Actin Depolymerization Agent*. J. Mol. Biol., 375:325–330.

[Hawkins et al., 1993] Hawkins, M., B. Pope, S. K. Maciver and A. G. Weeds (1993). *Human Actin Depolymerizing Factor Mediates a pH-Sensitive Destruction of Actin Filaments*. Biochemistry, 32:9985–9993.

[Head et al., 2003] Head, D. A., A. J. Levine and F. C. MacKintosh (2003). *Deformation of cross-linked semiflexible polymer networks*. Phys. Rev. Lett., 91.

[Heussinger et al., 2007] Heussinger, C., B. Schaefer and E. Frey (2007). *Nonaffine rubber elasticity for stiff polymer networks*. Phys. Rev. E, 76:031906.

[Howard, 2001] Howard, J. (2001). *Mechanics of Motor Proteins and the Cytoskeleton*. Sinauer Associates Inc.

[Howard, 2009] Howard, J. (2009). *Mechanical signaling in networks of motor and cytoskeletal proteins*. Annu. Rev. Biophys., 38:217–234.

[Huang et al., 2005] Huang, S., R. C. Robinson, L. Y. Gao, T. Matsumoto, A. Brunet, L. Blanchoin and C. J. Staiger (2005). *Arabidopsis VILLIN1 Generates Actin Filament Cables That Are Resistant to Depolymerization*. Plant Cell, 17:486–501.

[Huisman et al., 2007] Huisman, E. M., T. van Dillen, P. R. Onck and E. Van der Giessen (2007). *Three-dimensional cross-linked F-actin networks: relation between network architecture and mechanical behavior*. Phys. Rev. Lett., 99:208103.

[Huo and Müller, 1993] Huo, Y. and I. Müller (1993). *Nonequilibrium Thermodynamics of Pseudoelasticity*. Continuum Mech. Thermodyn., 5:163–204.

[Ishikawa et al., 2003] Ishikawa, R., T. Sakamoto, T. Ando, S. Higashi-Fujime and K. Kohama (2003). *Polarized actin bundles formed by human fascin-1: their sliding and disassembly on myosin II and myosin V in vitro*. J. Neurochem., 87:676–685.

[Jaffe and Hall, 2005] Jaffe, A. B. and A. Hall (2005). *Rho GTPases: Biochemistry and Biology*. Annu. Rev. Cell Dev. Biol., 21:247–269.

[Janmey et al., 1986] Janmey, P. A., J. Peetermans, K. S. Zaner, T. P. Stossel and T. Tanaka (1986). *Structure and Mobiltity of Actin Filaments as Measured by Quasielastic Light Scattering, Viscometry, and Electron Microscopy*. J. Biol. Chem., 261(18):8357–8362.

[Jégou et al., 2011] Jégou, A., M. F. Carlier and G. Romet-Lemonne (2011). *Microfluidics pushes forward microscopy analysis of actin dynamics*. BioArchitecture, 1:6:271–276.

[Kang et al., 2009] Kang, H., Q. Wen, P. A. Janmey, J. X. Tang, E. Conti and F. C. MacKintosh (2009). *Nonlinear Elasticity of Stiff Filament Networks: Strain Stiffening, Negative Normal Stress, and Filament Alignment in Fibrin Gels*. J. Phys. Chem. B., 113:3799–3805.

[Kasza et al., 2009] Kasza, K. E., G. H. Koenderink, Y. C. Lin, C. P. Broedersz, W. Messner, F. Nakamura, T. P. Stossel, F. C. MacKintosh and D. A. Weitz (2009). *Nonlinear elasticity of stiff biopolymers connected by flexible linkers*. Phys. Rev. E., 79:041928.

[Kasza et al., 2007] Kasza, K. E., A. C. Rowat, J. Liu, T. E. Angelini, C. P. Brangwynne, G. H. Koenderink and D. A. Weitz (2007). *The cell as a material*. Curr. Opin. Cell Biol., 19:101–107.

[Kasza and Zallen, 2011] Kasza, K. E. and J. A. Zallen (2011). *Dynamics and regulation of contractile actin-myosin networks in morphogenesis*. Curr. Opin. Cell Biol., 23:30–38.

[Kaufman et al., 2005] Kaufman, L. J., C. P. Brangwynne, K. E. Kasza, E. Filippidi, V. D. Gordon, T. S. Deisboeck and D. A. Weitz (2005). *Glioma Expansion in Collagen I Matrices: Analyzing Collagen Concentration-Dependent Growth and Motility Patterns*. Biophys. J., 89:635–650.

[Kawamura and Maruyama, 1970] Kawamura, M. and K. Maruyama (1970). *Electron Microscopic Particle Length of F-Actin Polymerized in Vitro*. J. Biochem., 67:437–457.

[Kinoshita et al., 2002] Kinoshita, M., C. M. Field, M. L. Coughlin, A. F. Straight and T. J. Mitchison (2002). *Self- and Actin-Templated Assembly of Mammalian Septins*. Dev. Cell, 3:791–802.

[Kinosian et al., 1993a] Kinosian, H. J., L. A. Selden, J. E. Estes and L. C. Gersham (1993a). *Nuceotide Binding to Actin*. J. Biol. Chem., 268:8683–8691.

[Kinosian et al., 1993b] Kinosian, H. J., L. A. Selden, J. E. Estes and L. C. Gershman (1993b). *Actin Filament Annealing in the Presence of ATP and Phallodin*. Biochemistry, 32:12353–12357.

[Köhler, 2012] Köhler, S. (2012). *Dynamics and structure formation in active actin networks*. PhD thesis, Technische Universität München.

[Korn et al., 1987] Korn, E. D., M.-F. Carlier and D. Pantaloni (1987). *Actin Polymerization and ATP Hydrolysis*. Science, 238:4827.

[Kouyama and Mihashi, 1981] Kouyama, T. and K. Mihashi (1981). *Fluorimetry Study of N-(1-Pyrenyl)iodoacetamide-Labelled F-Actin*. Eur. J. Biochem., 114:33–38.

[Kron and Spudich, 1986] Kron, S. J. and J. A. Spudich (1986). *Fluorescent actin filaments move on myosin fixed to a glass surface*. Proc. Natl. Acad. Sci. USA, 83 (17):6272–6276.

[Kroy and Frey, 1996] Kroy, K. and E. Frey (1996). *Force-Extension Relation and Plateau Modulus for Wormlike Chains*. Phys. Rev. Lett., 77.

[Kueh et al., 2008] Kueh, H. Y., W. M. Brieher and T. J. Mitchison (2008). *Dynamic stabilization of actin filaments*. Proc. Natl. Acad. Sci. USA, 105:16531–16536.

[Kueh and Mitchison, 2009] Kueh, H. Y. and T. J. Mitchison (2009). *Structural Plasticity in Actin and Tubulin Polymer Dynamics*. Science, 325:960–963.

[Kuhn and Pollard, 2005] Kuhn, J. R. and T. D. Pollard (2005). *Real-Time Measurements of Actin Filament Polymerization by Total Internal Reflection Fluorescence Microscopy*. Biophys. J., 88:1387–1402.

[Kumar and Lagoudas, 2008] Kumar, P. K. and D. C. Lagoudas (2008). *Introduction to Shape Memory Alloys*. Springer.

[Kurokawa et al., 1990] Kurokawa, H., W. Fujii, K. Ohmi, T. Sakurai and Y. Nonomura (1990). *Simple and rapid purification of brevin*. Biochem. Bioph. Res. Commun., 168(2):451–457.

[Lebart et al., 2004] Lebart, M.-C., F. Hubert, C. Boiteau, S. Venteo, C. Roustan and Y. Benyamin (2004). *Biochemical Characterization of the L-Plastin - Actin Interaction Shows a Resemblance with That of α-Actinin and Allows a Distinction To Be Made between the Two Actin-Binding Domains of the Molecule*. Biochemistry, 43:2428–2437.

[Lemke et al., 2007] Lemke, E. A., D. Summerer, B. H. Geierstanger, S. M. Brittain and P. G. Schutz (2007). *Control of protein phosphorylation with a genetically encoded photocaged amino acid*. Nat. Chem. Biol., 3:769–772.

[Li et al., 2009] Li, X., J. Kierfeld and R. Lipowsky (2009). *Actin Polymerization and Depolymerization Coupled to Cooperative Hydrolysis*. Phys. Rev. Lett., 103:048102.

[Lieleg and Bausch, 2007] Lieleg, O. and A. R. Bausch (2007). *Cross-linker unbinding and self-similarity in bundled cytoskeletal networks*. Phys. Rev. Lett., 99:158105.

[Lieleg et al., 2010] Lieleg, O., M. M. A. E. Claessens and A. R. Bausch (2010). *Structure and Dynamics of Cross-linked Actin Networks*. Soft Matter, 10:218–225.

[Lieleg et al., 2007] Lieleg, O., M. M. A. E. Claessens, C. Heussinger, E. Frey and A. R. Bausch (2007). *Mechanics of bundled semiflexible polymer networks*. Phys. Rev. Lett., 99:088102.

[Lieleg et al., 2008] Lieleg, O., M. M. A. E. Claessens, Y. Luan and A. R. Bausch (2008). *Transient Binding and Dissipation in Semi-flexible Polymer Networks*. Phys. Rev. Lett., 101:108101.

[Lieleg et al., 2011] Lieleg, O., J. Kayser, G. Brambilla, L. Cipelletti and A. R. Bausch (2011). *Slow dynamics and internal stress relaxation in bundled cytoskeletal networks*. Nature Mat., 10:236–242.

[Lieleg et al., 2009a] Lieleg, O., K. M. Schmoller, M. M. A. E. Claessens and A. R. Bausch (2009a). *Cytoskeletal Polymer Networks: Viscoelastic Properties are Determined by the Microscopic Interaction Potential of Cross-links*. Biophys. J., 96:4725–4732.

[Lieleg et al., 2009b] Lieleg, O., K. M. Schmoller, C. J. Cyron, W. A. Wall and A. R. Bausch (2009b). *Structural Polymorphism in Heterogeneous Cytoskeletal Networks*. Soft Matter, 5:1796–1803.

[Lim and McDowell, 1995] Lim, T. J. and D. L. McDowell (1995). *Path Dependence of Shape Memory Alloys during Cyclic Loading*. J. Intel. Mat. Syst. Str., 6:817–830.

[Liu et al., 2007] Liu, J., G. H. Koenderink, K. E. Kasza, F. C. MacKintosh and D. A. Weitz (2007). *Visualizing the Strain Field in Semiflexible Polymer Networks: Strain Fluctuations and Nonlinear Rheology of F-Actin Gels*. Phys. Rev. Lett., 98:198304.

[Loisel et al., 1999] Loisel, T. P., R. Boujemaa, D. Pantaloni and M. F. Carlier (1999). *Reconstitution of actin-based motility of Listeria and Shigella using pure proteins*. Nature, 401:613–616.

[Loomis et al., 2003] Loomis, P. A., L. Zheng, G. Sekerkova, B. Changyaleket, E. Mugnaini and J. R. Bartles (2003). *Espin cross-links cause the elongation of microvillus-type parallel actin bundles in vivo*. J. Cell Biol., 163:1045–1055.

[Ma et al., 2010] Ma, J., I. Karaman and Y. Chumlyakov (2010). *Superelastic memory effect in $Ti_{74}Nb_{26}$ shape memory alloy*. Scripta Mater., 63:265–268.

[MacLean-Fletcher and Pollard, 1980] MacLean-Fletcher, S. and T. D. Pollard (1980). *Identification of a factor in conventional muscle actin preparations which inhibits actin filament self-association*. Biochem. Bioph. Res. Commun., 96:18–27.

[Magalhaes et al., 2011] Magalhaes, M. A., D. R. Larson, C. C. Mader, J. J. Bravo-Cordero, H. Gil-Henn, M. Oser, X. Chen, A. J. Koleske and J. Condeelis (2011). *Cortactin phosphorylation regulates cell invasion through a pH-dependent pathway*. J. Cell. Biol., doi: 10.1083/jcb.201103045.

[Marckmann et al., 2002] Marckmann, G., E. Verron, L. Gornet, G. Chagnon, P. Charrier and F. P. (2002). *A theory of network alteration for the Mullins effect*. J. Mech. Phys. Solids, 50:2011–2028.

[Martin et al., 2009] Martin, A. C., M. Kaschube and E. F. Wieschaus (2009). *Pulsed contractions of an actin-myosin network drive apical constriction*. Nature, 457(7228):495–9.

[Martin et al., 2011] Martin, C., S. F. Pedersen, A. Schwab and C. Stock (2011). *Intracellular pH gradients in migrating cells*. Am. J. Physiol. Cell. Physiol., 300:C490–C495.

[Mayer and Heckel, 2006] Mayer, G. and A. Heckel (2006). *Biologically Active Molecules with a "Light Switch"*. Angew. Chem. Int. Ed., 45:4900–4921.

[Medeiros et al., 2006] Medeiros, N. A., D. T. Burnette and P. Forscher (2006). *Myosin II functions in actin-bundle turnover in neuronal growth cones*. Nat. Cell Biol., 8:215–226.

[Meima et al., 2009] Meima, M. E., B. A. Webb, H. E. Witkowska and D. L. Barber (2009). *The Sodium-Hydrogen Exchanger NHE1 Is and Akt Substrate Necessary for Actin Filament Reorganization by Growth Factors*. J. Biol. Chem., 284 (39):26666–26675.

[Melki et al., 1996] Melki, R., S. Fievez and M. F. Carlier (1996). *Continuous Monitoring of P_i Release Following Nucleotide Hydrolysis in Actin or Tubulin Assembly Using 2-Amino-6-mercapto-7-methylpurine Ribonucleoside and Purine-Nucleoside Phosphorylase as an Enzyme-Linked Assay*. Biochemistry, 35:12038–12045.

[Michelot et al., 2007] Michelot, A., C. G. Berro, R. Boujemaa-Paterski, C. J. Staiger, J.-L. Martiel and L. Blanchoin (2007). *Actin-Filament Stochastic Dynamics Mediated by ADF/Cofilin*. Curr. Biol., 17:825–833.

[Miyazaki et al., 1986] Miyazaki, S., T. Imai, Y. Igo and K. Otsuka (1986). *Effect of Cyclic Deformation on the Pseudoelasticity Characteristics of Ti-Ni Alloys*. Metall. Trans. A, 17A:115–150.

[Mooren et al., 2009] Mooren, O. L., T. I. Kotova, A. J. Moore and D. A. Schafer (2009). *Dynamin2 GTPase and Cortactin Remodel Actin Filaments*. J. Biol. Chem., 284:23995–24005.

[Moriyama and Yahara, 1999] Moriyama, K. and I. Yahara (1999). *Two activities of cofilin, severing and accelerating directional depolymerization of actin filaments, are affected differentially by mutations around the actin-binding helix*. EMBO J., 18:6752–6761.

[Mukhina et al., 2007] Mukhina, S., Y. Wang and M. Murata-Hori (2007). *α-Actinin Is Required for Tightly Regulated Remodeling of the Actin Cortical Network during Cytokinesis*. Dev. Cell, 13:554–565.

[Mullins, 1969] Mullins, L. (1969). *Softening of rubber by deformation*. Rubber Chem. Technol., 42:339–362.

[Mullins et al., 1998] Mullins, R. D., J. A. Heuse and T. D. Pollard (1998). *The interaction of Arp2/3 complex with actin: Nucleation, high affinity pointed end capping, and formation of branching networks of filaments*. Proc. Natl. Acad. Sci. USA, 95:6181–6186.

[Munoz et al., 2008] Munoz, M. J., J. A. Bea, J. F. Rodriguez, I. Ochoa, J. Grasa, A. Perez del Palomar, P. Zaragoza, R. Osta and M. Doblare (2008). *An experimental study of the mouse skin behaviour: Damage and inelastic aspects*. J. Biomech., 41:93–99.

[Olson and Nordheim, 2010] Olson, E. N. and A. Nordheim (2010). *Linking actin dynamics and gene transcription to drive cellular motile functions*. Nat. Rev. Mol. Cell Biol., 11:353–365.

[Ono and Ono, 2002] Ono, S. and K. Ono (2002). *Tropomyosin inhibits ADF/cofilin-dependent actin filament dynamics*. J. Cell Biol., 156:1065–1076.

[Ono et al., 1997] Ono, S., Y. Yamakita, S. Yamashiro, P. T. Matsudaira, J. R. Gnarra, T. Obinata and F. Matsumura (1997). *Identification of an actin binding region and a protein kinase C phosphorylation site on human fascin*. J. Biol. Chem., 272:2527–2533.

[Oser and Condeelis, 2009] Oser, M. and J. Condeelis (2009). *The Cofilin Activity Cycle in Lamellipodia and Invadopodia*. J. Cell. Biochem., 108:1252–1262.

[Otsuka and Ren, 1999] Otsuka, K. and X. Ren (1999). *Recent developments in the research of shape memory alloys*. Intermettalics, 7:511–528.

[Pardee et al., 1982] Pardee, J. D., P. A. Simpson, L. Stryer and Spu (1982). *Actin Filaments Undergo Limited Subunit Exchange in Physiological Salt Conditions*. J. Cell Biol., 94:316–324.

[Polak et al., 2001] Polak, Jaroslav, F. Fardoun and S. Degallaix (2001). *Analysis of the hysteresis loop in stainless steels I. Austenitic and ferritic steels*. Mater. Sci. Eng. A, 297:144–153.

[Pollard, 1986] Pollard, T. D. (1986). *Rate Constants for the Reactions of ATP- and ADP-Actin with the Ends of Actin Filaments*. J.Cell Biol., 103:2747–2754.

[Pollard and Mooseker, 1981] Pollard, T. D. and M. S. Mooseker (1981). *Direct Measurement of Actin Polymerization Rate Constants by Electron Microscopy of Actin Filaments Nucleated by Isolated Microvillus Cores*. J. Cell Biol., 88:654–659.

[Rabinowitz and Beardmore, 1974] Rabinowitz, S. and P. Beardmore (1974). *Cyclic deformation and fracture of polymers*. J. Mater. Sci., 9:81–99.

[Ren et al., 2009] Ren, Y., J. C. Effler, M. Norstrom, T. Luo, R. A. Firtel, P. A. Iglesias, R. S. Rock and D. N. Robinson (2009). *Mechanosensing through Cooperative Interactions between Myosin II and the Actin Cross-linker Cortexillin I*. Curr. Biol., 19:1421–1428.

[Rubod et al., 2008] Rubod, C., M. Boukerrou, M. Brieu, C. Jean-Charles, P. Dubois and M. Cosson (2008). *Biomechanical properties of vaginal tissue: preliminary results*. Int. Urogynecol. J., 19:811–816.

[Rzadzinska et al., 2005] Rzadzinska, A., M. Schneider, K. Noben-Trauth, J. R. Bartles and B. Kachar (2005). *Balanced Levels of Espin are Critical for Stereociliary Growth and Length Maintenance*. Cell Motil. Cytoskel., 62:157–165.

[Schmoller, 2008] Schmoller, K. M. (2008). *Composite Actin Networks*. Master's thesis, TU München.

[Schmoller et al., 2008a] Schmoller, K. M., O. Lieleg and A. R. Bausch (2008a). *Cross-Linking Molecules Modify Composite Actin Networks Independently*. Phys. Rev. Lett., 101:118102.

[Schmoller et al., 2008b] Schmoller, K. M., O. Lieleg and A. R. Bausch (2008b). *Internal stress in kinetically trapped actin bundle networks*. Soft Matter, 4:2365 – 2367.

[Semmrich et al., 2007] Semmrich, C., J. Glaser, R. Merkel, A. R. Bausch and K. Kroy (2007). *Glass Transition and Rheological Redundancy in F-Actin Solutions*. Proc. Natl. Acad. Sci. USA, 104 (51):20199–20203.

[Semmrich et al., 2008] Semmrich, C., R. J. Larsen and A. R. Bausch (2008). *Nonlinear Mechanics of Entangled F-Actin Solutions*. Soft Matter, 4:1675–1680.

[Sept et al., 1999] Sept, D., J. Xu, T. D. Pollard and J. A. McCammon (1999). *Annealing Accounts for the Length of Actin Filaments Formed by Spontaneous Polymerization*. Biophys. J., 77:2911–2919.

[Shin et al., 2004] Shin, J. H., M. L. Gardel, L. Mahadevan, P. Matsudaira and D. A. Weitz (2004). *Relating microstructure to rheology of a bundled and cross-linked F-actin network in vitro*. Proc. Natl. Acad. Sci. USA, 101:9636–9641.

[Shizuta et al., 1976] Shizuta, Y., H. Shizuta, M. Gallo, P. Davies and I. Pastan (1976). *Purification and properties of filamin, an actin binding protein from chicken gizzard*. J.Biol. Chem., 251 (21):6562–6567.

[Simpson, 1980] Simpson, P. A., Spudich J. A. (1980). *ATP-driven steady-state exchange of monomeric and filamentous actin from Dictyostelium discoideum*. Proc. Natl. Acad. Sci. USA, 77:4610–4613.

[Sitar et al., 2011] Sitar, T., J. Gallinger, A. M. Ducka, T. P. Ikonen, M. Wohlhoefler, K. M. Schmoller, A. R. Bausch, P. Joel, K. M. Trybus, A. A. Noegel, M. Schleicher, R. Huber and T. A. Holak (2011). *Molecular architecture of the Spire-actin nucleus and its implication for the actin filament assembly*. Proc. Natl. Acad. Sci. USA, 108:19575–19580.

[Small et al., 2002] Small, J. V., T. Stradal, E. Vignal and K. Rottner (2002). *The lamellipodium: where motility begins*. TRENDS Cell Biol., 12:112–120.

[Spudich and Watt, 1971] Spudich, J. A. and S. Watt (1971). *Regulation of Rabbit Skeletal Muscle Contraction .1. Biochemical Studies of Interaction of Tropomyosin-Troponin Complex with Actin and Proteolytic Fragments of Myosin*. J. Biol. Chem., 246:4866–71.

[Srivastava et al., 2007] Srivastava, J., D. L. Barber and M. P. Jacobson (2007). *Intracellular pH Sensors: Design Principles and Functional Signficance*. Physiology, 22:30–39.

[Srivastava et al., 2008] Srivastava, J., G. Barreiro, S. Groscurth, A. R. Gingras, B. T. Coult, D. R. Critchley, M. J. S. Kelly, M. P. Jacobson and D. L. Barber (2008). *Structural model and functional significance of pH-dependent talin-actin binding for focal adhesion remodeling*. Proc. Natl. Acad. Sci. USA, 105:14436–14441.

[Staiger et al., 2009] Staiger, C. J., M. B. Sheahan, P. Khurana, X. Wang, D. W. McCurdy and L. Blanchoin (2009). *Actin filament dynamics are dominated by rapid growth and severing activity in the Arabidopsis cortical array*. J. Cell Biol., 184:269–280.

[Steinmetz et al., 1998] Steinmetz, O. M., D. Stoffler, S. A. Mueller, W. Jahn, B. Wolpensinger, K. N. Goldie, A. Engel, H. Faulstich and U. Aebi (1998). *Evaluating Atomic Models of F-actin with an Undecagold-tagged Phalloidin Derivative*. J. Mol. Biol., 276:1–6.

[Stock and Schwab, 2009] Stock, C. and A. Schwab (2009). *Protons make tumor cells move like clockwork*. Eur. J. Physiol., 458:981–992.

[Stossel et al., 2001] Stossel, T. P., J. Condeelis, L. Cooley, J. H. Hartwig, A. Noegel, M. Schleicher and S. S. Shapiro (2001). *Filamins as Integrators of Cell Mechanics and Signalling*. Nat. Rev. Mol. Cell. Biol., 2:138–145.

[Stricker et al., 2010] Stricker, J., T. Falzone and M. L. Gardel (2010). *Mechanics of the F-actin cytoskeleton*. J. Biochem., 43:9–14.

[Tahara et al., 2009] Tahara, M., H. Y. Kim, H. Hosoda and S. Miyazaki (2009). *Cyclic deformation behavior of a Ti-26 at.% Nb alloy*. Acta Mater., 57:2461–2469.

[Tempel et al., 1996] Tempel, M., G. Isenberg and E. Sackmann (1996). *Temperature-induced sol-gel transition and microgel formation in α-actinin cross-linked actin networks: A rheological study*. Phys. Rev. E, 54:1802–1810.

[Tharmann et al., 2007] Tharmann, R., M. M. A. E. Claessens and A. R. Bausch (2007). *Viscoelasticity of Isotropically Cross-Linked Actin Networks*. Phys. Rev. Lett., 98:088103.

[Thoresen et al., 2011] Thoresen, T., M. Lenz and M. L. Gardel (2011). *Reconstitution of Contractile Actomyosin Bundles*. Biophys. J., 100:2698–2705.

[Tilney et al., 2003] Tilney, L. G., P. S. Connelly, L. Ruggiero, K. A. Vranich and G. M. Guild (2003). *Actin Filament Turnover Regulated by Cross-linking Accounts for the Size, Shape, Location, and Number of Actin Bundles in Drosophila Bristles*. Mol. Biol. Cell, 14:3953–3966.

[Tseng et al., 2001] Tseng, Y., E. Fedorov, J. M. McCaffery, S. C. Almo and D. Wirtz (2001). *Micromechanics and Ultrastructure of Actin Filament Networks Crosslinked by Human Fascin: A Comparison with a-Actinin*. J. Mol. Biol., 310:351–366.

[Tseng et al., 2005] Tseng, Y., T. P. Kole, J. S. H. Lee, E. Fedorov, S. C. Almo, B. W. Schafer and D. Wirtz (2005). *How actin crosslinking and bundling proteins cooperate to generate an enhanced cell mechanical response*. Biochem. Bioph. Res. Commun., 334:183–192.

[Tseng et al., 2004] Tseng, Yiider, K. M. An, O. Esue and D. Wirtz (2004). *The bimodal role of filamin in controlling the architecture and mechanics of F-actin networks*. J. Biol. Chem., 279 (3):1819–1826.

[Uhde et al., 2004] Uhde, J., M. Keller and E. Sackmann (2004). *Internal Motility in Stiffening Actin-Myosin Networks*. Phys. Rev. Lett., 93:268101.

[Vavylonis et al., 2008] Vavylonis, D., J.-Q. Wu, S. Hao, B. O'Shaughnessy and T. D. Pollard (2008). *Assembly mechanism of the contractile ring for cytokinesis by fission yeast*. Science, 319(5859):97–100.

[Vignjevic et al., 2006] Vignjevic, D., S. Kojima, Y. Aratyn, O. Danciu, T. Svitkina and G. G. Borisy (2006). *Role of fascin in filopodial protrusion*. J. Cell Biol., 174(6):863–785.

[Vignjevic et al., 2003] Vignjevic, D., D. Yarar, M. Welch, J. Peloquin, T. Svitkina and G. Borisy (2003). *Formation of filopodia-like bundles in vitro from a dendritic network*. J. Cell Biol., 160(6):951–962.

[Volkmer Ward et al., 2008] Volkmer Ward, S. M., A. Weins, M. R. Pollak and D. A. Weitz (2008). *Dynamic Viscoelasticity of Actin Cross-Linked with Wild-Type and Disease-Causing Muntant a-Actinin-4*. Biophys.J., 95:4915–4923.

[Wagenseil et al., 2003] Wagenseil, J. E., T. Wakatsuki, R. J. Okamoto, G. I. Zahalak and E. L. Elson (2003). *One-Dimensional Viscoelastic Behavior of Fibroblast Populated Collagen Matrices*. J. Biomech. Engrg., 125:719–725.

[Wagner et al., 2006] Wagner, B., R. Tharmann, I. Haase, M. Fischer and A. R. Bausch (2006). *Cytoskeletal polymer networks: molecular structure of cross-linkers determine macroscopic properties*. Proc. Natl. Acad. Sci. USA, 103:13974–13978.

[Walther and Eifler, 2007] Walther, F. and D. Eifler (2007). *Cyclic deformation behavior of steels and light-metal alloys*. Mater. Sci. Eng. A, 468-470:259–266.

[Wang et al., 1989] Wang, F., R. V. Sampogna and B. R. Ware (1989). *pH dependence of actin self-assembly*. Biophys. J., 55:293–298.

[Wang et al., 2000] Wang, H.-B., M. Dembo and Y.-L. Wang (2000). *Substrate flexibility regulates growth and apoptosis of normal but not transformed cells*. Am. J. Physiol. Cell. Physiol., 279 (5):C1345–C1350.

[Wang et al., 2009] Wang, N., J. D. Tytell and D. E. Ingber (2009). *Mechanotransduction at a distance: mechanically coupling the extracellular matrix with the nucleus*. Nat. Rev. Mol. Cell Biol., 10:75–82.

[Webb et al., 2011] Webb, B. A., M. Chimenti, M. P. Jacobson and D. L. Barber (2011). *Dysregulated pH: a perfect storm for cancer progression*. Nat. Rev. Cancer, 11:671–677.

[Webb, 1992] Webb, R. M. (1992). *A continuous spectrophotometric assay for inorganic phosphate and for measuring phosphate release kinetics in biological systems*. Proc. Natl. Acad. Sci. USA, 89:4884–4887.

[Webber et al., 2007] Webber, R. E., C. Creton, H. R. Brown and J. P. Gong (2007). *Large Strain Hysteresis and Mullins Effect of Tough Double-Network Hydrogels*. Macromolecules, 40:2919–2927.

[Wegner, 1976] Wegner (1976). *Head to Tail Polymerization of Actin*. J. Mol, 108:139–150.

[Wegner, 1982] Wegner, A. (1982). *Spontaneous fragmentation of actin filaments in physiological conditions*. Nature, 296:266–267.

[Wegner and Isenberg, 1983] Wegner, A. and G. Isenberg (1983). *12-Fold difference between the critical monomer concentrations of the two ends of actin filaments in physiological salt conditions*. Proc. Natl. Acad. Sci. USA, 80:4922–4925.

[Wegner and Neuhaus, 1981] Wegner, A. and J.-M. Neuhaus (1981). *Requirement of Divalent Cations for Fast Exchange of Actin Monomers and Actin Filament Subunits*. J. Mol. Biol., 153:681–693.

[Wendel and Dancker, 1986] Wendel, H. and P. Dancker (1986). *Kinetics of actin depolymerization: influence of ions, temperature, age of F-actin, cytochalasin B and phalloidin*. Biochim. Biophys. Acta, 873:387–396.

[Wilhelm and Frey, 2003] Wilhelm, J. and E. Frey (2003). *Elasticity of stiff polymer networks*. Phys. Rev. Lett., 91.

[Wu et al., 2009] Wu, Y. I., D. Frey, O. I. Lungu, A. Jaehrig, I. Schlichting, B. Kuhlman and K. M. Hahn (2009). *A genetically encoded photoactivatable Rac controls the motility of living cells*. Nature, 461:104–108.

[Wurm, 2011] Wurm, C. (2011). *Structure, Mechanics and Dynamics of Cytoskeletal Model Systems*. PhD thesis, Technische Universität München.

[Xu et al., 2010] Xu, Y., T. A. Bismar, J. Su, B. Xu, G. Kristiansen, V. Zsuzsanna, L. Teng, D. E. Ingber, A. Mammoto, R. Kumar and M. A. Alaoui-Jamali (2010). *Filamin A regulates focal adhesion disassembly and suppresses breast cancer cell migration and invasion*. J. Exp. Med., 207:2421–2437.

[Zigmond et al., 1992] Zigmond, S. H., R. Furukawa and M. Fechheimer (1992). *Inhibition of Actin Filament Depolymerization by the Dictyostelium 30,000-D Actin-bundling Protein*. J. Cell Biol., 119:559–567.

[Zimmerle and Frieden, 1988] Zimmerle, C. T. and C. Frieden (1988). *Effect of pH on the Mechanism of Actin Polymerization*. Biochemistry, 27:7766–7772.

List of Figures

1.1 Overview . . . 3

2.1 Bundled actin networks . . . 7
2.2 Stepwise shearing of actin solutions observed with confocal rheology . . . 13
2.3 Stepwise shearing of actin/HMM and actin/fascin networks . . . 14

3.1 Einstein polymer . . . 19
3.2 Experiment to visualize steady state dynamics of an F-actin ensemble . . . 22
3.3 Length distribution of steady state actin . . . 23
3.4 Fluorescence images of labeled actin fragments in an unlabeled actin solution 24
3.5 Time evolution of the length distribution of labeled actin fragments in an unlabeled actin solution . . . 25
3.6 Phosphate release of a steady state F-actin ensemble . . . 28
3.7 Fragmentation rate depends on the salt concentrations . . . 30

4.1 Pyrene assay monitoring depolymerization in the presence of fascin or HMM 34
4.2 Diffusion chamber . . . 35
4.3 Depolymerization induced by Latrunculin B . . . 36
4.4 Quantitative analysis of LatB induced depolymerization . . . 37
4.5 Depolymerization induced by dilution . . . 38
4.6 Actin disintegration induced by cofilin . . . 41
4.7 Quantitative analysis of cofilin induced disintegration . . . 42
4.8 Simultaneous action of cofilin and myosin II . . . 43
4.9 Depolymerization model . . . 44
4.10 Depolymerization of microtubules . . . 45
4.11 Cofilin model . . . 46
4.12 Depolymerization pathways of cross-linked actin filaments . . . 47

5.1 Confocal images of actin/filamin networks . . . 50
5.2 Branched actin/filamin bundle network . . . 51
5.3 Structural state diagram of actin/filamin networks . . . 52
5.4 Bundle thickness in actin/filamin networks . . . 53
5.5 Illustration of an aggregation controlled network formation . . . 54
5.6 Linear rheology of actin/filamin networks . . . 56

5.7 Non-linear rheology of actin/filamin networks 58
5.8 Shear rate dependence of the non-linear response of actin/filamin networks 59

6.1 Bundling can be induced by applying mechanical forces 62
6.2 Illustration of the Mullins effect 63
6.3 Actin/α-actinin networks show cyclic hardening. 64
6.4 Strain induced network reorganizations explain cyclic hardening in actin/α-actinin networks. 66
6.5 Cyclic hardening at different strain amplitudes. 67
6.6 Stepwise shearing of actin/α-actinin networks. 69
6.7 Rheological response of actin/α-actinin networks to stepwise shearing. . . 70
6.8 Cyclic hardening in actin/α-actinin networks depends on protein concentrations. 71
6.9 Cyclic hardening in actin/filamin networks. 72
6.10 Stepwise shearing of actin/filamin networks 73
6.11 SMA Phase diagram 76
6.12 Analogy to Shape Memory Alloys 77

7.1 pH dependence of actin/filamin networks 82
7.2 Polymerization speed of actin/filamin networks is pH dependent 83
7.3 pH dependence of actin/cortexillin networks 85
7.4 pH dependence of actin/fascin networks 87
7.5 pH dependence of the nonlinear response of actin/fascin networks 88
7.6 pH dependence of actin/HMM networks 89
7.7 Contractility of cross-linked active actin networks 90

8.1 Schematic illustration of cytoskeletal regulation 94

Acknowledgement

Abschließend möchte ich ganz herzlich allen danken, die zum Gelingen dieser Arbeit beigetragen haben, und dafür gesorgt haben, dass die letzten Jahre viel Spaß gemacht haben.

- Meinem Doktorvater **Prof. Andreas Bausch** danke ich für die Möglichkeit in seiner Arbeitsgruppe zu promovieren. Für die hervorragende Betreuung, Förderung und Unterstützung in jeder Hinsicht. Für die Möglichkeit an vielen Konferenzen teilzunehmen, und die Freiheit, eigene Ideen immer umsetzen zu können.
- Allen, die direkt an den Projekten dieser Doktorarbeit beteiligt waren, für die erfolgreiche Zusammenarbeit. Also: **Christine Wurm**, **Simone Köhler**, **Pablo Fernández**, **Oliver Lieleg**, **Carla Zensen**, **Alvaro Crevenna**, **Daniel Blair**, **Richard Arevalo** und **Thomas Niedermayer**. Bei der Arbeitsgruppe von Prof. Daniel Blair möchte ich mich speziell dafür bedanken, dass es mir ermöglicht wurde ihr konfokales Rheometer zu benutzen.
- Der gesamten **Aktin-Gruppe**, bzw. gleich dem gesamten **E27**: Christine, Volker, Jona, Simone, Uli, Markus, Heinrich, Bernhard, Sebastian, Carina, Martina, Schuppi, Felix, Matthias, Oli, Pablo, Michael, Carla, Bernd, Zlata... für die Hilfsbereitschaft, die vielen konstruktiven Diskussionen und Ratschläge, und das nette Zusammenarbeiten.
- Dem **Simone-Jona-Volker-Christine Büro** für viele beantwortete Fragen und meine inoffizielle Bürozugehörigkeit (besonders wichtig, wenn es Bürokuchen gab).
- **Simone Köhler** für die ständige Beantwortung biochemischer Fragen (Biochemie-Praktikum, Teil 1 bis viel).
- Den **TA's**, also **Monika Rusp**, **Gabriele Chmel**, **Karin Vogt** und **Daniela Scheikl** für die tägliche Unterstützung im Labor, ohne die vermutlich gar nichts funktionieren würde. Ganz besonders danken möchte ich Moni für das beste Aktin der Welt, sowie Gabi und Karin für das Aufreinigen verschiedenster Cross-linker.
- Den **Sekretärinnen**, also **Iris König-Decker**,**Elke Fehsenfeld**, **Katerina Girgensohn**, **Nicole Mittermüller** und **Katharina Scholz** für die Hilfe im Bürokratiedschungel.

- **Simone Köhler** und **Volker Schaller** fürs Korrekturlesen.
- All meinen **Bürokollegen** (Oli, Christina, Pablo, Michael, und viele mehr) für die angenehme Bürogemeinschaft.
- Dem *Dschungelbüro* und **Schuppi** für das regelmäßige Gehirnhälftenvernetzen bzw. das Erdulden desselben.
- Dem **Dschungelbüro** und dem **Schokoladen** für die Versorgung mit Zucker.
- Dem kompletten **E22**/**E27**/**E40** für das entspannte, positive Arbeitsklima und die gemeinsamen Arbeitspausen (Beachen, Fußball, Eiszeit...). Kurz, für die schöne gemeinsame Zeit.
- **Compint** und der **bayerischen Eliteförderung** für die finanzielle Unterstützung
- **Meiner Familie**, dafür dass sie mich immer unterstützt und mir mein Studium ermöglicht hat.

List of Publications

- S. Köhler*, **K. M. Schmoller***, A. H. Crevenna and A. R. Bausch.
  Regulating contractility of the actomyosin cytoskeleton by pH.
  submitted.

- **K. M. Schmoller**, S. Köhler, A. H. Crevenna, R. Wedlich-Soldner and A. R. Bausch.
  Modulation of cross-linked actin networks by pH.
  submitted.

- N. Elkhatib, M. Neu, C. Zensen, **K. M. Schmoller**, D. Louvard, A. R. Bausch and D. M. Vignjevic.
  Turnover of focal adhesions required for efficient cell migration is regulated by parallel actin bundles.
  submitted.

- T. Sitar*, J. Gallinger*, A. M. Ducka, T. P. Ikonen, M. Wohlhoefler, **K. M. Schmoller**, A. R. Bausch, P. Joel, K. M. Trybus, A. A. Noegel, M. Schleicher, R. Huber and T. A. Holak (2011).
  Molecular architecture of the Spire–actin nucleus and its implication for actin filament assembly.
  Proc. Natl. Acad. Sci. USA, 108, 19575-19580.

- **K. M. Schmoller**, T. Niedermayer, C. Zensen, C. Wurm and A. R. Bausch (2011).
  Fragmentation is Crucial for the Steady-State Dynamics of Actin Filaments.
  Biophys. J., 101, 803-808.

- **K. M. Schmoller***, C. Semmrich* and A. R. Bausch (2011).
  Slow down of actin depolymerisation by cross-linking molecules.
  J. Struct. Biol., 173, 350-357.

- **K. M. Schmoller**, P. Fernandez, R. C Arevalo, D. L. Blair and A. R. Bausch (2010).
  Cyclic Hardening in Bundled Actin Networks.
  Nat. Commun., 1, 134.

- O. Lieleg*, **K. M. Schmoller***, K. R. Purdy Drew, M. M. A. E. Claessens, C. Semmrich, L. Zheng, J. R. Bartles and A. R. Bausch (2009).
  Structural and Viscoelastic Properties of Actin Networks Formed by Espin or Pathologically Relevant Espin Mutants.
  ChemPhysChem, 10, 2813-2817.

- **K. M. Schmoller**, O. Lieleg, and A. R. Bausch (2009).
  Structural and Viscoelastic Properties of Actin/Filamin Networks: Cross-linked versus Bundled Networks.
  Biophys. J., 97, 83-89.

- O. Lieleg, **K. M.Schmoller**, C. J. Cyron, Y. Luan, W. A. Wall and A. R. Bausch (2009).
  Structural Polymorphism in Heterogeneous Cytoskeletal Networks.
  Soft Matter, 5, 1796-1803.

- O. Lieleg, **K. M. Schmoller**, M. M. A. E. Claessens and A. R. Bausch (2008).
  Cytoskeletal Polymer Networks: Viscoelastic Properties are Determined by the Microscopic Interaction Potential of Cross-links.
  Biophys. J., 96, 4725-32.

- **K. M. Schmoller**, O. Lieleg, and A. R. Bausch (2008).
  Internal stress in kinetically trapped actin bundle networks.
  Soft Matter, 4, 2365 – 2367.

- **K. M. Schmoller**, O. Lieleg, and A. R. Bausch (2008).
  Cross-linking Molecules Modify Composite Actin Networks Independently.
  Phys. Rev. Lett. 101, 118102.

* These authors contributed equally to this work.